

MINIMUM MEAN-SQUARED ERROR ADAPTIVE ANTENNA ARRAYS FOR
DIRECT-SEQUENCE CODE-DIVISION MULTIPLE ACCESS SYSTEMS

By

JOHN EARLE MILLER

A DISSERTATION PRESENTED TO THE GRADUATE SCHOOL
OF THE UNIVERSITY OF FLORIDA IN PARTIAL FULFILLMENT
OF THE REQUIREMENTS FOR THE DEGREE OF
DOCTOR OF PHILOSOPHY

UNIVERSITY OF FLORIDA

1996

Copyright 1996

by

John Earle Miller

This work is dedicated to my wife Kim, my children Marissa and Christopher and my parents Frank and Garnet.

ACKNOWLEDGMENTS

I would like to thank all of the members of my committee for their involvement, guidance and influence in this research. I would like to extend a special thanks to my chairman, Dr. Scott L. Miller, for his support, many insights and thoughtful suggestions which have influenced this work. The financial support provided by the Department of Electrical and Computer Engineering is also gratefully acknowledged.

TABLE OF CONTENTS

	<u>page</u>
ACKNOWLEDGMENTS	iv
ABSTRACT	vii
 CHAPTERS	
1 INTRODUCTION	1
Direct-Sequence Spread-Spectrum with Multiple-Access	3
Adaptive Antenna Arrays	7
Previous Work	13
Dissertation Outline	21
2 A MULTIUSER ANTENNA ARRAY PROCESSOR STEADY-STATE PERFORMANCE	24
The Multiuser MMSE Processor	25
Spatially Orthogonal Users	26
Nonorthogonal Users	30
Single-User System	34
One Weak User, One Strong User	34
Two Equal-Power Users	36
Two Strong Users	36
Numerical Results	37
3 THE MULTIUSER ARRAY PROCESSOR ADAPTIVE PERFORMANCE	42
Mean-Based Performance Measure	43
Variance-Based Performance Measure	47
Simulation Results	49
4 BASE STATION RECEIVER PERFORMANCE USING A SMART ANTENNA ARRAY IN A DS-CDMA SYSTEM WITH IMPERFECT POWER CONTROL	52

System Description	53
Analysis	54
Simulations and Results.....	61
Conclusions	65
 5 BASE STATION RECEIVER PERFORMANCE WITH A SMART ANTENNA ARRAY IN THE PRESENCE OF MULTIPATH FADING AND SHADOW FADING	 68
A Single Cell with Signals Subjected to Rayleigh Fading	69
Multiple Cells with Signals Subjected to Rayleigh Fading and Shadow Fading	 71
Analysis	76
Results.....	80
Conclusions/Discussion.....	88
Summary	89
 6 BASE STATION ANTENNA ARRAY ADAPTIVE PERFORMANCE.....	 91
Signal and Channel Model.....	92
Adaptive Receivers	94
Simulations	97
Conclusions/Summary.....	102
 7 SUMMARY	 106
Areas for Future Work.....	109
 APPENDIX	
A THE OUTPUT SNR PERFORMANCE SURFACE	113
LIST OF REFERENCES	117
BIOGRAPHICAL SKETCH	129

Abstract of Dissertation Presented to the Graduate School
of the University of Florida in Partial Fulfillment of the
Requirements for the Degree of Doctor of Philosophy

MINIMUM MEAN-SQUARED ERROR ADAPTIVE ANTENNA ARRAYS FOR
DIRECT-SEQUENCE CODE-DIVISION MULTIPLE-ACCESS SYSTEMS

By

John Earle Miller

August, 1996

Chairman: Dr. Scott L. Miller

Major Department: Electrical and Computer Engineering

This dissertation examines the performance of direct-sequence code-division multiple-access receivers which use a minimum mean-squared error adaptive antenna array as a predetection spatial filter. The array attenuates multi-access interference prior to conventional, direct-sequence matched-filter detection. Conventional detectors are vulnerable to heightened levels of multi-access interference. Minimum mean-squared error processing seems like a natural choice for optimization in a code-division multiple-access environment since several efficient search algorithms exist which are compatible with decision-directed equalizer structures.

Two array structures are examined. The first structure uses a single set of array weights to equalize more than one desired signal. For two strong incident signals of unequal power levels, the steady-state response gives output signal-to-noise ratios that are

leveled to a value near the maximum response of the weaker of the two users. The steady-state adaptive performance of the multi-user array based on a least-mean-squares algorithm is also examined. It is found that the maximum allowable step size based on stability arguments will also give adequate output signal-to-noise ratio performance of the multi-user processor.

The second structure uses a single set of weights per multiple-access signal and the array output feeds a conventional detector. The array/detector performance measure is outage probability and outage-based capacity as a function of the number of array elements and the degree of power control error. A robust, incremental measure of performance--the per-element capacity--is defined as the capacity per array element for a given outage probability. Steady-state performance is evaluated for the case of directional signals as well as for the case of signals subjected to multipath fading and shadowing. The adaptive performance of the recursive least-squares algorithm is also investigated.

CHAPTER 1 INTRODUCTION

Wireless communication based on direct-sequence spread spectrum (DS-SS) has received considerable attention as an efficient signaling format for code-division multiple-access systems (CDMA). While DS-SS has a long history of use in defense applications where jamming resistance and security are primary concerns,¹ some proponents maintain that it will also serve as a high-capacity format for the next-generation mobile-cellular and wireless systems for commercial use.^{2,3,4,5} System specifications for domestic use have been endorsed by industrial agencies,⁶ the results of field trials have been published^{7,8} and it has been studied as a possible format for third-generation mobile radio systems in Europe.^{9,10}

Despite a frenzy of activity and interest, DS-SS has a serious drawback: the near-far effect. This occurs when strong signals overwhelm a weaker desired signal during the detection process. In a commercial mobile-cellular system the near-far effect can occur at the cell-site base-station receiver. Incident signals originating from multiple-access, fixed-power transmitters geographically distributed throughout a cell can have incident power levels that change drastically as the transmitter positions vary. Signals originating from transmitters near the base station may overwhelm received signals from transmitters on the fringe of the cell. Vigorous proponents of commercial DS-SS systems have developed transmit power-control formats to adjust each user's RF transmit power in real time so that power levels of all multiple-access signals incident upon the base station are

approximately equal. Initially, it was stated that power control would need to be able to adjust the transmit power over a 80 dB dynamic range in a mobile cellular scenario.¹¹ Field tests indicate that 50 dB is more likely.^{7,12}

Another use for DS-SS is in the Global Positioning System (GPS). Originally implemented as a positioning system for the Department of Defense, it has enjoyed commercial applications in mapping, navigation, and surveying.¹³ The world-wide GPS uses a DS-SS signaling format to obtain relatively accurate estimates of geographical position. An earth-bound GPS receiver determines its position by measuring the path delays of several DS-SS signals which originate from earth-orbiting satellites. The near-far effect is not a critical issue for many commercial GPS applications, such as aviation or shipping, since the signals are subjected only to free-space path losses. Some commercial applications, such as surveying, suffer other forms of signal losses, such as multipath fading or shadow fading, and these can indirectly lead to near-far limited performance.

This work examines receiver performance when an adaptive antenna array is used at the DS-SS receiver. In such a system the array would act as a front-end spatial filter which preserves the integrity of the desired signal or signals, attenuates interferers and supplements the existing power control algorithm. Such an approach might be compatible with existing cellular CDMA standards. The remainder of this chapter is divided into several sections. The next section will give a qualitative review of DS-SS systems. The second section will review quantities and expressions used in the analysis of the minimum mean-squared-error (MMSE) beamforming antenna arrays. The third section will review previous work germane to the research presented here and the last section will provide an outline of the remainder of this dissertation.

Direct-Sequence Spread-Spectrum with Multiple-Access

Generating a DS-SS waveform involves multiplying a modulated baseband waveform by a pseudorandom sequence sometimes known as a pseudonoise (PN) code. In an asynchronous multi-access channel the incident DS-SS waveforms may be subjected to random time delays and carrier phase delays and corrupted by noise. For a single-channel receiver the multiple-access incident signals may be modeled by the expression:

$$Y(t) = \operatorname{Re} \left\{ \sum_{m=1}^K A_m c_m(t - \tau_m) b_m(t - \tau_m) \exp(j(\omega_c t + \theta_m)) + n(t) \right\} \quad (1.1)$$

where the index m refers to the m th of K signals. The quantity A_m is the incident signal level of the m th signal, $c_m(t - \tau_m)$ represents the m th PN code waveform which consists of a sequence (of length N_c) of pseudorandom square pulses, ($c_m \in \{+1, -1\}$) each with interval T_c . The quantity $b_m(t - \tau_m)$ represents independent binary phase-shift keyed (BPSK) modulation with equally-likely symbols ($b_m \in \{+1, -1\}$) obtained via ideal, square pulses. The time delay τ_m is uniformly distributed over a symbol interval $[0, T_b]$. The time delay τ_m arises because the channel allows asynchronous access; users may begin transmission at any time. The carrier frequency is designated by ω_c , and θ_m is the random carrier phase uniformly distributed over $[0, 2\pi)$. The quantity $n(t)$ is complex additive white Gaussian noise (AWGN) with a one-sided power spectral density of N_0 .

Note that in contrast to systems which use frequency-division multiple access (FDMA), all users in a CDMA system share a common frequency ω_c . Frequency-division channels are achieved by separating the carrier frequencies of multiple, bandlimited signals to the point that they do not interfere with one another in the receiver. Code-division

channels in CDMA systems, on the other hand, are achieved through the low crosscorrelation properties of the individual PN sequences. The PN sequences have many interesting properties, including low crosscorrelation¹⁴ defined as

$r_{mn}(\tau) = \int c_m(t)c_n(t+\tau)dt \ll Nc \quad \forall m \neq n$. The limits of the integral are from zero to $NcTc$. In a CDMA system the individual users share a common carrier frequency but are assigned distinct PN sequences that permit code-division channel links to a base station or other receiver.

This work assumes that detection of DS-SS signals is accomplished by a correlating detector also referred to as a *conventional detector*. The i th user's DS signal is multiplied by a synchronized replica of its PN sequence, passed to an integrate-and-dump filter and

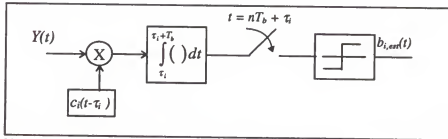


Figure 1.1 Conventional detector, baseband model.

hard-limited to provide an estimate of the modulation symbol, as shown in Figure 1.1.

The conventional detector provides optimum performance for a single user in AWGN but gives sub-optimum performance in a multi-access environment. The performance of a conventional detector in a multi-access environment depends roughly on the *processing gain* which is a measure of the interference rejection capability of the detector and is sometimes defined as the number of code symbols (or “chips”) per modulation symbol ($N_c = T_b/T_c$). For a fixed, finite processing gain it is always possible for strong interferers to

overwhelm the detection of a weaker signal and cause poor performance. The complex baseband output of the integrate-and-dump portion of the conventional detector devoted to user 1 consists of a desired signal component as well as multiaccess interference and noise components:

$$\begin{aligned}
 s_{o,1}(t) &= A_1 b_1(t) + \sum_{m=2}^K A_m \int_{\tau_1}^{\tau_1+\tau_b} c_1(t) c_m(t - \tau_m) b_m(t - \tau_m) dt + \int_{\tau_1}^{\tau_1+\tau_b} c_1(t) n(t) dt \\
 &= A_1 b_1(t) + \sum_{m=2}^K A_m [b_{m,-1} R_{m,1}(\tau_m) + b_{m,0} \hat{R}_{m,1}(\tau_m)] + \int_{\tau_1}^{\tau_1+\tau_b} c_1(t) n(t) dt
 \end{aligned} \tag{1.2}$$

$$\begin{aligned}
 R_{m,1}(\tau_m) &= \int_0^{\tau_b} c_m(t - \tau_m) c_1(t) dt \\
 \text{where:} \quad \hat{R}_{m,1}(\tau_m) &= \int_{\tau_m}^{\tau_b} c_m(t - \tau_m) c_1(t) dt
 \end{aligned}$$

where bit 1 of user 1 is the detected signal of interest and $\tau_1 = 0$. The quantities $R_{m,1}(\tau_m)$ and $\hat{R}_{m,1}(\tau_m)$ are the partial crosscorrelation functions. The quantities $b_{m,-1}$ and $b_{m,0}$ represent the contributions of the m th user's two bits which overlap the current bit interval of the desired user. The values of crosscorrelations depend upon the sequences and their relative time delays. The multi-access bit-error performance of the conventional detector has been studied extensively; the dependence of the detector performance on PN-code parameters has been well characterized.^{15,16} If one or more crosscorrelations are non-zero and the corresponding input levels are large, those components may overwhelm the desired signal in the detector. This is the near-far effect.

In mobile cellular or personal communication systems, signals incident on the base station (also referred to as the *uplink* signal path) can take wide-ranging incident power levels because of the random placement of users about the base station. The current

solution to this dilemma is to vary the transmitter power levels in real time via transmit power control. In a system using closed-loop power control the base station receiver monitors the detected power level of each multi-access signal. As the incident power levels of the multi-access signals vary because of changing channel conditions, instructions are sent from the base station to the mobile units, via an uncoded narrowband side channel, to individually increase or decrease transmit power. The aim of the power control is to force the effective bit-energy-to-noise spectral density ratio $((E_b/N_o)_{eff})$ of all the incident signals to the same threshold. In practice, however, the power control is unable to perfectly track changing channel conditions because of doppler-induced multipath fading and finite power control step size. Error in the power-controlled signal results in an effective bit energy to noise spectral density ratio $((E_b/N_o)_{eff})$ at the detector output which is approximately lognormal in distribution.^{17,18} Field trials indicate that high-mobility mobile users (such as in fast-moving automobiles) have $(E_b/N_o)_{eff}$ standard deviations of $\sigma_r = 2.5$ dB while lower values ($\sigma_r = 1.5$ dB) have been recorded for low-mobility users (pedestrians).⁷

Existing cellular CDMA specifications also have a contingency for open-loop power control.⁶ In an open-loop power-controlled system the mobile or personal units use the detected base-station carrier power as a reference to adjust their transmit power. No side channel is required. Some researchers have proposed estimation algorithms which would allow a mobile to make estimates of the base station carrier power. The researchers present evidence that the carrier-measurement error in terrestrial mobile cellular systems is well-approximated as lognormally distributed with a $\sigma_{pcc} \leq 3$ dB for vehicle speeds of up to 60 mph and 8 dB of shadow fading.¹⁹ Other researchers working in the field of mobile

cellular systems based on low-earth-orbiting-satellites (LEOS) have also found open-loop power control error to be well-approximated by a lognormally distributed random variable (r.v.).^{20,21}

If we generalize the previous work and assume that power control error may be approximated by a lognormal r.v., then equation (1.1) may be rewritten slightly:

$$Y(t) = \text{Re} \left\{ A \sum_{m=1}^K 10^{e_m/20} c_m(t - \tau_k) b_m(t - \tau_m) \exp(j(\omega_c t + \theta_m)) + n(t) \right\} \quad (1.3)$$

where e_m is normally distributed with zero mean and variance equal to $\sigma_{pce}^2 (N(0, \sigma_{pce}^2))$.

Note that in previous works the lognormal approximation of power control error applied to the incident power levels for open-loop power control, and to the $(E_b/N_o)_{eff}$ for the case of closed-loop power control. To simplify analysis, this research will assume that power control error results in lognormally distributed incident signal levels for closed-loop or open-loop power-controlled systems.

Adaptive Antenna Arrays

This research assumes an adaptive antenna array is used as a front-end spatial filter to attenuate direction-dependent cochannel interference prior to conventional detection of multi-access DS-CDMA signals. The anticipated role of the adaptive array will be to attenuate the strongest interferers and thereby lessen performance degradations due to the near-far effect. The antenna arrays explored here will be limited to beamforming arrays - linear combiners - which use a minimum mean-squared error (MMSE) optimization criterion. This technique is also referred to as Wiener filtering²² or optimum combining.²³ A MMSE optimization is well suited to a mobile DS-SS-CDMA scenario since each user's

PN sequence, required for DS-SS detection and decoding, can provide a convenient reference waveform. There are efficient MMSE adaptive algorithms which would require no more side information than the code sequence and its timing.²²

The array is composed of ideal isotropic sensors with no mutual coupling between the elements. Incident signals are spatially sampled by the sensors as they propagate across the array. The incident signals are assumed to be narrowband. This approximation is valid for spread spectrum signals as long as signal bandwidths are a small percentage of the carrier frequency. Current specifications⁶ call for bandwidths of 1.2288 MHz at a carrier frequency of 850 MHz. The resulting double-sided signal bandwidth is much less than one percent, so the narrowband approximation should be acceptable.

The physical displacements between the array sensors induce relative phase shifts on our spatially sampled, narrowband signals. The phase-shifts are constant over frequency and depend upon the array geometry and the signal's direction-of-arrival (DOA). The complex signal component outputs of the N discrete antenna elements for the m th incident signal can be described by a vector:

$$\begin{aligned} s_{c,m} &= g_m(t) \exp(jky_m - \omega_c t) = g_m(t) \exp(-j\omega_c t) \begin{bmatrix} \exp(j\phi_{m,0}) \\ \exp(j\phi_{m,1}) \\ \vdots \\ \exp(j\phi_{m,N-1}) \end{bmatrix} \\ &= g_m(t) \exp(-j\omega_c t) \mathbf{u}_m \end{aligned} \tag{1.4}$$

where:

$$\mathbf{u}_m = [\exp(j\phi_{m,0}) \quad \exp(j\phi_{m,1}) \quad \cdots \quad \exp(j\phi_{m,N-1})]^T$$

where the vector \mathbf{y}_m (see Figure (1.2)) represents the physical displacements between some reference point and the N array elements. An element of \mathbf{y}_m ($y_{m,n}$ $n = 0 \dots N-1$)

represents the physical distance between a reference point and the corresponding array element. The parameter k is the free-space wave number of the incident plane wave ($k = 2\pi/\lambda$). Carrier phase-shifts have been absorbed into the complex, baseband function $g_m(t)$. The vector \mathbf{u}_m contains electrical phase shifts resulting from the physical displacements \mathbf{y}_m between the elements and the point of reference. The individual elements of \mathbf{u}_m (i.e. $\phi_{m,n}$) represent the m th signal's phase shift between the reference point and the n th array element. The vector \mathbf{u}_m will be referred to as the *interelement phase-shift vector* or simply the *phase-shift vector* and will not be considered a function of time unless stated otherwise. For the remainder of the report constants will appear as normal block or script characters, vectors will be represented by lower-case boldface and matrices by upper-case boldface.

A diagram illustrating some of the physical quantities is shown in Figure 1.2. An incident signal propagates as a plane wave $s(t)$. The signals and noise are spatially sampled by each element of the array; ignoring an explicit time dependence allows the samples to be represented by x_n , $n = 0 \dots N-1$, and form the input vector \mathbf{x} . The inputs are weighted (via the weight vector $\mathbf{w} = [w_0 \ w_1 \ \dots \ w_{N-1}]^T$) and summed to form the beamformer output. The quantity $k y$ is the phase-shift of the propagating wave due to physical displacement y . As the wave propagates across the array the phase-shifts due to displacement give rise to interelement phase-shifts which are contained within the vector \mathbf{u} . The lower part of the figure illustrates how the direction-dependent phase-shift arises between two adjacent elements. The quantity ϕ is the phase shift between any two adjacent elements.

A change in array geometry would affect only the functional form of the relative phase-shifts between the array elements. The quantity $\phi = 2\pi d(\sin\theta)/\lambda$ in Figure 1.2 above

is the direction-dependent phase-shift between any two adjacent array elements for a linear array. Arrays composed of individual elements arranged in a circle will be examined in later chapters because, unlike linear arrays, they can resolve incident signals over the direction-of-arrival interval $[0, 2\pi)$. The phase-shift between any two adjacent elements is given by $\phi = (\pi d \cos[\theta - 2\pi/N]) / (\lambda \sin[\pi/N])$ for a circular array.

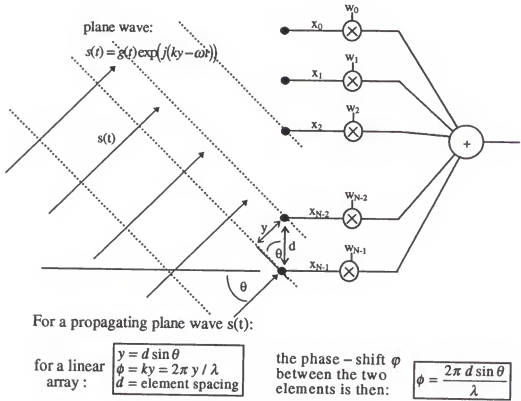


Figure 1.2 A directional plane wave incident on a linear array of sensors.

The baseband array output vector is the sum of the noise and signal vectors:

$$\mathbf{x} = \mathbf{n}(t) + \sum_{m=1}^K \mathbf{s}_m(t) = \mathbf{n}(t) + \sum_{m=1}^K g_m(t) \mathbf{u}_m \quad (1.5)$$

where $\mathbf{n}(t)$ is the AWGN vector. The noise is spatially and temporally white. The narrowband portion of the array autocorrelation matrix may be expressed as a sum of outer products or as a product of matrices:

$$\mathbf{R} = E[\mathbf{x} \mathbf{x}^T] = \sigma_n^2 \mathbf{I} + \sum_{m=1}^K A_m^2 \mathbf{u}_m^* \mathbf{u}_m^T = \sigma_n^2 \mathbf{I} + \mathbf{U}^* \mathbf{A}^2 \mathbf{U}^T \quad (1.6)$$

where \mathbf{U} is the matrix of phase-shift vectors and \mathbf{A} is a diagonal matrix of input amplitudes, $(\bullet)^*$ represents a complex conjugate and $(\bullet)^T$ a vector transpose, respectively. The expectation $E[\bullet]$ averages the AWGN, $\mathbf{n}(t)$ which is assumed to be $N(0, \sigma_n^2)$. The norm-squared of \mathbf{u}_m is:

$$\|\mathbf{u}_m\|^2 = \mathbf{u}_m^H \mathbf{u}_m = N \quad (1.7)$$

independent of signal DOA where $(\bullet)^H$ represents the hermitian transpose.

The MMSE weight vector minimizes the mean-squared error between the processor output and the reference signal. The weight vector is given by:

$$\mathbf{w}_o = \mathbf{R}^{-1} \mathbf{p} \quad (1.8)$$

where \mathbf{p} is the steering vector and is given by:

$$\mathbf{p} = E[r(t) \mathbf{s}_d^*] = A_d A_R \mathbf{u}_d^* \quad (1.9)$$

and \mathbf{s}_d and \mathbf{u}_d are the signal vector and phase-shift vector of the desired signal respectively. The quantity $r(t)$ is the time varying reference waveform with a peak amplitude of A_R . The MMSE weight vector maximizes the output signal-to-interference-and-noise-ratio²⁷ (SINR) which is defined as the quotient of the desired signal power and the sum of the interference and noise power $SINR = P_S/(P_I + P_N)$. The output signal-to-noise ratio (SNR) for the m th signal is the quotient of the output power of the m th signal and the output

noise power. It is given by:²⁷

$$SNR_{o_m} = \frac{P_{s,m}}{P_N} = SNR_{i_m} \frac{|\mathbf{w}_o^T \cdot \mathbf{u}_m|^2}{\|\mathbf{w}_o\|^2} \leq N \cdot SNR_{i_m} \quad (1.10)$$

The quantity $SNR_{i_m} = A_m^2/\sigma_n^2$ is the incident SNR for the m th signal, $P_{s,m}$ is the desired signal output power, P_I is the interference output power and P_N is the output noise power. For a single signal in AWGN, $\mathbf{w}_o = \mathbf{u}^*$, and the upper bound becomes an equality. The choice of $\mathbf{w}_o = \mathbf{u}_m^*$ represents the spatial equivalent of a matched filter (to the m th signal) and is referred to as a *conventional beamformer*²⁴, a *classical beamformer*²⁵, or a *maximal ratio combiner*.²⁶

The sum total of the number of beams and nulls an array is capable of directing simultaneously is $N-1$, one less than the number of array elements. This is also referred to as the *degrees-of-freedom*²⁷ of an array.

At this point, it may be important to explain the difference between the terms *adaptive array* and *diversity combiner*. The term *adaptive array* implies that the processor uses an array of sensors and exploits the phase and amplitude shifts between the array elements, induced by directional signals, to make processing decisions. A *diversity combiner*, on the other hand, exploits some degree of statistical independence between the input samples to ensure signal integrity at the summed output. For example, in the case of communication channels which contain multipath fading, an array of sensors might provide statistically independent spatial samples. If a signal is faded at one sensor, it might not be faded at another sensor; the statistical independence of the inputs is exploited by the processor to improve the integrity of the overall output response. There are many diversity combining strategies.²⁸ A popular strategy for analytical purposes, mentioned previously

as *maximal-ratio combining*, maximizes the output SNR but does not allow adaptive interference suppression. The diversity-combining counterpart to MMSE filtering is referred to as *optimum combining*. It is sometimes possible to achieve statistically independent samples through time sampling. Although not an issue in this research, a few examples of time diversity will be cited in the following section.

Previous Work

This section is a survey of previous work in adaptive beamforming antenna arrays and in CDMA that is pertinent to this research. The first part of the survey will give a historical perspective to research in adaptive antenna arrays. Details of the earlier work oriented towards radar and military communications is admittedly sparse. As the timeline and focus become more current the coverage will become more detailed. The second part of the survey will review the most recent work in which adaptive arrays function as an integral component of DS-CDMA systems. The last part of the survey will examine previous work in cellular CDMA (without antenna arrays) as it applies to this research.

A beam-steered array was investigated by Applebaum²⁹ but the results were not published in open literature until a decade later.³⁰ Widrow et al.³¹ reported on an antenna array using a least-mean-squares (LMS) processor in 1967. A special issue of the IEEE Transactions on Antennas and Propagation devoted to active and adaptive antennas was published in 1964,³² 1976³³ and 1986.³⁴ Other processors were investigated by Frost³⁵, Griffiths³⁶ and Schorr.³⁷ Much of the initial adaptive array work focused on the performance of particular processors or radar-oriented applications. One exception to this was the maximal ratio diversity combiner investigated by Brennan.²⁶

Subsequent work explored the role of adaptive arrays in communication systems.^{38, 39} In particular, Compton⁴⁰ presented a qualitative evaluation of an experimental adaptive array in a DS communication system. The evaluation focused on a single desired signal and a limited number of jammers. One of the conclusions reached by Compton is that the array makes appreciable contributions to interference suppression. Winters⁴¹ studied the acquisition performance of an LMS adaptive array in a DS system using four-phase modulation with two PN codes, a short code for rapid acquisition and a long code for protection against jammers. Ganz⁴² evaluated the bit-error-rate (BER) performance of a receiver employing an adaptive array and one of several detectors for binary-phase-shift-keying (BPSK), quadrature phase-shift keying (QPSK), or differential phase-shift keying (DPSK) modulation. The receiver was subjected to continuous-wave (CW) jamming.

Several authors have investigated the use of antenna arrays for mobile or personal communications. Bogachev and Kiselev⁴³ evaluated optimum-combining diversity arrays for the case of a single interferer. Winters²³ conducted a comparative study of optimum combining and maximal ratio combining base station arrays in a multiuser mobile environment with multipath fading but no shadow fading. The results quantify the possible improvement in SINR if optimum combining is selected over maximal ratio combining. Like optimum combining, maximal ratio combining preserves the integrity of the desired signal, but unlike optimum combining maximal ratio combining has no ability to adaptively suppress interference. Winters did propose the use of pseudonoise codes to generate the LMS reference, but transmit power control was mentioned only for its effect on the convergence properties of the LMS array. He did not investigate in any detail the condition when the number of users greatly exceeds the number of array elements. Winters

also explored the use of adaptive arrays on base stations for in-building systems using dynamic channel assignment.⁴⁴ He again considered a PN-coded PSK modulation and circumvented power control considerations by assuming interferers were of equal power and much stronger than the desired signal. A more recent study⁴⁵ investigated the acquisition and tracking performance of LMS and sample-matrix-inverse (SMI) beamformers in a time-division multiple-access system.

Yeh and Reudink⁴⁶ examined the contributions made by spatial diversity combiners to spectral efficiency in FDMA cellular systems when the arrays are located on the base station and on the mobiles. Glance and Greenstein⁴⁷ also examined the contributions of diversity order (the number of array elements) on average BER in a mobile FDMA system. Vaughan⁴⁸ discussed the benefit of MMSE combining at the mobile in an FDMA system and concluded with the comment that for MMSE combining to be successful wide bandwidth signals, such as those found in spread-spectrum systems, are necessary.

More recently, adaptive array research has examined commercially-oriented applications as CDMA and non-CDMA wireless systems gain popularity. At this time, antenna arrays are under investigation as a means of providing space-division channels in multiple-access systems. The technique, called space-division multiple access (SDMA) by some authors, utilizes the spatial filtering properties of the array to selectively receive signals which share the same time slot and the same frequency band. The SDMA technique might apply to either time-division multiple-access systems (TDMA) or CDMA systems. Swales et al.⁴⁹ established that a steerable, multi-beam antenna array can increase the capacity and spectral efficiency of a cellular system. Suard and Kailath⁵⁰ studied the upper bound of the information-based capacity of a wireless system which used a base-

station antenna array in the uplink path. Experimental studies have been conducted. Xu et al.⁵¹ and Lin et al.⁵² have examined algorithms based on direction-finding techniques MUSIC⁵³ and ESPRIT.⁵⁴ They have concluded that SDMA techniques based on DOA estimation will not be effective in multipath-rich environments. Xu and Li⁵⁵ developed an SDMA/TDMA protocol. Ward and Compton^{56,57} examined the contributions that a receiving array can make to the performance of an ALOHA system.

Arrays which include spatial and temporal adaptive processing nested within LMS feedback loops were proposed by Kohno et al.⁵⁸ and Ko et al.⁵⁹ Kohno used an LMS array in conjunction with adaptive temporal filtering which successively canceled DS signals due to multi-access interference. Ko described a null-steering beamformer nested within an LMS loop, not necessarily restricted to CDMA applications. Both considered limited multi-access scenarios with deterministic interference parameters.

Diversity combining is not necessarily restricted to space diversity. Balaban and Salz^{60,61} examined in detail the performance of a general multi-channel MMSE combiner working in conjunction with a decision-feedback equalizer. They established an upper bound on BER which is a function of the MMSE. A great deal of work has also been devoted to temporal diversity combiners which consist of a single input to a bank of matched filters, the outputs of which are coherently combined via maximal ratio combining. This is the basis for the RAKE⁶² receiver as well as variations studied by other authors. Several structures were examined by Turin⁶³ while Lehnert and Pursley⁶⁴ examined diversity combining in multiuser CDMA system in which successive bits are spread with different PN code subsequences. Wang et al. consider diversity for an indoor DS-CDMA system with Rician fading.⁶⁵

Some authors have studied the possible contributions made by arrays to the uplink path performance in cellular systems. Liberti and Rappaport have studied the effects of a directive, steered-beam base-station receiving array on uplink performance in a CDMA cellular system with perfect power control. The study focused on the effect of beam shape and beam width on the average BER. It was found that beam width has the greatest impact on performance and that adding a three-element array to the base station can improve BER performance by three orders of magnitude. Tsoulos, Beach and Swales have recently examined the role of adaptive antenna technology in large “umbrella” cells overlaying smaller microcells in cellular CDMA systems⁶⁶; they also examined the outage-based capacity enhancement due to an adaptive antenna array using a recursive least-squares (RLS) processor in a multi-cell CDMA environment.⁶⁷ The latter study was confined to simulations of the total interference to calculate outage. The authors concluded that an antenna with 6 dB of directivity gain can increase capacity by a factor of five.

Winters, Salz and Gitlin⁶⁸ studied the effects of optimum combining spatial diversity arrays on the capacity of a TDMA system in which the total number of incident signals was less than or equal to the array DOF. They applied previous work^{60,61} which resulted in an upper bound on BER. The assumption of high input SNR allowed a zero-forcing approximation to the optimum combining solution. Using these assumptions, and examining analytical expressions for BER, they found that optimum combining with N antennas and K interferers gives the same results as a maximal ratio combiner with $N-K+1$ elements and no interferers. Their theoretical results, as they point out, no longer apply when the number of interferers exceeds the number of antenna elements.

A structure which combines the spatial filtering of an antenna array and the temporal, diversity-combining properties of a RAKE receiver have been proposed and investigated by Khalaj in concert with several other authors.^{69,70,71} The structure is intended for use in channels with frequency-selective multipath fading. The structure allows the resolution of identifiable multipath rays by the time-filtering properties of the RAKE combiner and by the spatial filtering properties of the antenna array.

A number of authors have conducted brief simulation-based studies of adaptive arrays for DS-CDMA systems. Yoshino et al.⁷² examine the simulation performance of two RLS-based spatial diversity combiners operating in concert with (Viterbi) sequence estimators. One processor subtracts estimates of the cochannel interference from the output prior to estimation of the desired user's data sequence while the other processor does not. Wang and Cruz⁷³ examine the pattern behavior and BER of a six-element arrays based on the RLS and ESPRIT algorithms with six active users with well-separated DOAs. Liu⁷⁴ examined the performance of an LMS array with a scenario-dependent matrix preprocessor which aids in interference cancellation. Hanna et al.⁷⁵ investigated the BER performance of a two-element LMS array which operates in conjunction with an adaptive equalizer.

Perhaps the most in-depth study of the possible contributions of MMSE adaptive beamforming arrays to the performance of mobile cellular CDMA systems using closed-loop power control has been made by Naguib in concert with other authors. Initial work⁷⁶ focused on steady-state performance of an array of sensors, each followed by a DS conventional detector, which functions as a post-detection combiner (termed *code-filtering* by the authors). Analysis resulted in a simple expression for capacity. The signal

model was for unfaded signals originating in an isolated single cell. Power control error was modeled by assigning a single interferer an incident signal level 10 dB higher than the other signals.

Naguib, Paulraj and Kailath⁷⁷ extended the steady-state model in order to determine the outage probability in a cellular system with BPSK modulation, perfect power control, shadow fading, multipath fading, and cochannel interference equivalent to two tiers of surrounding cells. Assuming that the array pattern response consisted of a main lobe and no sidelobes resulted in a simple, closed-form expression for an upper bound on outage probability which simplified to the single-channel results of Gilhousen et al.¹¹ when the array is reduced to a single element. Modeling the MMSE processor as a maximal ratio processor and assuming the interference was Gaussian resulted in a simpler expression for the outage probability upper bound.⁷⁸ Naguib and Paulraj then modified the simulation model to include DPSK-modulated signals and determined the Erlang capacity.⁷⁹ The uplink performance with M-ary orthogonal modulation was examined as well.⁸⁰

A recursive beamforming algorithm was proposed by Naguib and Paulraj⁸¹ and simulated results were presented. The algorithm performed recursive updates on the matrix square root of the inverse of the covariance matrix. The authors claimed that the accumulation of numerical and quantization errors may cause the covariance matrix inverse to cease being hermitian definite and that updating the matrix square root will allow the covariance matrix inverse to remain hermitian definite even when the matrix square root is not. Thus, say the authors, numerical instabilities are avoided.

Naguib and Paulraj⁸² continued their investigation of cellular base station antenna arrays by examining the tradeoffs in coverage area, mobile transmit power, and capacity

that are available when an array is used and the users are subjected to perfect power control. Using simplifying assumptions the authors derived expressions which generalized the effect of the antenna array on performance. This research will attempt to extend some of the results to the case of imperfect power control.

Later investigations have resulted in detailed, simulation-based studies of an IS-95 system which uses orthogonal signaling, forward error-correction coding, closed-loop power control and a base-station antenna array. Unlike their previous studies Naguib and Paulraj applied a model for imperfect closed-loop power control. They studied the standard deviation of power control error, although where the error is defined is not clear in the paper. Using simulation results they show that power control error dependence on the power control step size, the number of array elements, and the maximum doppler frequency and the spread in DOA of the multipath rays.⁸³ The dependence of BER on the same parameters was the topic of a subsequent paper.⁸⁴

A multiuser LMS array for use in GPS receivers was examined by Beach et al.⁸⁵ in a simulation study. The results were confined to plots which show the evolution of the adaptive array pattern over time in the presence of CW jammers; no steady-state results were presented. The near/far effect was not an issue in the study.

A variety of authors have investigated the performance of cellular CDMA systems with imperfect power control and no antenna array. Simpsom and Holtzman⁸⁶ used simplified analytical models in order to provide insight into the interactions between power control, coding and interleaving. Stuber and Kchao⁸⁷ examined a multiple-cell CDMA system and evaluated the dependence of BER as a function of the distance from the base station. Jalali and Mermelstein⁸⁸ conducted a simulation study of a microcellular CDMA

system which included imperfect closed-loop power control and antenna diversity with square-law combining. Milstein et al.⁸⁹ studied the average BER performance of a multiple-cell system in which users were subjected to power control error which was described by a uniform random variable. Newson and Heath⁹⁰ examined a CDMA system which suffered from imperfect sectoring and lognormally-distributed power control error and made capacity comparisons to TDMA and FDMA systems.

Dissertation Outline

The remainder of the dissertation will be divided into six chapters. Chapter 2 will examine some aspects of the steady-state performance of a multiuser MMSE array; some limited aspects of an adaptive LMS version were investigated by Beach et al.⁸⁵ The near/far performance will first be investigated for strong, spatially orthogonal users and will then be extended to the case of two users with any DOA spacing. The analysis will focus on the ability of the array to confine the signal outputs to the same output SNR. The results will show that the array may be suitable when signals are well-separated in DOA and do not outnumber the array DOFs. The analysis will borrow some of the analytical techniques used by Gupta⁹¹ and apply them to evaluate the steady-state performance of the multi-user MMSE array. Unlike either previous study, however, the analysis will focus on the performance of the array in a near/far environment.

The third chapter will examine the adaptive performance of the multiuser MMSE array when it is implemented as an LMS processor. Analysis will show that the rule-of-thumb for picking step size to ensure stability also serves as a limit to reduce the spread in output signal levels due to LMS misadjustment.

The fourth chapter will examine the steady-state performance of an MMSE array feeding a conventional detector. Unlike the array of the first two chapters, this array will be dedicated to a single user among many multiple-access users. The single-cell users will not be subjected to many of the influences normally found in a mobile environment, such as multipath fading, shadow fading or interference which originates from surrounding cells. This will simplify the analysis: the intent is not to provide an analysis fraught with mathematical rigor, but to use simplifying assumptions to aid in the derivation of closed-form analytical expressions which accurately predict the uplink performance and which clearly show the dependence of uplink capacity on the system parameters, especially the array and the degree of power control error. The performance measures will be outage probability and outage-based capacity.

The analysis of chapter four will result in a simple closed-form expression for the capacity which is linear in the product of processing gain and the number of array elements and which decays exponentially with increasing power control error. The slope of the capacity line (the *per-element capacity*) will serve as a robust measure of the array's incremental contribution to capacity. Although some of the assumptions are highly idealized (i.e. no multipath fading), they will allow some well-understood quantities, such as array gain, to be exploited in the analysis. Some of the work in this chapter is related to that of Padovani⁷ and also to Naguib and Paulraj.⁸² The details will be discussed during the chapter's derivations and discussions.

Chapter 5 will extend the steady-state multi-access model of Chapter 4 to include the effects of multipath fading, shadow fading and outer-cell interference. The performance measures will again be the steady-state outage probability and outage-based capacity.

The sixth chapter will examine the recursive-least-squares (RLS) adaptive performance of the MMSE adaptive array in a mobile cellular scenario in a nonstationary channel. The discrete-event simulation model includes time-varying multipath fading, stationary shadow fading and time-varying outer-cell interference.

The last chapter will give a brief summary and some conclusions of this research. It will also identify some areas of future work.

This research makes contributions in two areas. First, analysis and numerical solutions provide more insight into the steady-state and the adaptive behavior of the multi-user MMSE array (chapters 2,3) than was provided by previous authors. Analysis shows that the array can remove the near-far effect and level the output SNRs to nearly the same level, under certain circumstances. Second, the analysis and simulation of a single-user array operating in conjunction with a conventional detector results in simple expressions for capacity when the signal sources are subjected to imperfect power control (chapters 4,5,6). The results characterize the incremental contributions an adaptive array can make to uplink performance. This is in contrast to previous works which examine the effects of closed-loop power control error only in simulation for limited scenarios.

CHAPTER 2

A MULTIUSER ANTENNA ARRAY PROCESSOR STEADY-STATE PERFORMANCE

This chapter examines the ideal, steady-state performance of the multiuser MMSE array proposed by Beach et al.⁸⁵ The authors conducted a simulation study of the pattern behavior of a multiuser LMS adaptive array with and without directional interference. They did not provide any analytical results which give general insight into the array's steady-state performance. In related work, Gupta⁹¹ examined a multi-user steered-beam array for non-CDMA applications and simplified his analysis by assuming the special case of spatially orthogonal users. Gupta was interested in using the array's effective aperture to improve the output SNR of the desired signals and in using the adaptive properties to reject interference. Other authors have shown that steered-beam arrays and LMS arrays give the same output SNR performance as long as the steering vectors differ by a constant.⁹² Using this rationale it might seem that Gupta's work could provide some insight to this problem. However, he was trying to configure the array processor to avoid the power leveling effect that this work is attempting to exploit.

This chapter will focus on the array output SNR performance for strong incident signals. The analysis will deemphasize the role of the spread-spectrum signalling other than to note that it provides a relatively easy way to provide separation and detection of the multiple, desired signals present at the single array output. The remainder of this chapter will be divided into several sections. The first section will provide some qualitative information about the multiuser MMSE array processor and give some refinements to the

general array equations given in the introduction. The second section will develop analytical expressions of the output SNR for $K \leq N-1$ spatially orthogonal users. The third section will present analytical expressions for two users which have arbitrary DOAs and are therefore not necessarily spatially orthogonal. The last section will compare the analytical and the numerical results and discuss their implications.

The Multiuser MMSE Processor

The multiuser array treats each of the K signals as a component of a single composite desired signal. This is accomplished via a reference signal which is a sum of the modulated PN sequences of the desired incident signals. A block diagram is shown below in Figure 2.1. In the figure all functions of time are ignored. For analytical simplicity we will assume that perfect estimates of the modulation and code waveforms are available for the generation of the reference waveform. This will not usually be the case. Generation of the reference signal can be a challenging issue and it has been investigated by other authors.^{27,40,41}

The array will force the outputs of the individual signals to the levels of that signal's component of the reference waveform. To avoid the near/far effect the individual components comprising the reference waveform have the same peak amplitudes. Since all of the incident signals share the same beamformer weights, the output SNRs will be leveled to approximately the same value. The analysis will show that the array will force the output SNRs to values very close to the maximum output SNR of the weakest user under certain conditions.

The steering vector defined by equation (1.9) represents the crosscorrelation between the reference signal and the multiple, independent input signals. It becomes a sum of single-user steering vectors:

$$\mathbf{p} = \sum_{m=1}^K \mathbf{p}_m = R \sum_{m=1}^K A_m \mathbf{u}_m^* \quad (2.1)$$

where A_m and \mathbf{u}_m are the incident amplitude and phase-shift vector of the m th signal, respectively.

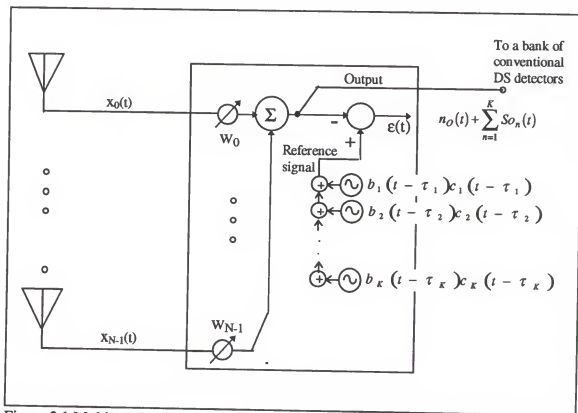


Figure 2.1 Multiuser MMSE processor

Spatially Orthogonal Users

Consider the limiting case of multiple users which are spatially orthogonal to one another ($\mathbf{u}_i^H \mathbf{u}_k = 0 \quad \forall i \neq k$). The minimum source separation (in DOA) which allows spatial orthogonality corresponds to the *Rayleigh limit*.²² The Rayleigh limit is generally

considered to be the minimum amount of source separation which still allows resolution of two sources by a beamformer.²⁴ If the users are orthogonal and the array elements are isotropic the inverse of the autocorrelation matrix is:⁹¹

$$\mathbf{R}^{-1} = \frac{1}{\sigma_n^2} \cdot \left(\mathbf{I} - \sum_{m=1}^K \frac{N \cdot SNR i_m}{1 + N \cdot SNR i_m} \mathbf{u}_m^* \cdot \mathbf{u}_m^T \right) \quad (2.2)$$

and the resulting MMSE weight vector, $\mathbf{w}_o = \mathbf{R}^{-1} \mathbf{p}$, is given by:

$$\mathbf{w}_o = \frac{R}{\sigma_n^2} \cdot \sum_{m=1}^K \frac{A_m}{1 + N \cdot SNR i_m} \cdot \mathbf{u}_m^* \quad (2.3)$$

Substituting these quantities into the general expression for the n'th users output SNR (equation (1.10)) gives:

$$SNR o_n = \left(\frac{N \cdot SNR i_n}{1 + N \cdot SNR i_n} \right)^2 \cdot \left(\sum_{m=1}^K \frac{N \cdot SNR i_m}{(1 + N \cdot SNR i_m)^2} \right)^{-1} \quad (2.4)$$

Some coarse judgements on performance for multiple users can be made using equation (2.4). If $\{SNR i_m \gg 1 \ \forall m = 1 \dots K\}$ the output SNRs for all of the users are approximately equal to:

$$SNR o \approx N \cdot \left(\sum_{m=1}^K \frac{1}{SNR i_m} \right)^{-1} \quad (2.5)$$

If there are K users with the same input SNR = $SNR i$ then equation (2.5) simplifies to:

$$SNR o = \frac{N \cdot SNR i}{K} \quad (2.6)$$

which shows that the users will all have output SNRs equal to the maximum possible SNR divided by the number of active users. If the array parameters remain constant, the performance will degrade as the number of users increases.

If there are S users with the same input $SNR_i = k_1 \cdot SNR$ and $K-S$ users with $SNR_i = SNR$ then the output SNR for the K users simplifies to:

$$SNR_o = N \cdot SNR \frac{k_1}{S + k_1 \cdot (K - S)} \quad (2.7)$$

If $k_1(K - S) \gg S$ (a possible near/far scenario) the expression for output SNR simplifies further:

$$SNR_o \approx \begin{cases} \frac{N \cdot SNR}{K - S} & K \neq S \\ \frac{k_1 \cdot N \cdot SNR}{K} & K \equiv S \end{cases} \quad (2.8)$$

where:

S = no. of strong users with input $SNR_i = k_1 \cdot SNR$, $k_1 \gg S$

K = total number of users

$K - S$ = no. of weaker users with input $SNR_i = SNR$

From the equation immediately above it is apparent that one weak user ($K - S = 1$) will dominate the overall performance of the array. This might make intuitive sense, even for the general case. A minimum MSE processor will try to force each output signal to have the same value as that signal's component of the reference waveform. This strategy will favor weaker incident signals which need large weight values to cause their array output to match their component of the reference waveform (i.e. minimum error power). Large incident signals will be attenuated via phase shifts and the noise power - the denominator of equation (2.4) - will be large thus causing a lower than maximum output SNR even for strong input signals.

Equation (2.8) above establishes that the weakest incident signal drastically affects the overall performance of the array. The worst array response towards an arbitrary signal (SNR_{o_n}) for a different input signal (SNR_{i_m}) can be found by finding the value of SNR_{i_m}

which forces $dSNRo_n/dSNRi_m$, the derivative of the n th signal's output SNR with respect to the m th signal's input SNR, to zero:

$$\frac{dSNRo_n}{dSNRi_m} = -\left(\frac{N \cdot SNRi_n}{1 + N \cdot SNRi_n}\right) \cdot \left(\frac{1 - N \cdot SNRi_m}{1 + N \cdot SNRi_m}\right) \cdot \left(\sum_{k=1}^D \frac{N \cdot SNRi_k}{(1 + N \cdot SNRi_k)^2}\right)^{-2} = 0 \quad (2.9)$$

From the equation above it is evident that a minimum occurs for $SNRi_m = 1/N$.

Substituting $SNRi_m = 1/N$ into equation (2.4) gives (for $SNRi_n \gg 1$, $n \neq m$):

$$\begin{aligned} SNRo_n &\approx 4 \cdot \left(\frac{N \cdot SNRi_n}{1 + N \cdot SNRi_n}\right)^2 \\ SNRo_m &\approx 1 \end{aligned} \quad (2.10)$$

For $SNRi_m = 1/N$ the value of the m th eigenvalue of \mathbf{R} is twice that of the noise-only eigenvalues. At this input level the array is barely able to resolve the m 'th input signal from the input noise.

It might be useful to define an output SNR "spread" which bounds the output SNRs for all of the users. From equation (2.4) it can be seen that the largest and smallest input signals result in the largest and smallest output SNRs respectively. We can predict the output spread by the difference between the largest and smallest output SNRs:

$$\begin{aligned} \Delta SNRo &= SNRo_{\max} - SNRo_{\min} \\ &= \left[\left(\frac{N \cdot SNRi_{\max}}{1 + N \cdot SNRi_{\max}}\right)^2 - \left(\frac{N \cdot SNRi_{\min}}{1 + N \cdot SNRi_{\min}}\right)^2 \right] \cdot \left(\sum_{m=1}^D \frac{N \cdot SNRi_m}{(1 + N \cdot SNRi_m)^2}\right)^{-1} \end{aligned} \quad (2.11)$$

If we let $SNRi_{\max}$ pass to infinity the output spread becomes:

$$\lim_{SNRi_{\max} \rightarrow \infty} \Delta SNRo = \left[1 - \left(\frac{N \cdot SNRi_{\min}}{1 + N \cdot SNRi_{\min}} \right)^2 \right] \cdot \left(\sum_{j \neq \max}^D \frac{N \cdot SNRi_j}{(1 + N \cdot SNRi_j)^2} \right)^{-1} \quad (2.12)$$

The equation above simplifies to:

$$\Delta SNRo = \frac{2 + 1/N \cdot SNRi_{\min}}{1 + \frac{(1 + N \cdot SNRi_{\min})^2}{N \cdot SNRi_{\min}} \cdot \sum_{j \neq \max, \min}^D \frac{N \cdot SNRi_j}{(1 + N \cdot SNRi_j)^2}} \quad (2.13)$$

An upper bound on the output SNR spread results:

$$\Delta SNRo \leq 2 + \frac{1}{N \cdot SNRi_{\min}} \quad (2.14)$$

In summary it would appear that for $N \cdot SNRi_m \gg 1$, $m=1 \dots D$, the user outputs will be near the value of the maximum output SNR for the weakest user and the output SNR spread will be equivalent to 2.

Nonorthogonal Users

Analyzing the general case of multiple narrowband users which are not spatially orthogonal is difficult because of the matrix inverse in equation (1.8). When the users are not orthogonal the analytical matrix inverse (via the matrix inversion lemma) quickly becomes intractable as the number of users increases beyond unity. The general case of only two users was examined in detail. The approach taken here is to derive expressions for the two output SNRs. The expressions are then interpreted as transfer functions with poles and zeros which are dependent upon the input levels and the DOAs. Critical points of the functions are then evaluated.

The autocorrelation matrix \mathbf{R} for two independent, narrowband users in AWGN (equation (1.6)), is given by:

$$\begin{aligned}\mathbf{R} &= \sigma_n^2 \cdot \mathbf{I} + A_1^2 \mathbf{u}_1^* \mathbf{u}_1^T + A_2^2 \mathbf{u}_2^* \mathbf{u}_2^T \\ &= \sigma_n^2 [\mathbf{I} + SNR_{i_1} \mathbf{u}_1^* \mathbf{u}_1^T + SNR_{i_2} \mathbf{u}_2^* \mathbf{u}_2^T]\end{aligned}\quad (2.15)$$

The inverse of \mathbf{R} (\mathbf{R}^{-1}) may be calculated via the matrix inversion lemma:

$$\begin{aligned}\mathbf{R}^{-1} &= \frac{1}{\sigma_n^2} \mathbf{I} - \frac{1}{\sigma_n^2} \frac{SNR_{i_1}}{1 + SNR_{i_1}} \mathbf{u}_1^* \mathbf{u}_1^T \\ &\quad - \frac{SNR_{i_2}}{\sigma_n^2} \frac{\left(\mathbf{u}_2 - \frac{\mathbf{u}_1^T \mathbf{u}_2 SNR_{i_1}}{1 + SNR_{i_1}} \mathbf{u}_1 \right)^* \left(\mathbf{u}_2 - \frac{\mathbf{u}_2^T \mathbf{u}_1^* SNR_{i_1}}{1 + SNR_{i_1}} \mathbf{u}_1 \right)^T}{1 + SNR_{i_2} - \frac{|\mathbf{u}_1^T \mathbf{u}_2|^2 SNR_{i_1} \cdot SNR_{i_2}}{1 + SNR_{i_1}}}\end{aligned}\quad (2.16)$$

The steering vector \mathbf{p} which results from equation (2.1) is:

$$\mathbf{p} = RA_1 \mathbf{u}_1^* + RA_2 \mathbf{u}_2^* = \sigma_n R \sqrt{SNR_{i_1}} \mathbf{u}_1^* + \sigma_n R \sqrt{SNR_{i_2}} \mathbf{u}_2^* \quad (2.17)$$

Substituting equations (2.16) and (2.17) into equation (1.8), $\mathbf{w}_o = \mathbf{R}^{-1} \mathbf{p}$, gives the MMSE weight vector:

$$\begin{aligned}\mathbf{w}_o = \mathbf{R}^{-1} \mathbf{p} &= \frac{R}{\sigma_n D_o} \left[\sqrt{SNR_{i_1}} (1 + SNR_{i_2}) - \mathbf{u}_1^T \mathbf{u}_2^* SNR_{i_1} \sqrt{SNR_{i_2}} \right] \mathbf{u}_1^* + \\ &\quad \frac{R}{\sigma_n D_o} \left[\sqrt{SNR_{i_2}} (1 + SNR_{i_1}) - \mathbf{u}_2^T \mathbf{u}_1^* SNR_{i_2} \sqrt{SNR_{i_1}} \right] \mathbf{u}_2^*\end{aligned}\quad (2.18)$$

The quantity D_o is defined by:

$$D_o = 1 + N(SNR_{i_1} + SNR_{i_2}) + \left(N - |\mathbf{u}_1^T \mathbf{u}_2^*|^2 \right) SNR_{i_1} SNR_{i_2} \quad (2.19)$$

Two vector inner products are required to find the output SNR defined in equation (1.10). If we assume the point of reference for the array is the same as the physical center of the array, the inner products will be real.²⁴ An inner product between two phase-shift

vectors may then be expressed in dot-product form: $\mathbf{u}_1^T \mathbf{u}_2^* = N \cos \alpha_{12}$ where α_{12} is the angle between the two vectors in signal space. Substituting this relationship into equation (2.18):

$$\begin{aligned} \|\mathbf{w}_o\|^2 &= \frac{R^2}{\sigma_n^2 D_o^2} N(SN Ri_1 + SN Ri_2) + 2N \sqrt{SN Ri_1 SN Ri_2} \cos \alpha_{12} + \\ &\quad \frac{R^2}{\sigma_n^2 D_o^2} N^2 SN Ri_1 SN Ri_2 \sin^2 \alpha_{12} (4 + NSN Ri_1 + NSN Ri_2 - 2N \sqrt{SN Ri_1 SN Ri_2} \cos \alpha_{12}) \end{aligned}$$

$$\text{where: } D_o = 1 + NSN Ri_1 + NSN Ri_2 + N^2 SN Ri_1 SN Ri_2 \sin^2 \alpha_{12} \quad (2.20)$$

Expressions for the numerator of equation (1.10), the output SNR, are possible for the two users:

$$|\mathbf{u}_{1,2}^T \mathbf{w}_o|^2 = \frac{R^2}{\sigma_n^2 D_o^2} \left[N \sqrt{SN Ri_{1,2}} (1 + NSN Ri_{2,1} \sin^2 \alpha_{12}) + N \sqrt{SN Ri_{2,1}} \cos \alpha_{12} \right]^2 \quad (2.21)$$

Substituting equations (2.20) and (2.21) into equation (1.10) will result in the steady-state output SNR for the two users at the point of minimum mean-squared error.

An additional substitution might simplify the expressions further. If we substitute the expression $SN Ri_j = a^2 SN Ri_2$ into equations (2.20) and (2.21) the output SNR can be expressed as a quotient of polynomials in a with coefficients that are functions of $NSN Ri_2$ and α_{12} . The numerators of the quotients are:

$$\begin{aligned} num_1 &= N^2 SN Ri_2 (1 + NSN Ri_2 \sin^2 \alpha_{12})^2 \left[a + \frac{\cos \alpha_{12}}{1 + NSN Ri_2 \sin^2 \alpha_{12}} \right]^2 \\ num_2 &= N^4 SN Ri_2^3 \sin^4 \alpha_{12} \left[a^2 + a \frac{\cos \alpha_{12}}{NSN Ri_2 \sin^2 \alpha_{12}} + \frac{1}{NSN Ri_2 \sin^2 \alpha_{12}} \right]^2 \end{aligned} \quad (2.22)$$

for user 1 and user 2 respectively. The denominator of both biquadratic terms is:

$$Den_{SNR} = a^2 N^2 SNR i_2^2 \sin^2 \alpha_{12} \left[4 + NSNR i_2 (a^2 - 2a \cos \alpha_{12} + 1) \right] + NSNR i_2 (a^2 + 2a \cos \alpha_{12} + 1) \quad (2.23)$$

and the expressions for the two output SNRs become:

$$SNR_{O_1} = a^2 SNR i_2 \frac{num_1}{Den_{SNR}} \quad SNR_{O_2} = SNR i_2 \frac{num_2}{Den_{SNR}} \quad (2.24)$$

The expressions for output SNRs may be interpreted as transfer functions in the variable a . The numerators may be treated as products of second order polynomials with easily determined roots which may be interpreted as real zeros of the output SNR "transfer function." The roots of the numerators are:

$$z_{num1} = 0, \quad -\frac{\cos \alpha_{12}}{1 + NSNR i_2 \sin^2 \alpha_{12}} \quad (2.25)$$

$$z_{num2} = \frac{\cos \alpha_{12}}{2NSNR i_2 \sin^2 \alpha_{12}} \left[1 \pm \sqrt{1 - 4NSNR i_2 \tan^2 \alpha_{12}} \right]$$

The denominator is a fourth-order polynomial in a and analytical expressions for its roots are not particularly useful in the general case. To circumvent this difficulty the analytical expressions for output SNR will be examined and approximated for specific cases of a^2 (the near-far ratio) and α_{12} (the angle between the phase-shift vectors in weight-space) and results will be compared to numerical solutions. Note that α_{12} is determined exclusively by the users' DOAs for a given antenna array configuration. The output SNR expressions will be examined for four *scenarios* of the variable a :

- | | |
|-----------------------|-------------------------------|
| 1. $a^2 = 0$ | (single user system) |
| 2. $0 < a^2 \ll 1$ | (1 weak, 1 strong user) |
| 3. $a^2 = 1$ | (2 strong, equal power users) |
| 4. $1 < a^2 < \infty$ | (2 strong, unequal powers) |

Two cases of DOA separation will be examined for each of the four scenarios listed immediately above. One case (referred to as *case a*) will be that of spatially orthogonal users ($\cos^2\alpha_{12} = 0$, $\sin^2\alpha_{12} = 1$). This will allow comparisons with the results in the previous section. The second case (*case b*) will be for DOAs with spacings greater than the Rayleigh limit ($0 < \cos^2\alpha_{12} \ll \sin^2\alpha_{12} < 1$) and will also be referred to as *well-separated*.

The following analysis will consider approximations to equations (2.22)-(2.25) for some combinations of the intervals of a listed above. Rather than being exhaustive the analysis will focus on critical points which will reveal trends in performance.

Single-User System

When $a = 0$ we have a single user system and :

$$SNR_{O_1} = a^2 SNR_{i_2} \frac{num_1}{Den_{SNR}} = 0 \quad (2.26)$$

$$SNR_{O_2} = SNR_{i_2} \frac{num_2}{Den_{SNR}} = NSNR_{i_2}$$

One Weak User, One Strong User

For the case of one weak user and a moderately strong user which are well separated (case b) the numerators and denominator of equation (2.24) can be approximated by:

$$num_1 \approx N^2 SNR_{i_2} (1 + NSNR_{i_2} \sin^2 \alpha_{12})^2 \left[a + \frac{\cos \alpha_{12}}{1 + NSNR_{i_2} \sin^2 \alpha_{12}} \right]^2 \quad (2.27)$$

$$num_2 \approx N^4 SNR_{i_2}^3 \sin^4 \alpha_{12} \left[a^2 + \frac{1}{NSNR_{i_2} \sin^2 \alpha_{12}} \right]^2$$

$$Den_{SNR} \approx N^2 SNRi_2^2 (4 + NSNRi_2) \sin^2 \alpha_{12} \left[a^2 + \frac{1}{NSNRi_2 (4 + NSNRi_2) \sin^2 \alpha_{12}} \right]$$

If we can further assume that $NSNRi_2 \gg 4$ then the output SNRs may be approximated

$$\begin{aligned} \text{by:} \quad SNRo_1 &= a^2 N \cdot SNRi_2 \sin^2 \alpha_{12} \frac{[a + (\cos \alpha_{12}) z_{2b}]^2}{[a^2 + p_{2b}]} \\ SNRo_2 &= N \cdot SNRi_2 \sin^2 \alpha_{12} \frac{[a^2 + z_{2b}]^2}{[a^2 + p_{2b}]} \end{aligned} \quad (2.28)$$

$$\text{where: } z_{2b} = \frac{1}{N \cdot SNRi_2 \sin^2 \alpha_{12}} \quad , \quad p_{2b} = \frac{1}{N^2 \cdot SNRi_2^2 \sin^2 \alpha_{12}} = \frac{z_{2b}}{N \cdot SNRi_2}$$

Where the notation z_{2b} represents the numerator zero for *scenario 2* and DOA case b.

Note that $p_{2b} < z_{2b}$. Also note that for *scenario 2*, $SNRo_1$ is small since it is multiplied by a second order zero at $a = 0$. As a increases, $SNRo_1$ increases with some possible wrinkles in the magnitude curve added by the numerator zeros ($a = z_{2b} \cos \alpha_{12}$) and denominator poles ($a = \sqrt{p_{2b}}$). Note that since the $\cos \alpha_{12}$ term in the numerator of equation (2.28) can be less than zero the possibility exists that $SNRo_1$ could equal zero for nonzero a . The most interesting behavior is displayed by $SNRo_2$. For very small a , $SNRo_2$ is near the maximum value $SNRo_2 = NSNRi_2$. As a increases away from zero, the $SNRo_2$ function rolls off at the -3 dB point of $a^2 = p_{2b}$ and continues to decrease until $a^2 = z_{2b}$ ($SNRi_1 = [N \sin^2 \alpha_{12}]^{-1}$). At $a^2 = z_{2b}$ the $SNRo_2$ roll-off attenuation is halted and $SNRo_2$ begins increasing since the pole at p_{2b} is canceled by the zero at $a^2 = z_{2b}$. Over the range of a specified by this scenario, the point $a^2 = z_{2b}$ represents a minimum of $SNRo_2$. Substituting $a^2 = z_{2b}$ into equation (2.28) gives $SNRo_1 = 1$ and $SNRo_2 = 4NSNRi_2 / (NSNRi_2 + 5) \approx 4$.

Note that similar expressions for the case of orthogonal users (case a above) can be readily found by simply setting $\sin^2\alpha_{12} = 1$ and $\cos^2\alpha_{12} = 0$ into equation (2.28).

In summary, for most of *scenario 2* the array is unable to resolve the low-power user 1 input signal from the input noise. The array can just begin to resolve the user 1 input signal from the input noise when $a^2 = z_{2b}$ ($SNR_{i1} = [N\sin^2\alpha_{12}]^{-1}$). At this point, $SNR_{o1} \approx 1$ and $SNR_{o2} \approx 4$ which represents a minimum value of SNR_{o2} over this scenario.

Two Equal-Power Users

If the two users have equal input power levels the output SNRs are equal:

$$SNR_o = \frac{NSNR_i}{2} \frac{(1 + \cos\alpha_{12} + NSNR_i \sin^2\alpha_{12})^2}{1 + \cos\alpha_{12} + NSNR_i \sin^2\alpha_{12} (2 + NSNR_i (1 - \cos\alpha_{12}))} \quad (2.30)$$

and for the *case* of well-separated users (case b: $0 < \cos^2\alpha_{12} << \sin^2\alpha_{12} < 1$) the output SNRs may be approximated as:

$$\begin{aligned} SNR_o &\approx \frac{NSNR_i}{2} \frac{(NSNR_i \sin^2\alpha_{12})^2}{NSNR_i \sin^2\alpha_{12} (NSNR_i (1 - \cos\alpha_{12}))} \\ &= \frac{NSNR_i}{2} (1 + \cos\alpha_{12}) \end{aligned} \quad (2.31)$$

If the users are spatially orthogonal (*case a*) then $\sin^2\alpha_{12} = 1$ and $\cos^2\alpha_{12} = 0$ and the output SNRs are exactly equal to $SNR_o = NSNR_i/2$, which is consistent with equation (2.6).

Two Strong Users

For this *scenario* (#4) we have two strong users with unequal input power levels.

For *case b* ($0 < \cos^2\alpha_{12} << \sin^2\alpha_{12} < 1$) the numerator terms of equation (2.26) may be modified by multiplying all SNR_{i2} terms by an additional $\sin^2\alpha_{12}$ term. The

denominator (equation (2.23)) changes slightly:

$$D_{4,b} = a^4 + a^2 \left[\frac{1}{N^2 SNR i_2^2 \sin^2 \alpha_{12}} + \frac{4}{NSNR i_2} + 1 \right] + \frac{1}{N^2 SNR i_2^2 \sin^2 \alpha_{12}} \quad (2.32)$$

Terms containing higher powers of a dominate the numerators (equation (2.22)) and denominator (equation (2.32)) of the output SNR expression (2.24). This condition represents the presence of two strong users of unequal power: $SNRo_1 \gg SNRo_2$. The expressions for the (*scenario 4, case b*) output SNRs may be approximated as:

$$\begin{aligned} SNRo_1 &\approx \frac{(1 + NSNR i_2 \sin^2 \alpha_{12})^2}{NSNR i_2 \sin^2 \alpha_{12}} \\ SNRo_2 &\approx NSNR i_2 \sin^2 \alpha_{12} \end{aligned} \quad (2.33)$$

Note that for large input SNR the expressions in equation (2.33) should be nearly equal.

The difference between the output SNRs for this scenario is:

$$\Delta SNRo = SNRo_1 - SNRo_2 \approx 2 + \frac{1}{NSNR i_2 \sin^2 \alpha_{12}} = 2 + \frac{1}{SNRo_2} \quad (2.34)$$

Which is very similar to the expression for output spread for orthogonal users given by equation (2.14).

Numerical Results

This section will first present numerical solutions to corroborate the two-user analysis of the previous section. The data will be presented in plots of the output SNRs (equation (2.26)) versus the input near-far ratio (a^2). Array performance will be evaluated for spatially orthogonal users and well separated users evaluated over a wide range of a^2 .

Specific comparisons between analytical and numerical solutions will be made for critical points identified in the analysis.

Performance for a linear MMSE array was investigated by plotting the output SNRs of two signals while varying one signal input level and holding the other at a fixed value of input SNR. For each point the MMSE weights and corresponding output SNRs were calculated using equations (1.6)-(1.10) and equation (2.1). The DOAs were fixed to specified values. The plot below shows the output SNRs for the case of a three element array with two users. User 1 is positioned broadside to the array (DOA = 0 degrees) with varying input SNR, and user 2 is positioned at 41.8 degrees from broadside with an input SNR of 10. This DOA condition gives the least amount of source separation which allows the sources to be spatially orthogonal.

Figure 2.2 shows the ($N = 3$) array output SNRs versus a^2 for a two-signal scenario over the range $10^{-5} \leq a^2 \leq 10^5$. The users are spatially orthogonal, $\alpha_{12} = 90$ degrees and the user 2 input SNR is 10. For $a^2 = 10^{-5}$ the array is in essence a single user system, $SNR_{O2} = NSNR_{i2} = 30$ which is the maximum possible output SNR for user 2 and $SNR_{O1} \approx 0$. As a (SNR_{i1}) increases, SNR_{O2} begins its roll-off attenuation: SNR_{O2} rolls off 3 dB by the time $a^2 = .0011$, as predicted by equation (2.28). As a increases the SNR_{O2} roll-off continues until it reaches the minimum value of 3.33 at $a^2 = 0.033$. At this point the array is just able to resolve signal 1 from the input noise and $SNR_{O1} = 0.89$. These numbers agree well with equations (2.10) and (2.28).

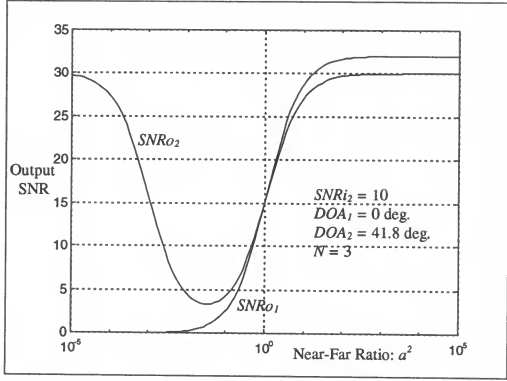


Figure 2.2 Output SNRs versus near-far ratio for spatially orthogonal incident signals

For the *scenario* $a^2 = 1$ the output SNRs are equal to 15 (see eqn. (2.6)). As a^2 becomes very large the output SNRs lose their dependence on a^2 and approach nearly the same value. This is shown in equations (2.33) and (2.34). At large near-far ratios ($a^2 = 10^5$) $SNRo_1 = 32.03$ and $SNRo_2 = 30$. The difference between their values is $\Delta SNRo = 2.03$ which agrees precisely with equations (2.14) and (2.34).

Figure 2.3 shows the performance for DOA spacings greater than the Rayleigh limit. For this scenario user 1 remains at array broadside and the DOA for user 2 moves to 90 degrees (in line with the array). This case gives the vector quantities $U_1^T U_2^* = N \cos \alpha_{12} = -1$, $\cos^2 \alpha_{12} = 1/9$ and $\sin^2 \alpha_{12} = 8/9$. When a^2 is small ($a^2 = 10^{-5}$) $SNRo_2 = NSNRi_2 = 30$ as in the previous case. As a^2 increases to 1.18×10^{-3} $SNRo_2$ rolls off approximately -3 dB

to a value of 15 and $SNRo_1$ increases from nearly zero to 6.5×10^{-3} . Note that equation (2.28) approximates $SNRo_1 = 5 \times 10^{-3}$ and a -3 dB roll-off point of $a^2 = 1.25 \times 10^{-3}$.

At $a^2 = 0.042$, $SNRo_1 = 0.798$ and $SNRo_2$ takes on a minimum value of 2.807.

Equation (2.28) predicts a minimum value of $SNRo_2 = 3.87$ will occur for $a^2 = z_{2b} = 0.0375$ and $SNRo_1 = 1.01$. From the plot $SNRo_1 = SNRo_2 = 9.94$ when $a^2 = 1$ which agrees with the approximations given by equation (2.31). When a^2 increases beyond unity the outputs quickly level to values near the maximum of $SNRo_2$: $SNRo_1 = 28.64$ and $SNRo_2 = 26.61$ at $a^2 = 1 \times 10^5$. This gives an output spread (eqn. (2.34)) of $\Delta SNRo = 2.03$.

Figure 2.4 shows what happens when the DOA spacings are less than the Rayleigh limit. In this case, signal source 1 remains at broadside while source 2 moves to $DOA_2 =$

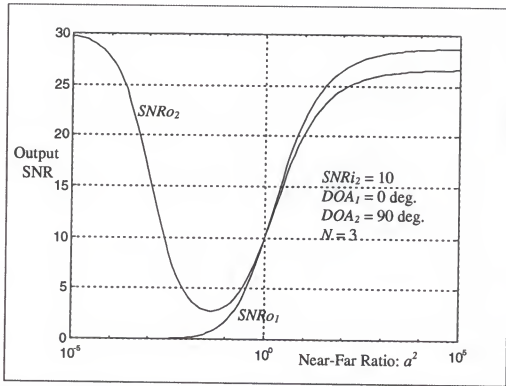


Figure 2.3 Output SNRs versus near-far ratio for nonorthogonal incident signals with DOA spacings greater than the Rayleigh limit.

20 deg., about half the Rayleigh limit. The outputs are degraded for $a^2 \gg 1$, compared to the two previous plots.

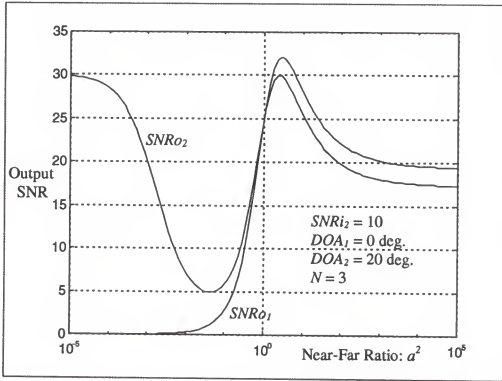


Figure 2.4 Output SNR versus near-far ratio for incident nonorthogonal signals with DOA spacings less than the Rayleigh limit

CHAPTER 3

THE MULTIUSER ARRAY PROCESSOR

ADAPTIVE PERFORMANCE

Consider for a moment that filter weights in an adaptive process are random variables with salient statistical properties. Adaptive processors are unable to perfectly track the corresponding steady-state solution; this induces a penalty known as misadjustment.⁹³ The goal of this chapter is determine the effect of the step size of the complex LMS algorithm⁹⁴ on the steady-state SNR-leveling performance of the multi-user processor. This concern is motivated by two factors. First, from an intuitive standpoint, it seems that the multi-user processor might cease to level the output SNRs if the misadjustment becomes too large. Second, the multi-user array processor might share some similarities to an LMS automatic line enhancer (ALE) for multiple time signals. Fisher and Bershad⁹⁷ studied the misadjustment performance of an LMS-ALE for the case of multiple sinusoids in AWGN and found the equalizer misadjustment to be especially sensitive to the step size.

This work will rely heavily of the work of Senne⁹⁵ who developed expressions for the time-dependent and steady-state weight covariance matrix of a real LMS adaptive processor. Other authors have investigated the transient and steady-state behavior of the complex LMS weight covariance matrix.^{96,97} and have found that the steady-state eigenvalues are very similar to those derived by Senne for the real LMS algorithm. This detail will be applied in a later section of this chapter.

Other authors have examined the performance of adaptive processors subjected to hard and soft constraints on SNR as well as optimizations of SNR itself subject to nonlinear constraints.^{98,99}

This chapter will be divided into three sections. The first section will give the development of a performance measure (cost function) which is based on the mean output SNR of the adaptive array. The second section develops a performance measure based on the variance of the array output SNR. The last section presents numerical results which allow comparisons between the analysis and simulations. The cost functions will be used to find acceptable bounds on the LMS step size. It is found that the upper bound on step-size arising from stability arguments also gives acceptable output SNR performance for the multi-user processor.

Mean-Based Performance Measure

If the adaptive weights of an LMS processor are considered to be time-varying random variables, $\mathbf{w}(n) = \mathbf{w}_0 + \mathbf{v}(n)$, the m th user's time-dependent output SNR results from substituting the expression for $\mathbf{w}(n)$ into equation (1.10):

$$SNR_o(n)_m = SNR_{i_m} \frac{\left| (\mathbf{w}_0 + \mathbf{v}(n))^T \mathbf{u}_m \right|^2}{\left\| \mathbf{w}_0 + \mathbf{v}(n) \right\|^2} \quad (3.1)$$

The random, time-varying weight component is represented by $\mathbf{v}(n)$, the mean of the weight vector is the steady-state MMSE weight vector, $\mathbf{w}_0 = \mathbf{R}^{-1}\mathbf{p}$, and the discrete time-dependence is introduced by the variable n . Note that the phase-shift vector \mathbf{u}_m and SNR_{i_m} are constants.

In order to derive an expression for the performance measure we need to find the mean of the output SNR. Some assumptions facilitate this effort:

1. $\|\mathbf{v}(n) + \mathbf{w}_o\| \approx \|\mathbf{w}_o\|$; instantaneous deviations of $\text{norm}(\mathbf{w})$ from $\text{norm}(\mathbf{w}_o)$ are negligible because of small step size μ .
2. $\mathbf{v}(n)$ are independent from sample-to-sample.
3. Input signals and noise are i.i.d., stationary and ergodic.
4. The elements of $\mathbf{w}(n)$ form a jointly Gaussian process.

The resulting mean of the output SNR is:

$$E[SNR_o(n)_m] = SNRi_m \cdot \frac{|\mathbf{w}_o^T \mathbf{u}_m|^2}{\|\mathbf{w}_o\|^2} + SNRi_m \cdot \frac{\mathbf{u}_m^T \mathbf{C}_{vv} \mathbf{u}_m}{\|\mathbf{w}_o\|^2} \quad (3.2)$$

where the first term on the right-hand side is SNR_o_m , the steady-state output SNR defined earlier in equation (1.10). The matrix $\mathbf{C}_{vv} = \text{cov}(\mathbf{v}(n))$ is the steady-state weight covariance matrix given by Senne.⁹⁵ The matrix is not a function of time, n , since $\mathbf{v}(n)$ components are i.i.d.

The last term on the right-hand side will cause the average output SNR for user m to increase as the adaptive weight covariance increases. This might have little effect for weak users; the term is not negligible for strong users. The average output SNRs may no longer be leveled if the term becomes too large. This point is clarified in Appendix A which presents some general characteristics of the SNR performance surface.

The first measure of performance is the difference between the average and steady-state output SNRs divided by the steady-state output SNR:

$$\frac{E[SNR_o(n)_m] - SNR_o_m}{SNR_o_m} = \frac{SNRi_m}{SNR_o_m} \frac{\mathbf{u}_m^T \mathbf{C}_{vv} \mathbf{u}_m}{\|\mathbf{w}_o\|^2} \leq C_1 \quad (3.3)$$

Where SNR_o_m is the steady-state output SNR for user m and is defined by the first term on

the right side of equation (3.2) above. The quantity $C_1 \propto 1/(NSNR_{i2}) \ll 1$ is a constant which serves as an upper bound which will limit the excursions of the time-dependent SNR (resulting from the adaptive process) from the steady-state solution. The constant will be defined in more detail later in the analysis. If the adaptive process is allowed to stray too far from the steady-state solution the output SNRs may no longer be held to nearly the same level and near/far limited performance may result. Using this relationship with equation (3.2) above gives an expression in which step size dependence is expressed indirectly through C_w :

$$\mathbf{u}_m^T \mathbf{C}_{vv} \mathbf{u}_m^* \leq C_1 \|\mathbf{w}_o\|^2 \frac{SNR_{o_m}}{SNR_{i_m}} \quad (3.4)$$

The quantity on the left-hand side may also be lower-bounded by using the *maximin theorem*²²:

$$\min_{\lambda_{vv}} (\lambda_{vv}) = \min_{\substack{\mathbf{q} \in \mathbb{C}^N \\ \mathbf{q} \neq 0}} \left(\frac{\mathbf{q}^T \mathbf{C}_{vv} \mathbf{q}^*}{\mathbf{q}^T \mathbf{q}^*} \right) \quad (3.5)$$

where \mathbb{C}^N denotes the complex N -dimensional space, \mathbf{q} is an N -length vector and $\lambda_{vv} = \min\{\text{all eigenvalues of } \mathbf{C}_{vv}\}$. Let \mathbf{q} of equation (3.5) equal \mathbf{u}_m of equation (3.4) where $\mathbf{u}_m^T \mathbf{u}_m^* = N$. Equation (3.5) may then be used to form a lower bound for equation (3.4).

The left-hand term of equation (3.4) would then be bounded by:

$$N \cdot \min_{\lambda_{vv}} (\lambda_{vv}) \leq \mathbf{u}_m^T \mathbf{C}_{vv} \mathbf{u}_m^* \leq C_1 \|\mathbf{w}_o\|^2 \frac{SNR_{o_m}}{SNR_{i_m}} \quad (3.6)$$

The next task is to find a useful expression for the lower bound of equation (3.6). Senne⁹⁵ has shown that the weight covariance matrix is diagonalized by the eigenvector matrix of \mathbf{R} , the input autocorrelation matrix. For an $N = 3$ array, the diagonal of Λ_{vv} , the

eigenvalue matrix of \mathbf{C}_w , is:

$$\text{diag}\{\lambda_w\} = \frac{\overline{\mu\epsilon^2_{\min}}}{2} \begin{bmatrix} (1-\mu\lambda_1)^{-1} \\ (1-\mu\lambda_2)^{-1} \\ (1-\mu\lambda_3)^{-1} \end{bmatrix} \left[1 - \frac{1}{2} \left(\frac{\mu\lambda_1}{1-\mu\lambda_1} \right) - \frac{1}{2} \left(\frac{\mu\lambda_2}{1-\mu\lambda_2} \right) - \frac{1}{2} \left(\frac{\mu\lambda_3}{1-\mu\lambda_3} \right) \right]^{-1} \quad (3.7)$$

where λ_1 , λ_2 , and λ_3 are the eigenvalues of \mathbf{R} , and μ is the LMS step size. Compton¹⁰⁰ has shown that when $SNR_{i1} \gg SNR_{i2} > 1$, the signal and noise eigenvalues of an N -by- N autocorrelation matrix \mathbf{R} are approximated by:

$$\begin{aligned} \lambda_1 &\approx \sigma_n^2 (1 + N \cdot SNR_{i1}) \\ \lambda_2 &\approx \sigma_n^2 \left(1 + SNR_{i2} \left(N - \frac{|\mathbf{u}_1^T \mathbf{u}_2|^2}{N} \right) \right) \\ \lambda_m &= \sigma_n^2 \quad m = 3 \dots N \end{aligned} \quad (3.8)$$

where the largest eigenvalue λ_1 is established by the strongest incident signal and λ_m are the noise-only eigenvalues.

If the step size is small ($\mu < 1/\lambda_1$) the smallest λ_w from equation (3.7) may be approximated by:

$$\begin{aligned} \min_{\lambda_w} \{\lambda_w\} &= \frac{\overline{\mu\epsilon^2_{\min}}}{2} (1-\mu\lambda_3)^{-1} \left[1 - \frac{1}{2} \left(\frac{\mu\lambda_1}{1-\mu\lambda_1} \right) - \frac{1}{2} \left(\frac{\mu\lambda_2}{1-\mu\lambda_2} \right) - \frac{1}{2} \left(\frac{\mu\lambda_3}{1-\mu\lambda_3} \right) \right]^{-1} \\ &\approx \frac{\overline{\mu\epsilon^2_{\min}}}{2} \end{aligned} \quad (3.9)$$

The simplification in equation (3.8) results directly from our assumption of small step size.

If μ is small the term in brackets and the term in parentheses outside of the brackets are equivalent to unity.

This establishes the upper and lower bounds on $\mathbf{u}_m^T \mathbf{C}_{vv} \mathbf{u}_m^*$:

$$\frac{1}{2} N \mu \overline{\varepsilon_{\min}^2} \leq \mathbf{u}_m^T \mathbf{C}_{vv} \mathbf{u}_m^* \leq C_1 \|\mathbf{w}_o\|^2 \frac{SNR_{O_m}}{SNR_{i_m}} \quad (3.10)$$

If all the incident signals are well-separated, strong and perfectly correlated to the reference waveforms the minimum MSE should be well-approximated by the output noise power: $\overline{\varepsilon_{\min}^2} \approx \sigma_n^2 \|\mathbf{w}_o\|^2$. If user $m = 1$ is the strongest user then SNR_{i_1} can be determined in terms of the eigenvalues via equation (3.8) ($N \cdot SNR_{i_1} = (\lambda_1 / \sigma_n^2) - 1 \approx \lambda_1 / \sigma_n^2$). The constant C_1 from equation (3.3) establishes a bound on the average excursions from the steady-state output SNR due to misadjustment, so it must be made suitably small. The strongest user - user 1 - should have a steady-state output SNR leveled to approximately the same value as user 2, therefore $SNR_{O_1} \approx SNR_{O_2} \approx N \cdot SNR_{i_2}$. Since even $SNR_{i_2} \gg 1$ then $C_1 = \mu_o / (2N \cdot SNR_{i_2})$ should give acceptable results where μ_o is a constant ($0 < \mu_o \leq 1$) and represents the unnormalized step size. This results in an upper bound on μ :

$$\mu \leq \frac{\mu_o}{\lambda_1} \quad (3.11)$$

which is similar to the upper bound on the LMS step size derived from stability arguments,^{22,93} and is consistent with our earlier assumption of a small step size.

Variance-Based Performance Measure

The second cost function is the variance of the adaptive output SNR divided by the squared mean of the adaptive output SNR. Choosing μ to keep this measure small will limit excursions from the mean of the adaptive process. The second moment of output SNR is:

$$E[SNRo(n)_m^2] = \frac{SNR i_m^2}{\|\mathbf{w}_o\|^4} \cdot E\left[\left(\mathbf{w}_o + \mathbf{v}(n)\right)^T \mathbf{u}_m\right]^4 \quad (3.12)$$

Senne assumed that the filter weights, $\mathbf{w}(n) = \mathbf{w}_o + \mathbf{v}(n)$, form a jointly Gaussian process.

In the following analysis this assumption is used to expand fourth-order joint moments in terms of the second-order moments via the Gaussian moment factoring theorem.¹⁰¹

If we assume the vector $\mathbf{v}(n)$ is multivariate and complex Gaussian we can express the fourth order moments as functions of the second-order moments.¹⁰¹ Expanding the bracketed vector term and discarding terms that would give odd-ordered moments of $\mathbf{v}(n)$ results in several terms:

$$\begin{aligned} E\left[\left(\mathbf{w}_o + \mathbf{v}\right)^T \mathbf{u}_m\right]^4 &= \left|\mathbf{w}_o^T \mathbf{u}_m\right|^4 + 4 \cdot \left|\mathbf{w}_o^T \mathbf{u}_m\right|^2 \mathbf{u}_m^T \mathbf{C}_{\mathbf{v}\mathbf{v}} \mathbf{u}_m^* \\ &\quad + E\left[\left(\mathbf{w}_o^T \mathbf{u}_m\right)^2 \left(\mathbf{v}_o^H \mathbf{u}_m^*\right)^2 + \left(\mathbf{w}_o^H \mathbf{u}_m^*\right)^2 \left(\mathbf{v}_o^T \mathbf{u}_m\right)^2\right] \\ &\quad + \sum_{i_1=1}^N \sum_{i_2=1}^N \sum_{i_3=1}^N \sum_{i_4=1}^N u_{i_1} u_{i_2}^* u_{i_3} u_{i_4}^* E\left[v_{i_1} v_{i_2}^* v_{i_3} v_{i_4}^*\right] \end{aligned} \quad (3.13)$$

where we have dropped the time-dependent notation from the weights. The third term on the right is zero. The fourth-order moment may be expanded in terms of the second-order moments:

$$E\left[v_{i_1} v_{i_2}^* v_{i_3} v_{i_4}^*\right] = E\left[v_{i_1} v_{i_2}^*\right] E\left[v_{i_3} v_{i_4}^*\right] + E\left[v_{i_1} v_{i_3}^*\right] E\left[v_{i_2} v_{i_4}^*\right] \quad (3.14)$$

The summation term becomes:

$$\sum_{i_1=1}^N \sum_{i_2=1}^N \sum_{i_3=1}^N \sum_{i_4=1}^N u_{i_1} u_{i_2}^* u_{i_3} u_{i_4}^* E\left[v_{i_1} v_{i_2}^* v_{i_3} v_{i_4}^*\right] = 2 \cdot \left(\mathbf{u}_m^T \mathbf{C}_{\mathbf{v}\mathbf{v}} \mathbf{u}_m^*\right)^2 \quad (3.15)$$

The second moment of the output SNR is:

$$E[SNRo(n)_m^2] = SNR i_m^2 \cdot \frac{2\left(\left|\mathbf{w}_o^T \mathbf{u}_m\right|^2 + \mathbf{u}_m^T \mathbf{C}_{\mathbf{v}\mathbf{v}} \mathbf{u}_m^*\right)^2 - \left|\mathbf{w}_o^T \mathbf{u}_m\right|^4}{\|\mathbf{w}_o\|^4} \quad (3.16)$$

and the variance of the output SNR is (from equation (3.2)):

$$\begin{aligned}\sigma_{SNR_{oj}(n)}^2 &= SNR_{i_m}^2 \cdot \frac{\left(\left| \mathbf{w}_o^T \mathbf{u}_m \right|^2 + \mathbf{u}_m^T \mathbf{C}_{vv} \mathbf{u}_m \right)^2 - \left| \mathbf{w}_o^T \mathbf{u}_m \right|^4}{\left\| \mathbf{w}_o \right\|^4} \\ &= E[SNR_{o_m}(n)]^2 - SNR_{o_m}^2\end{aligned}\quad (3.17)$$

where the second line of equation (3.17) follows from (3.2) and SNR_{o_m} is the *steady-state* output SNR of the m 'th signal. The performance measure becomes:

$$\frac{\sigma_{SNR_{o_m}(n)}^2}{E[SNR_{o_m}(n)]^2} = 1 - \frac{SNR_{o_m}^2}{E[SNR_{o_m}(n)]^2} \leq C_2 \quad (3.18)$$

where $C_2 \propto 1/(NSNR_{i_2}) \ll 1$ is a constant to be defined later.

Substituting quantities from equation (3.2) into equation (3.18) results in the inequality:

$$\mathbf{u}_m^T \mathbf{C}_{vv} \mathbf{u}_m \leq \left\| \mathbf{w}_o \right\|^2 \frac{SNR_{o_m}}{SNR_{i_m}} \left[\frac{1}{\sqrt{1-C_2}} - 1 \right] \quad (3.19)$$

Since $C_2 < 1$ the radical term may be approximated by a two-term series

$(1 - C_2)^{-\frac{1}{2}} \approx 1 + C_2/2$ and the inequality takes the same form as equation (3.4). The same procedure used to determine the step size upper bound for the first performance measure may be followed for this second performance measure with the same results: $\mu \leq \mu_o/\lambda_1$.

Simulation Results

This section will use simulations to corroborate the steady-state analytical results of previous sections.

The next two plots show curves of the quantities obtained from equations (3.2) and (3.18). Figure 3.1 shows the average output SNRs versus the step size coefficient for means resulting from simulation and from expression (3.2). The input scenario is $SNR_{i1} = 10$, $SNR_{i2} = 10^6$, $DOA_1 = 0$ deg., $DOA_2 = 90$ deg., $N = 3$. The initial weight for the LMS simulation was MMSE weight vector from equation (1.8), $\mathbf{w}_0 = \mathbf{R}^{-1}\mathbf{p}$.

Plots of the variance-based performance measure are shown in Figure 3.2. The input scenario is identical to the one described in Figure 3.1. The curves show the ratio of variance divided by the squared mean of the output SNR obtained through analysis

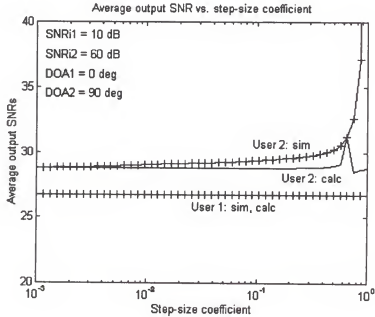


Figure 3.1 Output SNR versus step-size coefficient μ_0 . The step size is normalized by the input power

(equation (3.18)) and simulation. The curves show, as we might expect, that the performance will be worst for the strongest user. Selecting step size for acceptable strong user performance will lower-bound the performance for the remaining weaker users.

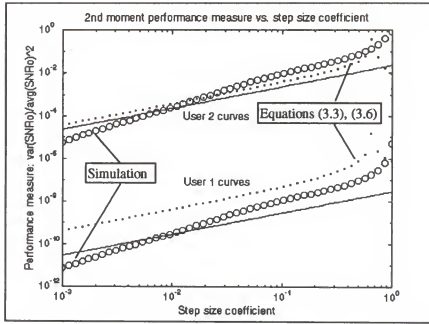


Figure 3.2 Variance-based estimator versus step-size coefficient μ_0 . The step size is normalized by the input power. The input scenario is identical to the one described in Figure 3.1

Selecting a small performance measure will limit the point-by-point excursions of the output SNR from the steady-state value and will give results which are acceptable in the mean. If 1% is selected as an acceptable value of the performance measure then from the curves for user 2 above it would appear that $\mu \approx 0.1/\text{Tr}(\mathbf{R})$ is the maximum allowable step size. This is in agreement with existing rules-of-thumb for selecting step size for stability and convergence. For these conditions, it would appear that upper bounds on LMS step size derived from convergence arguments will give acceptable performance of the multiuser processor.

CHAPTER 4

BASE STATION RECEIVER PERFORMANCE USING A SMART ANTENNA ARRAY IN A DS-CDMA SYSTEM WITH IMPERFECT POWER CONTROL

This chapter examines the steady-state outage probability and outage-based capacity of a single cell containing multiple directional signal sources transmitting to a central base station. The only fluctuation in the signal levels is due to lognormally-distributed power control error in the multiple transmitters. The central receiver consists of an array of N isotropic sensors, K minimum mean-squared error single-user beamforming processors and a bank of conventional detectors. The performance measures are outage probability and outage-based capacity. The goal is to find simple expressions which relate the outage-based capacity to the antenna array parameters, the number of active signal sources and the degree of power control error. The analytical results are expressed in terms of the number of users per array element which may be supported for a given outage probability. Analytical results are found to agree closely with those obtained from Monte Carlo simulations.

This work is unique in several respects. First, most previous work examined uplink performance for a traditional single-channel receiver. Second, the authors which considered a base station antenna and imperfect power control presented simulation results for the case of closed-loop power control.^{84,85} As was mentioned in Chapter 1, power control error will be modeled by incident power levels which are lognormally distributed. This model has gained some acceptance for open-loop power-controlled

systems. Its suitability as a model for closed-loop power-controlled systems remains an open issue.

The remainder of the chapter is divided into several sections. A qualitative description of the array and the receiver is given in the next section. The third section outlines the development of the analytical model and the derivation of the expressions for uplink capacity. The fourth section describes the Monte Carlo simulations and compares the analytical and the simulated results. The last section presents the conclusions.

System Description

The incident DS-CDMA signals are independent and originate from independent transmitters which are arbitrarily placed about the base station receiving antenna. The K active transmitters (located in a single cell) result in incident signals with independent directions-of-arrival (DOA) uniformly distributed over the interval $[0, 2\pi)$. The transmitters' output levels are continuously adjustable and have an infinite dynamic range. The output power - adjusted by an unspecified power control algorithm - results in output power which is independent between sources and which is also lognormally distributed. The modulation format is BPSK.

The base station receiving array consists of N ideal isotropic sensors arranged in a circle. Adjacent sensors are separated by a distance with the electrical equivalent of one-half wavelength. The sensor array feeds K separate banks of N complex weights controlled by K MMSE beamforming processors. The optimum steady-state weight vector for each beamformer is given by equation (1.8), $\mathbf{w}_0 = \mathbf{R}^{-1}\mathbf{p}$. Each of the K beamformer outputs feeds a distinct conventional DS-SS detector which in turn provides

an estimate of the demodulated output. The receiver is assumed to be capable of perfect carrier tracking of the desired signal. Unlike the multiple-user array of the previous chapters, the array/detector combination is devoted to detection of a single desired signal amidst multi-access interference. A diagram is shown in Figure 4.1.

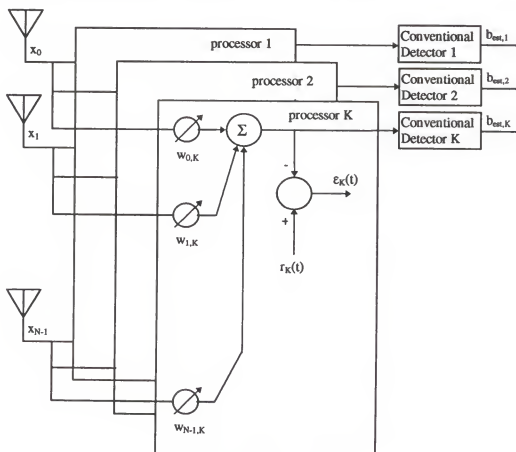


Figure 4.1 A bank of baseband single-user beamformers and conventional detectors sharing an array of sensors

Analysis

The stationary, complex base-band output of the sensor array is found by combining equations (1.3) and (1.4):

$$\underline{Y}(t) = A \sum_{m=1}^K 10^{e_m/20} \cdot c_m(t - \tau_m) b_m(t - \tau_m) \mathbf{u}_m + \mathbf{n}(t) \quad (4.1)$$

where A is the peak amplitude and e_m is $N(0, \sigma_{pcc}^2)$. The sensor outputs are weighted and summed by the beamformer and then processed by the conventional detector which forms an estimate of the current output bit. The signal from source 1 is considered the desired signal. The remaining $K-1$ signals are considered multi-access interference.

The array tends to steer a pattern lobe towards the desired signal and also tends to steer nulls of finite depth towards the $N-2$ strongest interferers when $K \geq N-1$. Because the strongest signals are attenuated, no single signal dominates the output statistics and the output may be well-approximated as Gaussian. An additional assumption of long codes (codes which span more than one data symbol) allows the PN sequences to be modeled as random codes. The random code model of Pursley¹⁰² will be used here. More refined models exist, but the additional complexity they introduce tends to improve accuracy when only a few users are present.^{103,104,105}

From Pickholtz et al.¹⁰⁶ we know that the effective bit energy to noise spectral density ratio may be approximated by $(Eb/No)_{eff} \approx N_c SINR$. The random code approximation may be modified to account for varying input amplitudes among the incident signals due to their power control error. Using one of the intermediate steps (equation (14) from Pursley¹⁰²) allows a convenient expression for $(Eb/No)_{eff}$ while retaining the cross-correlative properties of the PN codes:

$$\left(\frac{E_b}{N_o} \right)_{eff} \approx N_c SINR = \frac{N_c SINR_{o1}}{\frac{1}{3N_c^2} \sum_{m=2}^K SINR_{om} \cdot r_{m,1} + 1} \quad (4.2)$$

where $SINR_{om}$ is the array output SNR of the m th incident signal and $r_{m,1}$ is a

crosscorrelation parameter between the first and m th PN codes. If $SNRo_m$ is replaced by its sample mean and the remaining sum of $r_{m,i}$ terms is replaced by the random code approximation (equation (16) from Pursley¹⁰²) the expression becomes:

$$\left(\frac{E_b}{N_o} \right)_{eff} = \frac{N_c SNRo_1}{\frac{2}{3} \sum_{m=2}^K SNRo_m + 1} \quad (4.3)$$

The quantity $SNRo_k$ may be rewritten as:

$$SNRo_m = 10^{\epsilon_m/10} \cdot Gp_m \cdot SNRi \quad (4.4)$$

where $Gp_m = \left| \mathbf{w}_0^T \mathbf{u}_m \right|^2 / \left\| \mathbf{w}_0 \right\|^2$ is the normalized power gain of the array towards the m th signal and $SNRi = A^2 / \sigma_n^2$.

The power gain is a complicated function of the input scenario and the array geometry. In order to simplify the analysis we will use a simplifying assumption that the array power gain with respect to the first user, $Gp_1 = Gp_d$, will be approximately equal to its upper bound N , the number of array elements. The MMSE array gain towards the *interferers* ($Gp_m, m = 2 \dots K$) is difficult to characterize. Intuitively, we might expect that the $\text{avg}\{Gp_m\} = Gp_i$ might be well-approximated by the *average* (over DOA) normalized power gain (Gp_{avg}) of a classical beamformer ($\mathbf{w}_0 = \mathbf{u}_1$) with no adaptive null-steering capability. The value of Gp_{avg} ranges from unity for a single element to 1.6 for a 30-element circular array. Simulated results presented shortly will show that these assumptions with regard to the individual quantities (Gp_d, Gp_i) are not always valid over the conditions of interest. The average of the ratio Gp_d/Gp_i , however, does provide a reasonably good fit to the simulated results when the above assumptions ($Gp_d \approx N, Gp_i \approx N$) are used.

If there are many interfering signals the sum in the denominator of equation (4.3) may be approximated by averages:

$$\left(\frac{E_b}{N_o}\right)_{eff} = \frac{N_e N SNR_i 10^{x/10}}{\frac{2}{3}(K-1) SNR_i G_{p_i} 10^{\frac{\ln 10}{200} \sigma^2_{\mu^*}} + 1} \quad (4.5)$$

Further explanation is required. The sum in the denominator of equation (4.3) is almost a sample mean and may be approximated by an ensemble average. Assume the power gain and the exponential of equation (4.4) are independent: the expectations apply separately. This results in the base-10 exponential term, the $(K-1)$ term and G_{p_i} in the denominator of (4.5). This approximation causes a slight overestimation of interference: by breaking a sum of products into a product of sums we have invoked Schwartz's inequality twice in succession to get from (4.2) to (4.3) and to get from (4.3) to (4.5). Our simplifications have equated sample means and ensemble averages and also ignored the complicated nature of the array response by treating the power gain as an averaged quantity.

Simulations of the power gain show our assumptions regarding G_p may give acceptable results. Figure 4.2 shows the results of Monte Carlo simulations of averaged values of (MMSE) G_p for a desired signal (G_{p_d}), an interferer (G_{p_i}) and their quotient for a varying number of users, 3 dB of power control error and a 30-element array. The curves show that as the number of users exceeds the degrees-of-freedom of the array our simulated values for the individual gains are not very close to approximated values of $G_{p_d} \approx N = 30$ and $G_{p_i} \approx G_{p_{avg}} = 1.6$ but their quotient $G_{p_d}/G_{p_i} \approx N = 30$. So, for this circumstance it might be useful to approximate the gains in equation (4.5) as $G_{p_d} \approx N$ and $G_{p_i} = 1$.

Why will this work? As the number of users increases and the system becomes interference-limited the “1” term in the denominator of equation (4.5) becomes negligible leaving a good approximation of the quotient of the gains as $Gp_d/Gp_i \approx N$. When there are few users the multi-access interference is negligible, $Gp_d \approx N$ and the approximation will still hold. These gain approximations do not hold separately to predict the desired signal output power or the interference output power, but their combination might prove useful in calculating outage.

What about more extreme scenarios? Figure 4.3 shows the gains and the gain ratio for a power control error of 10 dB. The individual approximations $Gp_d \approx N$ and $Gp_i \approx Gp_{avg} = 1.6$ are even worse than before. However, the simulated gain ratio $Gp_d/Gp_i \approx N/1.3$ for $K > N$. This is a little closer to the ratio of the individual gains $Gp_d/Gp_{avg} = N/1.6$. This,

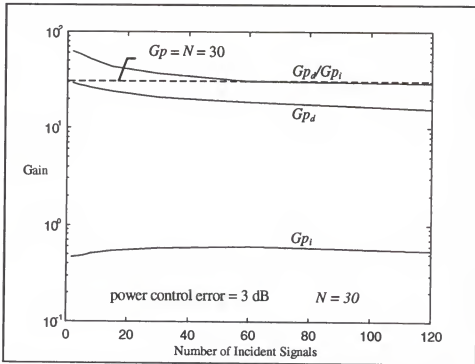


Figure 4.2 Gain versus the number of incident signals. Power control error is 3 dB.

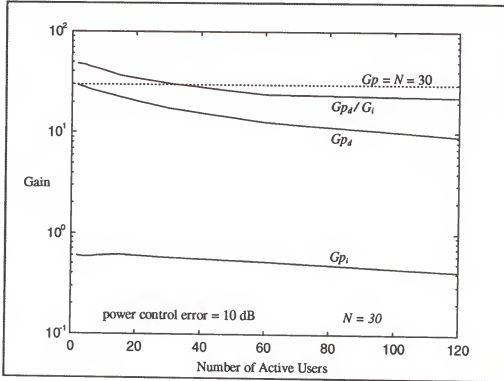


Figure 4.3 Gain versus the number of incident signals. Power control error is 10 dB.

and other simulations, indicate that choosing $Gp_d = N$ and $Gp_i \approx Gp_{avg} = 1.3$ for this model is a good approximation for outage calculations over the ranges of power control error examined here ($0 \leq \sigma_{pce} \leq 10$). Note that $Gp_i \approx Gp_{avg} = 1.3$ also arises from a sample mean (over N) of the average power gain (over DOA) for $N = 1, 2, 4, 8, 15$ and 30-element arrays for a classical beamformer.

Approximating the interference as an average quantity in equation (4.5) eliminates complex scenario-by-scenario interactions between the desired signal and the interference in the analytical model. It also leaves the lognormally distributed desired signal as the only random variable in the model. The resulting distribution of the $(Eb/No)_{eff}$ in equation (4.5) is therefore log-normal and results in simple expressions for the outage probability and the

capacity. Outage occurs when the $(E_b/N_o)_{eff}$ is less than some threshold. Converting equation (4.5) to dB and noting that e_I is $N(0, \sigma_{pce}^2)$ results in a simple expression for the outage probability:

$$\Pr_{outage} = \Pr\left(\left(\frac{E_b}{N_o}\right)_{eff, dB} < \xi_{dB}\right) = Q\left(\frac{Z_{dB} - \xi_{dB}}{\sigma_{pce}}\right) \quad (4.6)$$

where $Q(x)$ is the complementary Gaussian CDF, ξ_{dB} is the desired threshold in dB and:

$$Z_{dB} = 10 * \log_{10}\left(\frac{N \cdot \frac{E_b}{N_o}}{D}\right) \quad (4.7)$$

The quantity D is the denominator of equation (4.5). The quantity $E_b/N_o \approx (T_b/T_c)SNR_i = N_c SNR_i$ represents the equivalent bit energy to noise density ratio for a single incident signal and a single array element. Note that Naguib et al.⁷⁸ has also developed a Q-function upper bound for outage probability for the case of perfect power control. For the case of imperfect closed-loop power control Naguib et al.⁸¹ presented the simulated means and variances of $(E_b/N_o)_{eff}$.

Some simple algebraic manipulations result in the average capacity as a function of desired outage probability:

$$K = C \cdot \left[\frac{N}{\xi} 10^{\left(\frac{\sigma_{pce} Q^{-1}(\Pr_{outage})}{10}\right)} - \left(\frac{E_b}{N_o}\right)^{-1} \right] + 1 \quad (4.8)$$

where:

$$C = \frac{3N_c}{2Gp_i} 10^{\left(\frac{\ln 10}{200} \sigma_{pce}^2\right)}$$

where for high E_b/N_o the capacity is approximately linear in processing gain, N_c , or the

number of array elements N but decays exponentially as the power control error increases. Note also that the threshold ξ is no longer in dB. Note that if we interpret equation (4.8) as being linear in N , we can define a *per-element capacity* by noting the slope of the line. Note also that the capacity asymptotically approaches a finite maximum as E_b/N_0 increases. A similar effect was noted by Naguib and Paulraj⁸² for the case of a 2-D RAKE combiner at the base station receiver and perfect power control in the mobiles. They examined the capacity as the equal incident signal levels went to infinity and named the parameter *asymptotic capacity*. A simple expression for uplink capacity was also formulated by Suard et. al.⁷⁶ for a post-detection combiner. The model for power control error was restricted to a single user with an incident power level 10 dB higher than the other users.

Simulations and Results

Monte-Carlo simulations were used to corroborate the analytical results given by equation (4.6). Autocorrelation matrices for the desired signal, interferers and noise were generated by ensemble averages as in equation (1.6). Signal DOAs were uniformly distributed over $[0, 2\pi)$. The processing gain was 127 and $E_b/N_0 = 7$ for a single antenna element and no power control error. For a single trial the MMSE weights were calculated via equation (1.8) and the desired signal, interference and noise power out of the array were then used to calculate $(E_b/N_0)_{eff}$ via equation (4.3). An outage condition was judged to exist for that trial if $(E_b/N_0)_{eff} < 7$ dB (i.e. from equation (4.6), $\xi_{dB} = 7$ dB). The quantities were averaged over 20,000 trials for each combination of power control error, number of users and number of array elements.

Curves of the outage probability - $\Pr((Eb/No)_{eff} < 7 \text{ dB})$ - versus the number of users are shown in Figure 4.4. The figure contains curves from equation (4.6) as well as the Monte Carlo simulations. Power control error is 4 dB. Note that for 20,000 trials, curves in Fig. 4.4 might be inaccurate for outage less than 10^{-2} .

Figure 4.5 shows the total array/receiver capacity versus the number of array elements with outage probability as a parameter. The curves are formed by plotting constant contours of a three-dimensional surface formed by $\Pr((Eb/No)_{eff} < 7 \text{ dB})$ as it varies over K and N . The solid curves show simulated results; dashed lines show the constant-value contours of equation (4.6) for power control error equal to 4 dB.

The curves of Figure 4.5 show the user capacity of the array/detector is roughly linear in N . We may therefore use as a performance measure *per-element capacity*, the number of users per array element which may be supported for the given values of outage probability and power control error. As noted earlier the analytical expression for the per-element capacity may be obtained by noting the slope of the total capacity line in equation (4.8) with N as the independent variable. A point of note: the average power gain (Gp_{avg}) in equation (4.8) has a slight dependence on N : it is equal to unity for a single element and is equal to 1.6 for a 30-element array. For the sake of simplicity, this slight dependence is ignored and a mean value of $Gp_{avg} = 1.3$ is assumed, which was noted earlier when comparing simulated Gp_d/Gp_i curves in figures 4.2 and 4.3.

The per-element capacity versus the power control error for $\Pr((Eb/No)_{eff} < 7 \text{ dB}) = 0.02$ is shown in the upper plot of Figure 4.6. For simulated data, the normalized capacity was determined by extracting the approximate slopes of the capacity curves (as shown in Figure 4.4) via a linear least-squares curve fit. The analytical results were calculated from

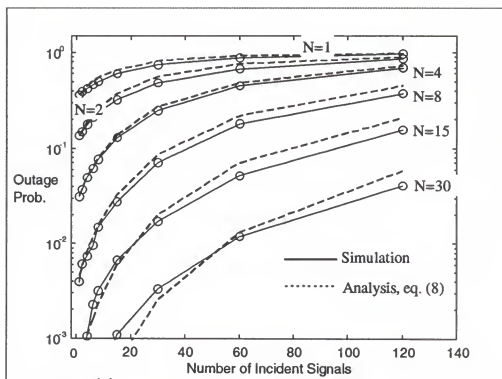


Figure 4.4 Outage probability versus the number of incident signals. Power control error is 4 dB. The number of array elements N is a parameter

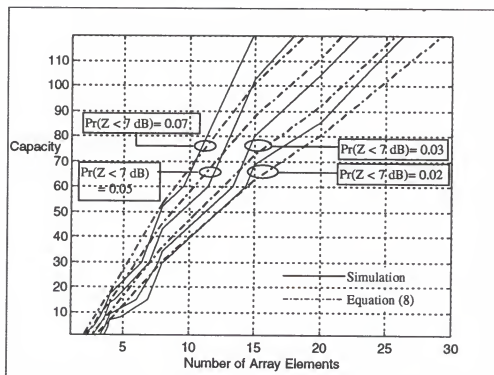


Figure 4.5 Capacity versus the number of array elements with outage probability as a parameter. The power control error is 3 dB.

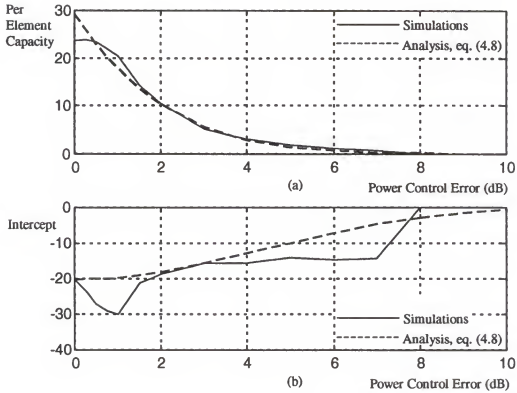


Figure 4.6 Normalized array capacity versus power control error in dB.

the slope of the system capacity line given in equation (4.8). As the curves show, the analytical and simulated results for the per-element capacity are in close agreement. The lower plot of Figure 4.6 shows the intercept point of the line in equation (4.8). Obviously the analytical and simulated results are not in as close agreement as the upper plot. Note that to determine the overall system capacity - given an array of N elements - it would be necessary to know the per-element capacity as well as the intercept.

Conclusions

In this chapter we attempted to develop accurate, simple analytical expressions for the outage-based uplink capacity in an idealized single-cell DS-CDMA system with multiple, possibly near/far, signals incident on a base-station receiving array. Power control error was assumed to be lognormally distributed. Some simplifying assumptions regarding the interference and the array response allowed an approximate expression for the uplink capacity that was compared with results from Monte Carlo simulations.

The approximate expression - given in equation (4.8) - shows that a roughly linear relationship exists between the capacity and the number of array elements. The overall capacity K consists of two components. The first component is the slope of the line in N and has been defined as the per-element capacity, the number of users per array element which may be supported for a given level of outage probability and power control error.

Equation (4.8) indicates that the per-element capacity is not dependent on the nominal input level (i.e. the input level without power control error: SNR_i) but decreases exponentially with increasing power control error. For the levels of power control error examined here the term which dominates the exponential roll-off is $\sigma_{pce} Q^{-1}(P_{outage})/10$ of equation (4.8). The decrease in the per-element capacity is therefore dependent on the outage requirements and the standard deviation - in dB - of the power control error. Since the per-element capacity is insensitive to the nominal input levels and the array size, but is keenly dependent on the degree of power control error and the outage, it might serve as a useful asymptotic measure of the performance for this array/receiver.

The second component of equation (4.8) is the intercept term equal to $1-C(Eb/No)^{-1}$ where C is defined in (4.8). The intercept is inversely proportional to the nominal input levels. As the input levels decrease this term becomes larger, diminishing the overall capacity. In a plot of capacity (K) versus array elements (N), the capacity line moves away from the origin along the horizontal N -axis as the nominal input levels decrease. The intercept is weakly dependent on the power control error (via C) and also on the number of array elements (via Gp_{avg}) and is not dependent on the outage probability. Analytical and simulated results do not agree as closely as those for per-element capacity.

The agreement - or lack of it - between the analytical and simulated results for per-element capacity and the intercept can be interpreted in terms of outage probability curves shown in Figure (4.4). The analytical model can predict well the horizontal spacing between the continuous outage probability curves. The per element capacity predicts the incremental increase in capacity with increasing array elements and is a measure of the horizontal displacements of the outage curves relative to one-another. The less reliable prediction made by the model is the horizontal placement of the outage curves relative to a point on the horizontal axis. This enters into the model via the intercept parameter described above.

The simple model presented here was based on some simplifying assumptions regarding the array response towards the incident signals. In spite of this, the analytical model accurately predicts some aspects of the array/receiver performance when directional signals are employed with lognormally distributed power control error. The directional signals originated in a single cell and were not subjected to any kind of environmentally-

induced fading. The system performance in the presence of fading and interference resulting from outer cells is the topic of the next chapter.

CHAPTER 5

BASE STATION RECEIVER PERFORMANCE WITH A SMART ANTENNA ARRAY IN THE PRESENCE OF MULTIPATH FADING AND SHADOW FADING

This chapter examines base station receiver performance when incident signals are subjected to frequency-nonselective Rayleigh multipath fading and lognormally distributed shadow fading. The effects of multi-access interference from outer cells - subjected to shadow fading - will also be included in the incident signal model. The power control error model will continue to be described by a lognormally-distributed random variable and the receiver still consists of an array of N ideal isotropic sensors, K minimum mean-squared error single-user array processors and a bank of conventional detectors (see Figure 4.1).

The goal of this chapter is to determine the performance dependence on the number of active signal sources, the number of array elements and the degree of power control error. As before, the performance will be expressed by outage probability and per-element capacity. Unfortunately the introduction of fading and outer cell interference further complicates the development of simple analytical models. In spite of these complications the simulated results closely follow some general trends established by the model in Chapter 4. In particular, curves of outage-based capacity continue to be linear in N with slopes that decrease exponentially with increasing power control error.

Previous authors have investigated the performance of optimum combining from the standpoint of interference rejection. Winters^{23,44} and other authors^{60,61} have examined contributions to TDMA system performance while Naguib et al.⁷⁶⁻⁸⁴ have studied CDMA

systems. Unlike previous work, this research examines the outage-based capacity for the case of imperfect power control and attempts to provide some analytical models which would allow easy assessment of performance.

The remainder of this chapter is divided into six sections. The first section will present the receiver model for single-cell signals subjected to Rayleigh fading. The second section will extend the model to the multi-cell case. The third section will quickly revisit the model of chapter four and introduce a second analytical technique. The fourth section will give a brief description of the simulation parameters and compare the simulated results with the analytical results.. The fifth section entitled Conclusions and Discussion will review the results in some detail. The last section gives a summary.

A Single Cell with Signals Subjected to Rayleigh Fading

Multipath fading arises when propagating electromagnetic waves originating from a single signal source arrive at a receiver via different propagation paths. The individual paths may include line-of-sight propagation as well as paths resulting from reflection off of one or more surfaces. The individual waves - as well as their sum - are highly dependent upon the frequency of the propagating waves, their path lengths as well as the reflective properties and geometric arrangement of the encountered surfaces.

This research will exploit the assumption that multipath fading of a signal from a single source results from the sum of many reflected waves. The individual waves have roughly equal power as well as independent amplitudes and independent phases. This allows the fading component of the incident signal to be modeled as a complex Gaussian random variable with uniformly distributed phase and an envelope which is Rayleigh

distributed.¹⁰⁷ If the channel is well-approximated by a constant frequency response characteristic then relative time delays between arriving wave fronts are negligible. This is known as *frequency-nonselective Rayleigh fading* or *flat Rayleigh fading*. The flat-fading condition is probably an accurate approximation for indoor communication systems with large path losses and mobile systems with scatterers located in close proximity to the mobile. It represents a worst-case condition from the standpoint of detection since it will not allow the use of a RAKE receiver⁶² to provide resolution of individual time-delayed paths.

The complex base-band output of a sensor array outwardly resembles the expression given in equation (4.1):

$$\mathbf{y}(t) = A \sum_{m=1}^K 10^{\epsilon_m/20} \cdot c_m(t - \tau_m) b_m(t - \tau_m) \mathbf{u}_m + \mathbf{n}(t) \quad (5.1)$$

where the elements of the phase shift vector \mathbf{u}_m are complex Gaussian random variables which result from Rayleigh fading. This is in contrast to equations (1.4) and (4.1) in which the components of \mathbf{u}_m are complex exponentials resulting from directional, unfaded signals.

The components of \mathbf{u}_m may have any permissible degree of correlation. The study of spatial diversity combiners is dedicated to antenna array structures which force the correlation of fading components between array elements to be low (ideally zero).¹⁰⁸ A base station diversity array must have larger element spacings than the customary half-wavelength spacings used in a mobile radio receiver.²⁸ Lee conducted an empirical study of fading correlations in a two-element base station array. He concluded that, for low correlation, the interelement spacings must be $15\lambda - 20\lambda$ if the signal arrives from

broadside and 70λ - 80λ if the signal arrives along the axial direction. Salz and Winters¹⁰⁹ examined a linear array and developed closed-form expressions for the direction-dependent fading correlations between array elements when multipath rays are “dense” throughout a range of DOAs. Raleigh et al.¹¹⁰ proposed an analytical model which describes the spatially-dependent correlations of the fading process. Verification of the latter two models through experiment remains an open issue, as does more refined spatially-dependent channel models. Naguib and Paulraj⁸³ examined the effects of the Salz and Winters fading model on a base-station diversity array in an IS-95 system using closed-loop power control.

Because spatial channel models remain an open issue this research will exploit the assumption that the fading process is independent between antenna elements and the elements of \mathbf{u}_m in equation (5.1) are complex i.i.d. $N(0,1)$. Spatial dependence of the incident signals - via the interelement phase-shifts - no longer exists and the array geometry is critical only in that it results in independent fading between elements. Winters²³ has shown that even when directional information is not used by the processor (i.e. the array functions as a diversity combiner) an optimum combiner will outperform, in steady state, a maximal ratio combiner because it is able to adaptively attenuate cochannel interference.

Multiple Cells with Signals Subjected to Rayleigh Fading and Shadow Fading

The models and results from the last subsection will be extended here to include the effects of outer-cell interference. Like the previous section of this chapter the incident signals will be subjected to flat Rayleigh fading. Unlike the previous section, however, the

cell which contains the desired user will be surrounded by several layers of cells containing sources of multi-access interference (i.e. other DS CDMA users). The interference will be subjected to multipath fading and shadow fading. Shadow fading occurs when structures (such as buildings, hills or mountains) attenuate propagating signals. Shadow fading varies more slowly than the multipath fading component of the signal and is interpreted as the time-varying mean of the rapid, multipath-induced signal fluctuations.²⁸

The incident signal model may be modified slightly:

$$y(t) = A \sum_{m=1}^K 10^{e_m/20} \cdot c_m(t - \tau_m) b_m(t - \tau_m) \mathbf{u}_m + \sum_{n=1}^{K \cdot N_{oc}} A_n \cdot 10^{e_n/20} \cdot \left(\frac{10^{s_n/20}}{r_{n,o}^4} \right) \cdot c_n(t - \tau_n) b_n(t - \tau_n) \mathbf{u}_n + \mathbf{n}(t) \quad (5.2)$$

where the first summation is for center-cell and the second summation (with index n) results from the outer-cell interference. All users have lognormally distributed power control error where e_m is $N(0, \sigma_{pce}^2)$. The quantity N_{oc} is the number of outer cells while K remains the number of users/cell. The variable s_n is $N(0, 64)$ which in turn specifies lognormally distributed shadow fading with 8 dB standard deviation. The quantity $r_{n,o}^4$ is the distance-dependent, fourth-order propagation loss between the n 'th interferer and the center cell base station. The phase-shift vectors \mathbf{u}_m and \mathbf{u}_n are, as in the previous subsection of this chapter, composed of i.i.d. random variables which are $N(0, 1)$. Note that the incident amplitude A_n is an indexed quantity unlike the first summation representing the center-cell users. This is because the outer-cell amplitudes are determined by a hand-off to the outer-cell base station with the least path loss. This will be discussed in more detail shortly. The quantity $\mathbf{n}(t)$ is a vector of complex AWGN with power σ_n^2 .

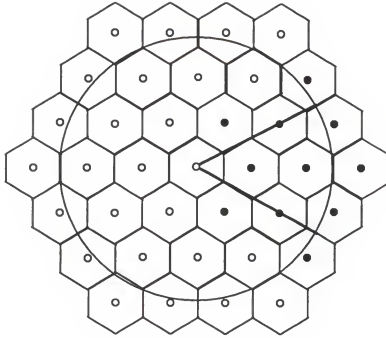


Figure 5.1 Spatial region for simulation of outer-cell interference.

Figure 5.6 below shows a diagram of the arrangement of the hexagonal cells, each with a unit radius (cell area = $3\sqrt{3}/2$). The region of interest is circular and contains the equivalent area of $N_{oc} = 21.67$ cells, excluding the center cell. The small circle at the center of each cell designates the position of each cell's base station. The wedge-shaped region within the larger circle contains the equivalent area of 3.61 cells and it is over this region that the spatial distribution of outer cell interferers is uniform, excluding the portion containing the center cell. The interference from this wedge-shaped region will be determined for each scenario and the results replicated to generate the interference components for the remainder of the circular region.

The path loss which occurs between an outer-cell user and an outer-cell base station contains a deterministic propagation loss ($\propto r^4$) as well as lognormally distributed

shadowing. The random components complicate the hand-off - or membership - of a user to a cell: a user is not necessarily serviced by the closest base station. Viterbi et al.¹¹¹ investigated the properties of outer cell interference for the case of perfect power control and lognormal shadowing while Lee et al.¹¹² investigated the effects of imperfect power control and lognormal shadowing. These previous works examined the case of up to 4 base stations involved in the hand-off. Increasing the number of base stations in the hand-off beyond $N_B = 4$ will only slightly decrease the outer cell interference for a given degree of shadowing and power control error.

The hand-off was computed by selecting the base station path with the minimum base-station-to-mobile path loss. For the m th outer-cell user, this results minimizing a convenient ratio of path losses between the outer cell mobile and the outer cell base station and the outer cell mobile and the center-cell base station:

$$L_m = \min_{n=1 \dots N_B} \left[\frac{r_{m,n}^4 \cdot 10^{\frac{\epsilon_{m,n}}{10}}}{r_{m,o}^4 \cdot 10^{\frac{\epsilon_{m,o}}{10}} \cdot 10^{\frac{\epsilon_m}{10}}} \right] \quad \text{where: } m = 1 \dots K \cdot N_{oc} \quad (5.3)$$

where m represents the index over the outer-cell users in the wedge-shaped region and n is the index over the $N_B = 11$ base stations denoted by the solid black circles in Figure 5.6 above. The quantities $r_{m,n}^4$ and $10^{\epsilon_{m,n}/10}$ are the propagation loss and lognormal shadowing respectively between the m th mobile and the n th base station. The quantities $r_{m,o}^4$, $10^{\epsilon_{m,o}/10}$ and $10^{\epsilon_m/10}$ are the propagation loss and shadowing between the m th mobile and the center cell at the origin. The quantity $10^{\epsilon_m/10}$ is the power control error of the m th user with respect to the base station chosen for hand-off. As the figure shows, base stations just

outside of the wedge-shaped region are utilized in the hand-off calculations for the outer cell interferers. The shadowing and power control error components are assumed to be independent from path-to-path. Some authors^{113,114} maintain that spatial correlations exist in shadowing components, but those effects are not incorporated into this model. The incident levels (A_n 's of equation (5.3)) resulting from hand-offs in the wedge-shaped region of Figure 5.6 were replicated to generate interference levels for the remaining portions of the large circular region. The model used in this research agrees precisely with the results of Viterbi et al.¹¹¹ which reported that for $N_B = 3$ the ratio of the outer cell to inner cell interference is 0.57.

It was assumed that power control error correlates perfectly between hand-off base stations and does not enter into interference calculations until hand-off is chosen based on minimum path loss. This is in contrast to the work of Lee et al.¹¹² which assumed closed-loop power control error was uncorrelated between hand-off base stations. The authors minimized the quantity:

$$L_m = \min_{n=1 \dots N_B} \left[\frac{r_{m,n}^4 \cdot 10^{\frac{s_{m,n}}{10}} \cdot 10^{\frac{e_{m,n}}{10}}}{r_{m,o}^4 \cdot 10^{\frac{s_{m,n}}{10}}} \right] \quad \text{where: } m = 1 \dots K \cdot N_B \quad (5.4)$$

where $10^{\frac{e_{m,n}}{10}}$ is the power control error between the m th user and the n th hand-off base station. They assumed that $N_B = 3$; hand-off occurred to one of the three closest base stations.

Analysis

This section will briefly revisit the analytical results of chapter four which gave an asymptotic expression for capacity when signals were directional. Another analytical model will then be introduced which exploits the assumption of lognormal interferers.

The expression given in equation (4.3) for the $(Eb/No)_{eff}$ may be rewritten slightly using equation (4.4) for a single cell:

$$\left(\frac{E_b}{N_o} \right)_{eff} = \frac{N_c SNR i_1 G_{p_1} 10^{\epsilon_n/10}}{\frac{2}{3} SNR i \sum_m G_{p_m} 10^{\epsilon_n/10} + 1} \quad (5.5)$$

where $SNR i_m = (A_m^2 / \sigma_n^2) \cdot 10^{\epsilon_n/10}$ is the input SNR and $G_{p_m} = |\mathbf{w}_o^T \mathbf{u}_m|^2 / \|\mathbf{w}_o\|^2$ is the normalized array gain towards the m th signal. In chapter four some assumptions (via equation (4.4)) allowed the sum term in the denominator of the expression for $(Eb/No)_{eff}$ to simplify into products of average terms, some of which are not explicit functions of the input parameters (i.e. $avg\{G_{p_m}\} = G_{p_i}$, $m \neq 1$, the interference signal gain). In addition, the gain towards the desired user $G_{p_1} = G_{p_d}$ was modeled by its upper bound N , the number of array elements. While these approximations were not accurate when considered separately, their quotient resulted in a convenient form and gave acceptable results (see Figures 4.2 and 4.3). The per-element capacity was the slope of equation (4.8):

$$K_E = \frac{3NN_c}{2\xi G_{p_i}} \exp\left(-\frac{\ln(10)Q^{-1}(\Pr_{outage})}{10}\sigma_{pce} - \frac{\ln^2 10}{200}\sigma_{pce}^2\right) \quad (5.6)$$

where the term containing the Q -function is dominant for the range of power control error considered here. The term - analogous to a single-pole roll-off - resulted from modeling

the multi-access interference as an averaged quantity. The averaging operation left the desired signal as the only random variable and resulted in a lognormal distribution of $(Eb/No)_{eff}$ in which the standard deviation (in dB) is determined solely by the power control error standard deviation σ_{pce} (see equations (4.5), (4.6)). Under this simplified analytical model, the number of users K and the number of array elements N affect the mean of $(Eb/No)_{eff}$ but not the standard deviation.

This series of assumptions gave acceptable results for the asymptotic case of strong nominal input levels if the signals were directional and had a moderate degree of power control error. With the addition of multipath fading the results of chapter four are less precise. The roll-off of a diversity combiner's per-element capacity is slower for low values of power control error because the standard deviation of $(Eb/No)_{eff}$ is not determined solely by the power control error σ_{pce} .

A different analysis technique which might approximate the standard deviation of $(Eb/No)_{eff}$ more accurately has been examined by other authors. The model assumes that a sum of lognormally distributed random variables is also lognormal. Along this line, Schwartz and Yeh developed an iterative version of Wilkinson's method¹¹⁵ and then used their model to evaluate the outage probability of a multi-cell AMPS system.¹¹⁶ Beaulieu et al. examined several methods for approximating a sum of lognormal random variables and concluded that the "best" choice of model depends upon the system parameters (i.e. the degree of shadowing and the magnitude of the outage probability).

This research will supplement the analysis of previous sections by approximating the multi-access interference as a sum of lognormal r.v.'s. This method will result in a closed-

form expression for outage probability. An explicit equation for the per-element capacity will not be possible.

If the array gain towards the interference may be modeled by a constant, the resulting noise and multi-access interference is approximated by:

$$I_{MA} = \sum_{m=2}^K 10^{\frac{z_m}{10}} + \frac{F}{Gp_i} \cdot \sum_{n=1}^K 10^{\frac{y_n}{10}} + \frac{3}{2Gp_i SNR_i} \quad (5.7)$$

where the left-most summation represents the inner-cell interference and the second summation represents the outer-cell interference. The right-most term results from the presence of noise. The outer-cell interference has been modelled as a quantity normalized by the inner-cell interference: the outer-cell summation is over K rather than KN_{oc} . This approach has been used for incident signals by previous authors^{111,112} and will be extended to the diversity array output via the gain constant F .

Wilkinson's method begins with the assumption that the multi-access interference is a lognormal r.v. The first two moments of the I_{MA} are then matched to the first two moments of the sums of lognormal random variables. The mean and second moment of I_{MA} are given in equation (5.8) below:

$$\begin{aligned} E[I_{MA}] &= E\left[\exp\left(\ln(10)\frac{z}{10}\right)\right] = \exp(\beta m_z + \beta^2 \sigma_z^2 / 2) \\ &= (K-1)\exp(\beta^2 \sigma_x^2 / 2) + \frac{F}{Gp_i} K \exp(\beta^2 \sigma_y^2 / 2) + \frac{3}{2Gp_i SNR_i} = b_1 \end{aligned}$$

$$\begin{aligned}
E[I_{MA}^2] &= E\left[\exp\left(2\ln(10)\frac{z}{10}\right)\right] = \exp(2\beta m_z + 2\beta^2 \sigma_z^2) \\
&= E\left[\left(\sum_{m=2}^K \exp(xe_m) + \frac{F}{G_{p_i}} \sum_{n=1}^K \exp(\beta y_n) + \frac{3}{2G_{p_i} SNR_i}\right)^2\right] \\
E[I_{MA}^2] &= \left[\begin{aligned} &(K-1)\exp(2\beta^2 \sigma_x^2) + (K-1)(K-2)\exp(\beta^2 \sigma_x^2) \\ &+ \left(\frac{F}{G_{p_i}}\right)^2 \left(K\exp(2\beta^2 \sigma_y^2) + K(K-1)\exp(\beta^2 \sigma_y^2)\right) \\ &+ 2\left(\frac{F}{G_{p_i}}\right) K(K-1)\exp(\beta^2 (\sigma_x^2 + \sigma_y^2)/2) + \left(\frac{3}{2G_{p_i} SNR_i}\right)^2 \\ &+ \frac{3}{G_{p_i} SNR_i} (K-1)\exp(\beta^2 \sigma_x^2/2) \\ &+ \frac{3F}{G_{p_i}^2 SNR_i} K\exp(\beta^2 \sigma_y^2/2) \end{aligned} \right] = b_2 \quad (5.8)
\end{aligned}$$

where the variable z is $N(m_z, \sigma_z^2)$ and $\beta = \ln(10)/10$. Note that the exponential terms of the inner and outer cell interference are specified as $N(0, \sigma_x^2)$ and $N(0, \sigma_y^2)$ respectively.

The logarithms of the moments allow linear solutions of m_z and σ_z^2 in terms of the moments of the sums (b_1, b_2):

$$\begin{aligned}
m_z &= 2\ln(b_1) - \frac{1}{2}\ln(b_2) \\
\sigma_z^2 &= \ln(b_2) - 2\ln(b_1)
\end{aligned} \quad (5.9)$$

Once the interference moments are determined then $(Eb/No)_{eff}$ may be expressed as:

$$\left(\frac{E_b}{N_o} \right)_{eff} = \frac{3}{2} N_c \frac{Gp_d}{Gp_i} 10^{\frac{x_1 - 10 \log(\exp(1))z}{10}} \quad (5.10)$$

and the outage probability is given by equation (5.11) below where $\log(\bullet)$ denotes the base-10 logarithm. This method does not allow an explicit closed-form expression for the per-element capacity. It will, however, allow that quantity to be extracted from outage probability contours as was done for the simulated results. The expression for the outage probability from the approximated moments:

$$\Pr \left(\left(\frac{E_b}{N_o} \right)_{eff, df} < \xi_{dB} \right) = Q \left(\frac{\eta - \xi_{dB} - 10 \log(\exp(1))m_z}{\sigma_c} \right)$$

where:

$$\eta = 10 * \log \left(\frac{3}{2} N_c \frac{Gp_d}{Gp_i} \right) = 10 * \log \left(\frac{3}{2} N_c \frac{N}{Gp_i} \right) \quad (5.11)$$

$$\sigma_c = \sqrt{\sigma_x^2 + 100 \log^2(\exp(1)) \sigma_z^2}$$

Results

Most of the details of the simulation procedure are outlined in the section Simulations and Results of Chapter 4 with one difference: the faded, incident signals were no longer directional and a DOA was not specified. Each signal was specified by its power control error (and shadowing for the outer cell interferers), and its phase-shift vector which consisted of complex, i.i.d. unit-variance Gaussian random variables. For each trial the $(Eb/No)_{eff}$ was determined via equations (1.8), (1.10), (5.3) and (5.5) and was then compared to an outage threshold of 7 dB. A sample mean was tabulated over the trials for each combination of users and array elements. Even with fading the resulting outage

contours were roughly linear in N with slopes which decrease with increasing power control error.

Figure 5.2 shows $Pr((Eb/No)_{eff} < 7 \text{ dB})$ versus the number of users with the power control error equal to 4 dB and with no outer cell interference. As in previous plots, the curves are plotted parametrically. The different curves represent outage probability for different numbers array elements N . For this value of power control error the performance is not drastically different than for the nonfaded case shown in Figure 4.4. The nominal input signal levels (without power control error) are such that $Eb/No = 7$ (or $SNR_i = 7/Nc = 7/127 = -12.6 \text{ dB}$) for a single signal incident on a single array element feeding a

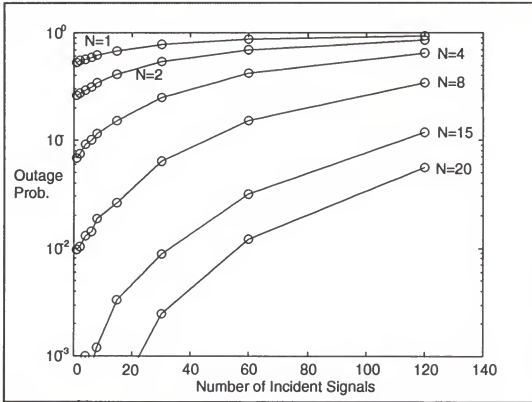


Figure 5.2 Outage probability versus the number of incident signals with power control equal to 4 dB. The number of array elements N is a parameter.

conventional detector. When comparing Figures 4.4 and 5.2 it is easy to see the faded and unfaded systems have roughly the same outage performance. This similarity ceases for other values of power control error.

Figure 5.3 shows simulated outage contours as the power control error varied. The top two plots show contours of $Pr((Eb/No)_{eff} < 7 \text{ dB}) = 0.02$ as the power control error varied from 0 to 7 dB with no outer cell interference. The upper plot (a) is for a nominal input condition (without power control error) of $SNR_i = 7/N_c = -12.6 \text{ dB}$ while plot (b) shows contours for a nominal input condition of $SNR_i = 10^8/N_c = 59 \text{ dB}$. Plots (c) and (d) show the same conditions but include outer cell interference. The plots show that, even with fading, outage-based capacity continues to be linear in N . Note also that as the nominal input levels increase, the intercepts of the approximately linear contours move towards the origin. This general behavior was predicted for the nonfaded case by equation (4.8).

The slopes of the lines in Figure 5.3 were extracted using a least-squares curve fit and plotted as the per-element capacity in Figure 5.4. Note that the per-element capacity is less than that for the case of no Rayleigh fading as long as the power control error is less than approximately 1.5 dB. As long as the power control error is greater than 1.5 dB the receiver employing a diversity array combiner in the presence of fading outperforms a receiver using a beamformer to equalize signals which are not subjected to multipath fading.

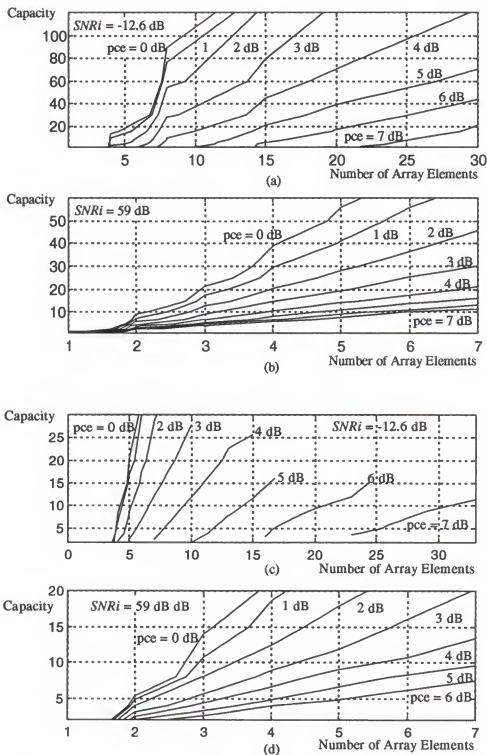


Figure 5.3 Capacity versus the number of array elements with power control error as a parameter. Outage probability = 0.02. Plots (a), (b) are without outer cell interference. Plots (c), (d) include outer cell interference.

Note that in Figure 5.4 there is degradation in the per-element capacity as the nominal input levels increase and outer cell interference is present (plot (b)). When the nominal signal level is small ($SNR_i = -12.6$ dB) the individual outer cell signals incident on the inner cell are very weak (compared to ambient noise and the inner cell interferers) due to the path loss. In this circumstance the outer cell interference probably just adds to the ambient AWGN. When the nominal input signals are large ($SNR_i = 59.6$ dB), outer cell interferers can overcome the outer-cell to center-cell path loss and can have signal levels much higher than the ambient noise, even at the center cell. In this case some percentage of individual outer cell signals compete with the inner cell interference for attention from the array processor, and performance suffers.

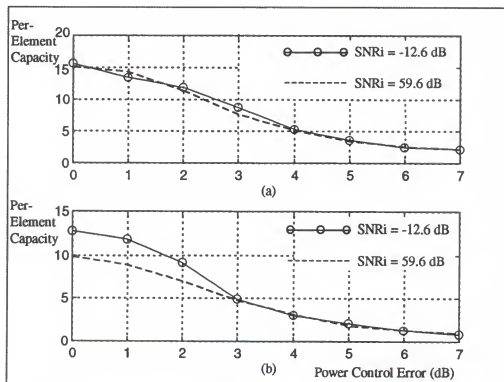


Figure 5.4 Per-element capacity (users/array element) versus power control error (dB) for an outage probability = 0.02. The upper plot is for the case of no outer cell interference. The lower plot includes outer cell interference.

Figure 5.5 below shows the per-element capacity from the simulated results of Figure 5.4b (with outer cell interference) and the approximation given in equation (5.2) with $\xi = 7$ dB and $Gp_i = 2$. Agreement between (5.2) and the simulated results for the case no outer cell interference was poor, and the results are not presented here. The value of Gp_i accounts for the fact that the output power of the outer cell interference is about equal to the output power of the inner cell interference when averaged over most of the possible combinations of user population, array elements and power control error. The rapid roll-off of the curve from equation (5.2) is due to the use of averaged multi-access interference when computing $(Eb/No)_{eff}$, as discussed in a previous section.

Figure 5.6 shows the per-element capacity resulting from the application of Wilkinson's method to model the multi-access interference as a sum of lognormal variables (equations (5.7) through 5.11)). The lognormal statistics of the inner cell interferers are assumed to be due to power control error only while the outer cell interference combines power control error and 8 dB of shadowing (x_m of equation (5.7) is $N(0, \sigma_{pcc}^2)$ while y_m is $N(0, \sigma_{pcc}^2 + 64)$). Simulations show that the average interference gain Gp_i for the inner cell interferers can vary from zero to unity depending on the number of elements, the number of users and the nominal input level. Interestingly enough, Gp_i does not seem sensitive to the power control error. Averaging over these conditions results in $Gp_i \approx 0.7$. The gain constant for the outer cell interferers - F of equation (5.7) - is taken to be unity. Simulations have shown that the array attenuates the interference so that the average output power due to the inner and outer cell interferers is about equal

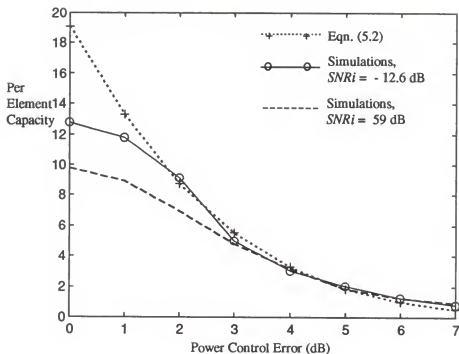


Figure 5.5 Per-element capacity versus power control error (dB) with outer cell interference. The capacity is from equation (5.2).

over many scenarios of interest. Interestingly enough, simulations show the ratio of the *incident* signal power from the outer cell and inner cell sources is 0.57.

The upper two plots of Figure 5.6 show that Wilkinson's method does not provide a particularly useful approximation when there is no outer cell interference. The lower two plots include the effects of outer cell interference and tend to agree more closely with simulated results for a range of power control error from 1 to 6 dB. For power control error = 7 dB the simulated per-element capacity is almost an order of magnitude greater than the analytical results.

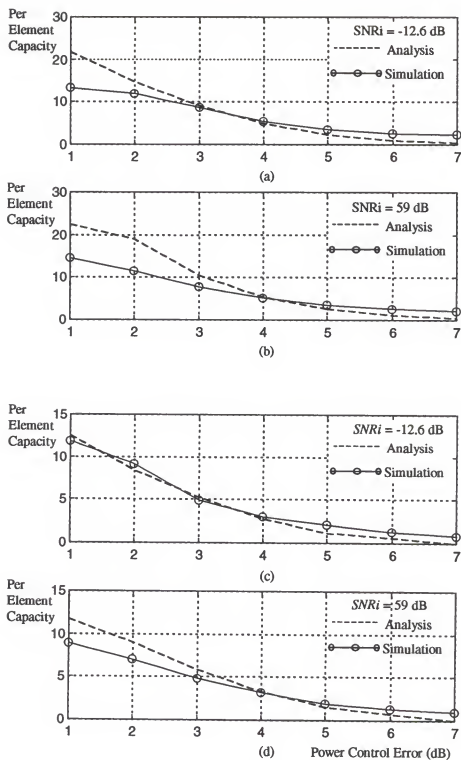


Figure 5.6 Per-element capacity versus power control error (dB) for outage probability = 0.02. Plots (a) and (b) are without outer cell interference. Plots (c) and (d) include outer cell interference. Curves from analysis result from equations (5.8) - (5.11).

Conclusions/Discussion

Simulations showed that even in the presence of multipath fading, the per-element outage-based capacity might serve as a useful performance measure for a wide range of conditions when considering a single-cell with multi-access interferers. As the nominal input levels increase for the multiple-cell case the per-element capacity deteriorates for pcc ≤ 3 dB compared to the single-cell case. The reason: for low nominal input levels the array treats the outer cell signals like AWGN. When the nominal input levels are high all interferers incident on the base station are well above the noise and the array must dedicate some processing to attenuate the outer cell interferers, at a loss in performance.

The simulated results presented in this chapter show that for low nominal input levels ($SNR_i = 7/127 = -12.90$ dB) and power control error ≥ 1.5 dB a single-cell system with multipath faded signals will have a higher per-element capacity than a system with directional, unfaded signals. The addition of outer-cell cochannel interference degrades the per-element capacity by about 80-90% for p.c.e. ≤ 2 dB and 60-70% for p.c.e. > 2 dB. For strong nominal input levels ($SNR_i = 59.6$ dB) the addition of outer cell interference degrades the per-element capacity by a factor of 2/3 to 3/4 for power control error ≤ 2.5 dB.

The two analytical models for per-element capacity gave mixed results. The model developed in Chapter 4 - which averaged multi-access interference - degrades too rapidly with increasing power control error to be of much use in a single-cell scenario. In a multi-cell scenario with low input levels the model gives a good fit to simulated results for power control error ≥ 1 dB. When input levels are high, the array output power due to the

outer cell interferers can be as much as twice the power of the inner cell interferers (there are 21.67 times more signals originating in the outer cells than the inner cells). This accounts for the decrease in the capacity in Figure 5.5 as the nominal input levels increase.

This model is limited in several ways. First, we are modeling the interference as an averaged quantity so the complex trial-to-trial interactions between the interference, the desired signal and the noise are lost. Second, we are attempting to absorb the relatively complicated behavior of the processor into two parameters, Gp_i and N , which do not vary with the number of users or the power control scenario.

The model based on Wilkinson's method of evaluating sums of lognormal random variables was introduced in an attempt to resolve the first of these two issues. It was hoped that the accuracy of the analytical model might be improved by approximating the interference as a sum of variables rather than an average. The plots in Figure 5.6 show that this model might offer some improvement in accuracy - compared to simulations - for the select case of multiple cells. If more accuracy is required for the case of a single-cell system or power control > 6 dB, then refinements of the models would be necessary.

Summary

This chapter presented simulation results of the outage-based capacity for incident signals subjected to frequency-nonselective Rayleigh multipath fading and lognormally distributed power control error. The models included single-cell and multi-cell scenarios where outer cell interferers were subjected to lognormal shadow fading. The multipath fading model assumed that the spatial interactions between the faded incident signals and the antenna array allowed the fading process to be fully decorrelated between array

elements. Under these conditions the array functioned as a diversity combiner rather than a beamforming antenna array.

The per-element capacity - the number of users/array element which may be supported for a required outage probability - was evaluated via simulations. The motivation behind the use of per-element capacity was to find a performance measure which was robust to the variations in user population and array size and which would reflect the possible contributions a receiving array would make to the capacity of a power-controlled CDMA system.. An additional goal was to formulate approximations which would allow easy assessments of the per-element capacity.

Physical arguments in conjunction with semi-empirical curve fits resulted in two analytical models. The first model was adapted from the model in Chapter 4 in which the signal, the interference and the noise were averaged. The complex interactions between even these quantities was overlooked for the sake of simplicity. Array outputs were modeled as averages of input quantities and gain constants. Values of these constants were derived empirically from simulations.

The second model exploited Wilkinson's method of approximating lognormal variables so that averaging of the interference could be avoided. This model resulted in slightly improved accuracy - compared to the first model - for power control error ≤ 2 dB but was somewhat worse for power control error ≥ 6 dB.

CHAPTER 6

BASE STATION ANTENNA ARRAY ADAPTIVE PERFORMANCE

This chapter examines the steady-state performance of the Recursive Least Squares (RLS) adaptive algorithms for a base station diversity array receiving faded incident signals with power control error. A simulation approach is used since the scenarios are too complicated to allow useful analytical solutions. The simulations were discrete-event simulations of transmitted bits through a nonstationary AWGN channel with time-varying multipath fading as well as stationary power control error and shadow fading. The simulation results will be given in terms of histograms of the effective E_b/N_0 which can facilitate outage calculations. The performance of an RLS array in the presence of cochannel interference has been examined by several authors,^{67,72,73} but of these only Tsoulos et al.⁶⁷ considered near/far scenarios with fading and outer cell interference. They used simulations to determine the outage probability when the ($N = 8$) array functioned as a beamformer, not a diversity combiner.

Simulation results show that the RLS algorithm can track the time-varying solution effectively and that the adaptive solution is close to the steady-state solution. The structure of this chapter is similar to the two previous chapters. The first section revisits the now-familiar signal model from previous chapters and also introduces the time-dependent fading process. Approximations of the fading process used in this research are also presented. The second section outlines the RLS adaptive algorithms and the receiver

structure used in the simulations. The third section gives the results of the discrete-event simulations and provides some discussion. The last section gives the conclusions.

Signal and Channel Model

The signal model is the same as in the previous chapter:

$$\underline{Y}(t) = A \sum_{m=1}^K 10^{\epsilon_m/20} \cdot c_m(t - \tau_m) b_m(t - \tau_m) \mathbf{u}_m + \sum_{n=1}^{K \cdot N_{oc}} A_n \cdot 10^{\epsilon_n/20} \cdot \left(\frac{10^{\epsilon_n/20}}{r_{n,o}^4} \right) \cdot c_n(t - \tau_n) b_n(t - \tau_n) \mathbf{u}_n + \mathbf{n}(t) \quad (6.1)$$

where the first summation is for center-cell and the second summation (with index n) results from the outer-cell interference when it is taken into account. Power control error and shadow fading are lognormally distributed (e_x is $N(0, \sigma_{pce}^2)$, s_x is $N(0, 64)$). The quantity N_{oc} is the number of outer cells while K remains the number of users/cell. The quantity r_n^4 is the distance-dependent, fourth-order propagation loss between the n th interferer and the center cell base station. As in Chapter five the amplitude A_n accounts for the hand-off with the least path loss when outer cell interference is taken into account. The quantities $c_n(\cdot)$ and $b_n(\cdot)$ represent the spreading code and the BPSK modulation with ideal, square pulses. We assume the beginning and end of a PN sequence corresponds to the beginning and end of an information bit. In this chapter the PN sequences, no longer random, are Gold codes of length 127. The quantity $\mathbf{n}(t)$ is a vector of complex AWGN with power σ_n^2 which is temporally and spatially white. The power control error and shadow fading are assumed to be constant over the observed interval.

Time-varying, flat Rayleigh fading, is introduced into the incident signals by the phase-shift vectors \mathbf{u}_m and \mathbf{u}_n . The fading process is independent between array elements (spatial samples) but is correlated between time samples. The time autocorrelation function is given by:

$$R(\tau) = J_0(\omega_D \tau) \quad (6.2)$$

where ω_D is the Doppler frequency in radians/sec., τ is a time delay and $J_0(\bullet)$ is a Bessel function of the first kind with order zero. The Doppler frequency arises from relative motion between the signal source and the observation point; it represents a velocity-induced shift in the signal carrier frequency. The Doppler frequency is given by $\omega_D = kv$ where k is the free-space wave number ($k = 2\pi/\lambda$) and v is the relative velocity.

The fading of the incident signals was accomplished by superimposing a time-varying complex Gaussian component on the time-dependent data waveforms. The fading component was generated by a third-order autoregressive (AR) filter. The filter response to white noise has an autocorrelation function with a damped sinusoid characteristic which has been adjusted to closely match the major lobe and first minor lobe of the Bessel function in equation (6.2). The impulse response of the filter is given by:¹¹⁷

$$h(t) = \left(e^{-0.91f_D t} \left[2.66f_D \sin(5.15f_D t) - 3.17f_D \cos(5.15f_D t) + 3.17e^{-5.23f_D t} \right] \right) u(t) \quad (6.3)$$

where f_D is the Doppler frequency in hertz and $u(t)$ is a step function at $t = 0$. The filter is used in the following manner. First, complex white Gaussian noise is processed with the filter specified in equation (6.3). The data waveform is then multiplied point-by-point by

the filter output to simulate the fading process. This approach preserves the salient properties of the fading and allows an efficient simulation procedure.

Adaptive Receivers

The RLS processor has an advantage over the LMS algorithm in that its convergence rate is not dependent upon the eigenvalue spreads of \mathbf{R} , the input autocorrelation matrix. The disadvantage of this algorithm is that the computational burden ($O(N^2)$) is relatively large compared to the computationally efficient Least-Mean-Squares (LMS) algorithm. Unfortunately an LMS array cannot track the time-dependent fading, especially at higher vehicle speeds.⁴⁵

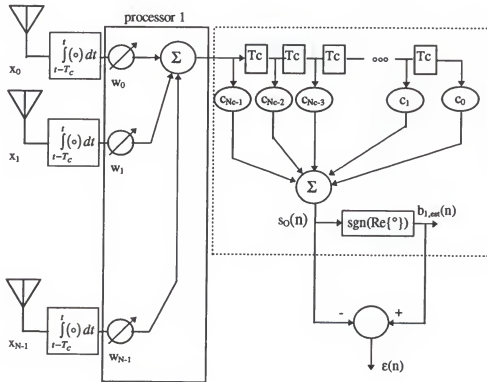


Figure 6.1 Adaptive array with a discrete-time conventional detector.

The discrete-time adaptive receiver structure for user 1 is shown in Figure 6.1 below. The outputs of the antenna elements are passed through integrate-and-dump filters matched to the chip transitions of the desired signal waveform. The sensor array outputs are then weighted and summed. The array output is passed through a discrete-time version of a conventional detector which consists of a delay-line filter with N_c discrete time-delay elements each with a duration of one chip (dotted box). Once every bit the contents of the delay line are weighted by the elements of the PN sequence ($\mathbf{c}_1 = [c_1^0 \ c_1^1 \ c_1^2 \dots c_1^{N-1}]^T \in \{1, -1\}$) of the desired signal and summed to form the output. The estimate of the current output bit is taken as $b_{1,est}(n) = \text{sign}(\text{Real}\{s_{o,1}(n)\})$. The array weights are updated once a bit. For the n th bit interval the input of the array and the weights are given by:

$$\mathbf{w}(n) = [w_0(n) \ w_1(n) \ \dots \ w_{N-1}(n)]^T \quad (6.4)$$

$$\mathbf{X}(n) = \begin{bmatrix} x_0^0(n) & x_0^1(n) & \dots & x_0^{N_c-1}(n) \\ x_1^0(n) & x_1^1(n) & \dots & x_1^{N_c-1}(n) \\ \vdots & \vdots & \ddots & \vdots \\ x_{N-1}^0(n) & x_{N-1}^1(n) & \dots & x_{N-1}^{N_c-1}(n) \end{bmatrix}$$

where $x_g^m(n)$ represents the array input at the g th element during the m th chip interval of the n th bit. The inputs are processed by the integrate-and-dump filters. The input to the bank of weights is given by:

$$\mathbf{Y}(n) = \begin{bmatrix} \int_{nT-T_c}^{nT} x_0^0(n) dt & \int_{nT-2T_c}^{nT-T_c} x_0^1(n) dt & \dots & \int_{nT-N_c T_c}^{nT-(N_c-1)T_c} x_0^{N_c-1}(n) dt \\ \vdots & \vdots & \ddots & \vdots \\ \int_{nT-T_c}^{nT} x_{N-1}^0(n) dt & \int_{nT-2T_c}^{nT-T_c} x_{N-1}^1(n) dt & \dots & \int_{nT-N_c T_c}^{nT-(N_c-1)T_c} x_{N-1}^{N_c-1}(n) dt \end{bmatrix} \quad (6.5)$$

The inputs are weighted and summed by the array and the resulting output stream is

weighted and summed by the tapped delay-line. The array/detector attempts to minimize the output error:

$$\begin{aligned}\varepsilon(n) &= b_{1,est}(n) - \mathbf{w}^T(n)\mathbf{Y}(n)\mathbf{c}_1 = b_{1,est}(n) - \mathbf{w}^T(n)\mathbf{z}(n) \\ \mathbf{c}_1 &= [c_1^0 \quad c_1^1 \quad \cdots \quad c_1^{N_c-1}]^T\end{aligned}\tag{6.6}$$

where the random variable is $\mathbf{z}(n) = \mathbf{y}(n)\mathbf{c}_1$. A single element of $\mathbf{z}(n)$ is the inner product between the output of one array element - filtered chip-by-chip over the bit interval - and the desired user's PN sequence \mathbf{c}_1 . The vector $\mathbf{z}(n)$ will be the sample vector over which the adaptive filter operates.

The RLS algorithm recursively computes an estimate of the optimum weight vector \mathbf{w}_0 . The recursive equations are given by (version 2, Haykin.²²):

$$\begin{aligned}\mathbf{k}(n) &= \frac{\gamma^{-1}\mathbf{R}^{-1}(n-1)\mathbf{z}(n)}{1 + \gamma^{-1}\mathbf{z}^H(n)\mathbf{R}^{-1}(n-1)\mathbf{z}(n)} \\ \alpha(n) &= r(n) - \tilde{\mathbf{w}}^H(n-1)\mathbf{z}(n) \\ \tilde{\mathbf{w}}(n) &= \tilde{\mathbf{w}}(n-1) + \mathbf{k}(n)\alpha^*(n) \\ \mathbf{R}^{-1}(n) &= \gamma^{-1}\mathbf{R}^{-1}(n-1) - \gamma^{-1}\mathbf{k}(n)\mathbf{z}^H(n)\mathbf{R}^{-1}(n-1)\end{aligned}\tag{6.7}$$

where $\alpha(n)$ is the a priori estimation error and is an estimate of the error between the current value of the reference signal $r(n)$ and the output based on the previous value of the weight vector at iteration $n-1$. The weight vector is updated by the product of $\mathbf{k}(n)$ and the a priori estimation error. The vector $\mathbf{k}(n)$ may therefore be interpreted as a gain vector and is sometimes called the *Kalman gain*. Note that the matrix inverse is updated recursively, rather than by a block computation.

The quantity γ serves to exponentially window the data. Eleftheriou and Falconer¹¹⁸ investigated the influence of γ in the adaptation process. They examined the role of γ on the total misadjustment, the sum of the “estimation noise,” which results in the displacement of the filter weight vector from the optimum value, and the “lag error” which occurs when the filter tries to track channel nonstationarities. Too large a value of γ will cause a filter to use outdated statistics when tracking channel nonstationarities. An excessively small value of γ will allow fast adaptation but will cause too little information to be used in the adaptation process and result in excessive misadjustment. In this work the selection of γ was empirical. More details will be given in the next section.

In the adaptive receiver shown in Figure 6.1 the bit estimate $b_{est}(n)$ serves as the reference signal $r(n)$ for the RLS processor. The structure shown is for decision-directed operation only. Training and transient response issues as well as issues arising from fixed-point arithmetic were not addressed by this research.

Simulations

Monte Carlo simulations were conducted for the discrete-event case. Rather than examining exhaustive combinations of power control error, user populations and array sizes, discrete-event simulations focused on a few combinations of these quantities in an effort to show that the adaptive solution does not differ appreciably from the steady-state results presented in an earlier chapter.

Results in this chapter are presented in terms of the histograms of the $(Eb/No)_{eff, dB}$. When $(Eb/No)_{eff}$ is tabulated in dB units for many trials the resulting histogram is

approximately Gaussian but contains some slight asymmetries. This result is not surprising considering that the mean incident signal amplitudes are lognormally distributed.^{115,116} Some authors have found that a sum of lognormally distributed random variables is well-approximated by another lognormally distributed random variable.

All signal sources were assumed to have velocities of 55 mph relative to the base station. This corresponds to a Doppler frequency of 74 Hz. A real mobile communication system must cope with multiple signals Doppler-shifted over a range of values: zero for a car sitting still or 114 Hz for a driver going 85 mph. Note that the Doppler frequency or frequencies could have an appreciable impact on the selection of γ_R , the RLS memory factor.

Incident signal levels were modeled via the signal description given earlier in the chapter (equation (6.1)). All incident signals consisted of random, equally-likely BPSK bits (rate = 9600 bits/sec) which were spread with Gold codes of length 127 and chip-filtered via the integrate-and-dump filters of Figure 6.1. The effects of multipath fading were introduced via u_m and u_n - the independent array samples - in equation (6.1) and the multipath fading simulator described in an earlier section. The fading was generated at the chip rate and was not considered constant over a bit interval. A single *scenario* consisted of multiple signal vectors of 51 bits in which power control error and shadow fading were constants and only the multipath fading component of the incident signals varied with time.

The RLS processor was modeled via equation (6.4) above. In order to avoid transient-related issues the initial weight vector for the RLS algorithm was the steady-state

MMSE weight vector averaged over the first bit. Output signals were then tabulated over the next 50-bit interval and $(Eb/No)_{eff}$ was calculated for each single bit. Six hundred scenarios for a total of 30,000 RLS-adapted bits were simulated. The nominal input SNR is $= -12.6$ dB.

The choice of γ was made empirically. A scenario was considered with 5 inner-cell

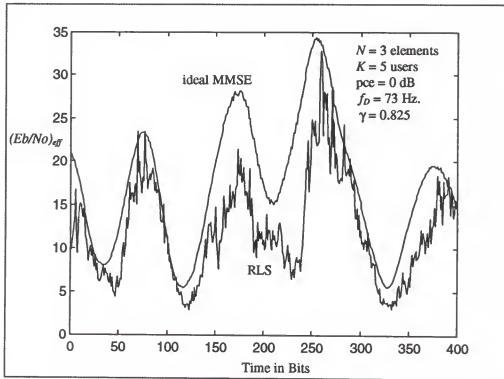


Figure 6.2 The time-varying $(Eb/No)_{eff}$ for an RLS processor and an ideal MMSE processor. There are 5 users with $pce = 0$ dB incident on a 3-element array. The Doppler frequency is 73 Hz. and γ is 0.825

users with $pce = 0$ dB subjected to multipath fading. The $(Eb/No)_{eff}$ was tabulated on a bit-by-bit basis for an interval of 400 bits using the output of an RLS processor $((Eb/No)_{eff,RLS})$ and the output of an ideal MMSE $((Eb/No)_{eff,MMSE})$ processor. For these conditions a value of $\lambda_R = 0.82$ was found to minimize the quantity:

$$\text{avg}\left[\left(\varepsilon_{RLS}\right)^2\right] = \frac{1}{400} \sum_{n=1}^{400} \left(\left(\frac{Eb}{No} \right)_{\text{eff},RLS} - \left(\frac{Eb}{No} \right)_{\text{eff},MMSE} \right)^2 \quad (6.5)$$

and was used to produce the results that follow. Figure 6.2 shows the time-varying $(Eb/No)_{\text{eff}}$ for the ideal MMSE processor and the RLS processor over the 400-bit interval.

The results of simulations for 5 users with $\sigma_{\text{pcc}} = 0$ dB is shown in Figure 6.3 below.

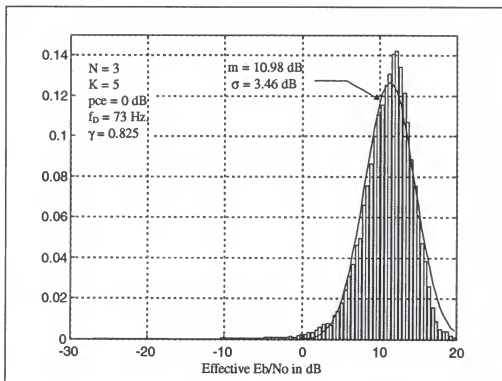


Figure 6.3 Bar chart of histogram of $(Eb/No)_{\text{eff}}$ in dB. The solid line curve outlines a Gaussian pdf with mean = 10.98, st. dev. = 3.46. There are 5 users with $\text{pcc} = 0$ dB incident on a 3-element array. The Doppler frequency is 73 Hz, and γ is 0.825.

The plot shows a bar-chart histogram of $(Eb/No)_{\text{eff}}$ in dB. Superimposed on this is Gaussian curve with mean and standard deviation taken as sample means ($m = 10.98$, $\sigma = 3.46$) from the data which generated the histogram. The match between the curves is good except for the peak and the tail regions. Unfortunately, the lower tail region is critical for

outage calculations and the poor fit might prevent accurate results if a lognormally distributed output is assumed and the outage probability is low.

Another interesting feature of Figure 6.3 is the slight asymmetry between the upper tail regions of the bar-chart curve. The asymmetry is also present in histograms generated by steady-state simulations. Using the histograms to calculate the outage probability gives $\Pr((Eb/No)_{eff} \leq 7 \text{ dB}) = 0.105, .125$ for the bar-chart and Gaussian curve respectively. Under the same conditions an ideal MMSE processor gave a mean output of $(Eb/No)_{eff} = 12 \text{ dB}$, a standard deviation of 3.27 dB and $\Pr((Eb/No)_{eff} \leq 7 \text{ dB}) = 0.066$. Figure 6.4 shows the same conditions except that power control error has been increased to 4 dB. Note that the mean is only slightly decreased to 10.7 but the standard deviation is increased to 5.37.

Histograms which include the effects of outer cell interference are shown below. Figure 6.5 shows the histogram of $(Eb/No)_{eff}$ for the case of perfect power control in which outer cell users are subjected to 8 dB of lognormal shadow fading. The assignment of the power levels for the outer cell users is the same as described in Chapter 5. As in the previous plots a Gaussian distribution with the same mean and variance as the bar chart histogram is shown. The mean ($\approx 10.6 \text{ dB}$) decreased slightly compared to the case of no outer cell interference ($\approx 10.98 \text{ dB}$). The standard deviation ($\approx 3.33 \text{ dB}$) decreased slightly from a value of 3.46 dB for no outer cell interference. Using the empirical histogram results in an outage probability of $\Pr((Eb/No)_{eff} \leq 7 \text{ dB}) = 0.15$, a slight increase compared to the case of no outer cell interference. This seems to agree with the general trends noted in the steady-state results which show only a slight degradation in

capacity when outer cell interference is included. The case of $p_{ce} = 4$ dB is shown in Figure 6.6. The mean of the empirical bar-chart histogram is 9.75 dB and the standard deviation is 5.17 dB. Unlike the previous figures, these curves resulted from 10000 bits of data.

Conclusions/Summary

This chapter has examined via simulation the outage performance of an adaptive diversity antenna array updated with the RLS algorithm. The output performance was tabulated by histograms of $(Eb/No)_{eff}$ in dB. The adaptive performance did not vary drastically from the steady-state performance. It appears that the RLS algorithm operating in a decision-directed mode is capable of tracking the time-varying channel when Rayleigh multipath fading is present.

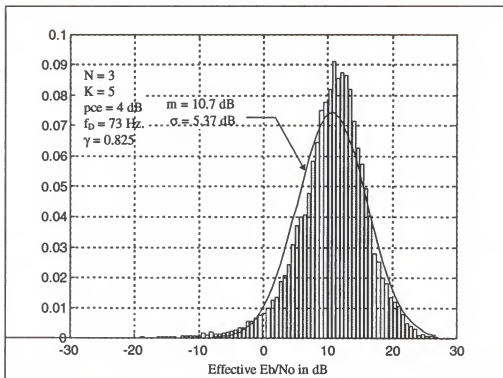


Figure 6.4 Bar chart of histogram of $(E_b/N_0)_{eff}$ in dB. The solid line curve outlines a Gaussian pdf with mean = 10.98, st. dev. = 3.46. There are 5 users with $pce = 4$ dB incident on a 3-element array. The Doppler frequency is 73 Hz. and γ is 0.825.

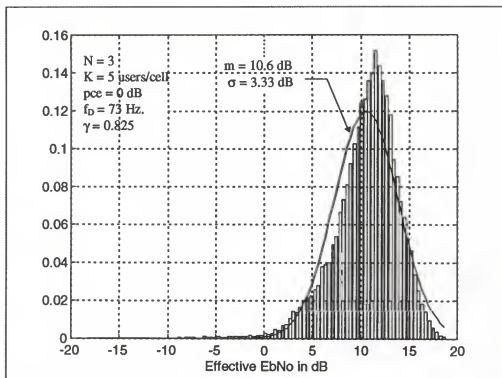


Figure 6.5 Bar chart of histogram of $(E_b/N_0)_{eff}$ in dB for the case of outer cell interference. The solid line curve outlines a Gaussian pdf with mean = 10.6, st. dev. = 3.33. There are 5 users with $p_{ce} = 0$ dB incident on a 3-element array. The Doppler frequency is 73 Hz. and γ is 0.825.

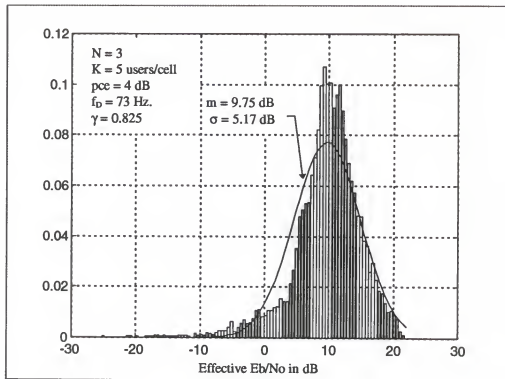


Figure 6.6 Bar chart of histogram of $(E_b/N_0)_{eff}$ in dB for the case of outer cell interference. The solid line curve outlines a Gaussian pdf with mean = 9.75, st. dev. = 5.17. There are 5 users with pce = 4 dB incident on a 3-element array. The Doppler frequency is 73 Hz, and γ is 0.825.

CHAPTER 7

SUMMARY

In this work we have examined the possible performance contributions that adaptive antenna arrays can make to DS-CDMA base station performance. This final chapter will provide a results-oriented summary of the previous chapters. In addition, a section entitled Areas for Future Work will outline some of the issues which have arisen during this research which are related to array processing and channel modeling.

The system model has consisted of an array of antennas whose weights are controlled by a MMSE processor. This work has examined two system configurations. First, a multi-user antenna array was investigated which consisted of an array of sensors and a single beamforming processor. The processor with a single set of weights attempted to equalize the multiple incident signals. The second structure used an array of sensors which was shared by multiple processors, each dedicated to a single incident signal. Each distinct output fed a DS conventional detector.

Chapter two examined the steady-state performance of the multi-user processor. Unlike most analyses of MMSE filters, this analysis focused on output SNR as the performance measure. First, the case of $K \leq N-1$ spatially orthogonal users was examined, followed by the case of 2 incident signals with an unspecified DOA spacing. The analysis showed that for strong incident signals the output SNRs of the various signals were leveled to a value near that of the weakest user.

Chapter three investigated the steady-state adaptive performance of an LMS multi-user processor and attempted to establish a link between the misadjustment of the LMS algorithm and the output SNR performance. The performance was determined by examining first two moments of the output SNR. The first performance measure was a cost function based of the difference between the mean SNR response of the processor and the steady-state output performance. An upper bound for the cost function was formulated which limited the excursion of the mean output SNR from the ideal steady-state value. The second cost function was the quotient of the output variance and the mean squared. Analysis and simulations showed that both cost functions were found to be held to acceptable limits if the step size was selected using the well-known rules based on convergence arguments of the LMS algorithm.

Chapter four examined the steady-state performance of a single-user processor. The performance for this and the remaining chapters was judged on the ability of the array to recover the desired signal and reject multi-access interference. This chapter attempted to provide some insight into the contributions an array could make to the base station receiver performance when multi-access users limited their transmit power via imperfect power control. Rather than performing a rigorous analysis, an approximate analysis - which replaced the interference response with its average - resulted in simple expressions for the outage-based capacity. The outage-based capacity was found to be linear in a quantity which was the product of the processing gain and the number of array elements. A robust performance measure - per-element capacity - was defined as the slope of this line with the processing gain held constant. Analytical results were corroborated with exhaustive simulations.

The next chapter introduced multipath fading and outer cell interference into the steady-state channel model. The approximate analysis based on the techniques of chapter four gave mixed results. The approximate analytical model based on techniques from Chapter four did not provide a good fit to simulated results for the per-element capacity in the case of a single cell. The same model agreed well with simulated results for the multiple-cell case as long as the power control error exceeded 2 dB and the nominal input level was low ($SNR_i = -12$ dB). Another model was introduced which approximated the array gain by an average. The incident signals themselves were modeled using Wilkinson's method of approximating sums of lognormal variables. The resulting expressions for the per-element capacity were more accurate than the models from chapter four, for the faded-signal case. When the asymptotic case of strong incident signals was considered, the analytical expressions for per-element capacity gave slightly optimistic results compared to simulations for power control error less than 4 dB.

Chapter six examined the adaptive performance of the MMSE processor via simulation using the RLS algorithm. Performance was expressed through histograms of $(E_b/N_0)_{eff,AB}$ and Gaussian curves with same mean and variance as the simulated data. It was found that the mean and variance of the adaptive results agreed closely with those of the steady-state simulated results. Unfortunately, the histograms were slightly skewed, with the peak higher than the sample mean and a lower tail more pronounced than the upper tail. The output was not exactly lognormal and that the skew might prevent accurate analytical assessments of outage performance if the outage probability is small.

Areas for Future Work

Two issues have arisen during the course of this research which might warrant further investigation. The first issue is the application and extension of previous work to provide rigorous, useful measures of array performance, particularly when the number of users is large. The second is the extension of existing channel models to include the effects of spatially-dependent multipath fading.

This research provided semi-empirical approximations as convenient - but limited - measures of outage-based performance. A more rigorous analysis is warranted. The analysis might best focus on the joint statistics of the desired signal, the multi-access interference and the noise. One possible approach is to find the pdf of the SINR:

$$SINR = \mathbf{s}^T \mathbf{Q}^{-1} \mathbf{s}^* = tr(\mathbf{s}^* \mathbf{s}^T \mathbf{Q}^{-1}) \quad (7.1)$$

where \mathbf{Q} is the covariance matrix and \mathbf{s} is the signal vector of the desired signal. If signals are subjected to independent Rayleigh fading then phase-shift vectors will consist of zero mean jointly Gaussian i.i.d. elements. The joint distribution of the multi-access interference components of \mathbf{Q} are known to be Wishart distributed.¹¹⁹ It might be possible to formulate a pdf using these statistical relationships. This problem was noted, but not solved, by Dlugos and Scholtz.¹²⁰

Using previous work resulting from investigations into the Sample Matrix Inverse processor (SMI) might provide a good starting point. The SMI processor uses a sample-mean estimate of the covariance matrix \mathbf{Q} :

$$\hat{\mathbf{Q}} = \frac{1}{M} \sum_{m=1}^M \mathbf{x}_m \mathbf{x}_m^T \quad (7.1)$$

to compute an estimate of the weights, $\hat{\mathbf{w}}_0 = \hat{\mathbf{Q}}^{-1}\mathbf{s}^*$, where \mathbf{x}_m is the array output vector of jointly distributed complex i.i.d. $N(0, \sigma_x^2)$ variables at the m th time sample. The vector \mathbf{s} is the N -length, phase-shift vector of the desired signal and consists of unit-amplitude, complex exponentials. Obviously $M > N$ so that $\hat{\mathbf{Q}}$ is full rank. Previous work has examined the relationship between the window length M and functions and various functions of the output power for stationary^{121,122} and nonstationary noise.¹²³ It has been shown that the output SINR normalized by its steady-state value is a random variable with a beta distribution¹²¹ for the case of stationary noise.

Reinterpreting this previous work may lead to some convenient results for diversity combining. Recall that the samples that led to $\hat{\mathbf{Q}}$ were interpreted as samples of the Gaussian, zero-mean interference and noise. If the samples are instead phase-shift vectors of Rayleigh-faded multi-access interferers, then $\hat{\mathbf{Q}}$ may still be interpreted as a sum of outer products of jointly Gaussian vectors. The results of some previous radar-oriented research might be reinterpreted in terms of diversity combining. If a meaningful, unambiguous measure of the output SINR of an optimum combining array is possible, based on previous results, it might provide a robust solution to the problem of calculating array performance when the number of users exceeds the number of array elements. This is currently an active area of research.^{124,125}

The second area of future work is the extension of general channel models to include the effects of spatially-dependent multipath fading. A great deal of work has been done in the area of temporal single-channel fading models but relatively few models exist which include spatial effects for multi-channel receivers. The interest in antenna arrays as a

component in commercial communication systems has grown quickly in recent years. Unfortunately, developments in array theory have outpaced the channel models. For antenna arrays to reach their full potential as a communication system component accurate, useful models must be developed which provide a unified, integrated description of the temporal and spatial characteristics of the channel.

One such model is an extension of the single-channel with multipath fading which assumes that multiple plane waves originate from the same source but arrive at a point in space via different paths. In the single-channel model the effects of the individual waves are modeled by “rays” which result in a Rayleigh-distributed amplitude and can result in relative time delays between same-source arrivals. This model has been crudely extended to include spatial effects by assuming individually faded, dominant rays arrive at points in space from different directions. This type of model focuses on the distribution of large, dominant reflectors in the environment about the receiver but ignores the smaller-scale spatial effects at the receiver itself. This is the basis of ray tracing techniques^{126,127} which use site-specific measurements to predict path loss. Even current ray-tracing models focus on single-channel measurements of power-delay profiles. This gives a macroscopic description of the transmission amplitude versus delay but ignores local spatial characteristics at the receiver.

Other models have also been proposed which describe the impact of the spatial channel locally at the receiver but do not consider the surrounding environment. Salz and Winters¹⁰⁹ examined the effects of a continuum of wavefronts with a nonzero DOA spread on the crosscorrelations between array elements. As an example, the simple fading model used in this research assumes the crosscorrelations are zero. Raleigh et al.¹¹⁰ have also

proposed a time/space model to describe the effects of multipath on the spatial samples from an array. There is plenty of room for additional local models which incorporate space/time descriptions for an array-based receiver.

These models seem like a first tentative step towards a unified channel description. Local receiver models need to be integrated into the larger-scale models of the surrounding environment. This may dictate new, or at least more detailed, descriptions of the processes which comprise the unified time/space channel.

APPENDIX A

THE OUTPUT SNR PERFORMANCE SURFACE

This appendix gives some of the general aspects of the output SNR as a performance surface. There are some important differences between the MSE and the SNR performance surfaces. Some general qualities of the surface in weight-space are noted, such as the contours and the gradient, along with the impact of misadjustment on the multi-user processor.

The best way to get an intuitive feel for the SNR performance of an MMSE processor is to examine the case of a single user in additive white Gaussian noise. The weight-space diagram for a single-user case is shown in the figure below. The elliptical curves are the customary constant MSE contours and the straight lines represent contours of constant output SNR. Notice that the constant SNR contours are lines which pass through the origin and only the slopes change with changing SNR_o. As the weight vector moves away from the MMSE weight vector, \mathbf{w}_o , the output SNR decreases from the maximum output SNR_{o_{max}} = NSNR_i (= 20 for this scenario). As the MSE increases the output SNR decreases.

For a single user, two-weight array the relationship between SNR_o and the weights is easily shown through the relationship:

$$SNR_o + 1 = \frac{\mathbf{w}^T \mathbf{R} \mathbf{w}^*}{\sigma_n^2 \mathbf{w}^T \mathbf{w}^*} = \frac{\mathbf{w}^T \mathbf{M} \mathbf{L} \mathbf{M}^H \mathbf{w}^*}{\sigma_n^2 \mathbf{w}^T \mathbf{w}^*} = \frac{\mathbf{v}^T \mathbf{L} \mathbf{v}^*}{\sigma_n^2 \mathbf{v}^T \mathbf{v}^*} \quad (\text{A.1})$$

Where \mathbf{L} and \mathbf{M} are the eigenvalue and eigenvector matrices of \mathbf{R} respectively. The

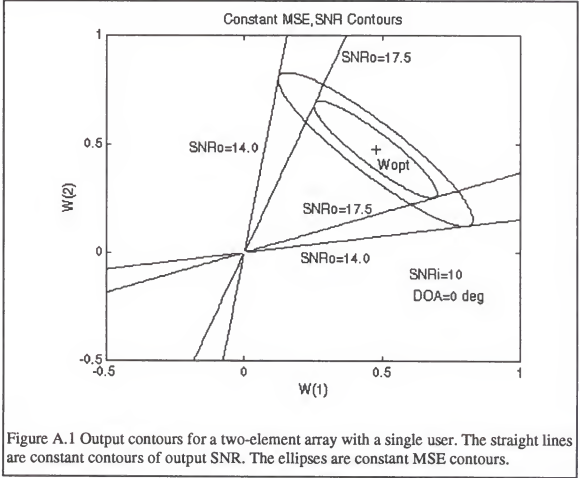


Figure A.1 Output contours for a two-element array with a single user. The straight lines are constant contours of output SNR. The ellipses are constant MSE contours.

equation for the constant-value contour is $\mathbf{v}^H \mathbf{L} \mathbf{v} - \sigma_n^2 (SNR_o + 1) \mathbf{v}^H \mathbf{v} = 0$.

For a single user in AWGN the eigenvalues are $\lambda_1 = \sigma_n^2$, $\lambda_2 = A^2 + \sigma_n^2$, and the two weights in the rotated coordinate system are related by the expression:

$$v_1 = \pm v_2 \sqrt{\frac{SNR_o}{SNR_i - SNR_o}} \quad (A.2)$$

which is a set of lines in two-dimensional, rotated weight-space. The SNR surface in weight-space is concave. These relationships have been attributed to Winkler,¹²⁸ but the original reference does not seem to be available. In the two-dimensional system shown in

the figure above the major axis of the constant MSE ellipse is parallel to the noise-only eigenvector and the ellipse minor axis is parallel to the signal and noise eigenvector. The optimum MMSE weight vector \mathbf{w}_o will be almost orthogonal to the noise-only eigenvector.

The gradient of the output SNR is given by:

$$\nabla_{\mathbf{w}} SNRo = \frac{2SNRo}{\|\mathbf{w}\|^2} \left[\mathbf{u} \mathbf{u}^T - \frac{SNRo}{SNRi} \mathbf{I} \right] \mathbf{w} \quad (\text{A.3})$$

where \mathbf{u} is the phase-shift vector defined in equation (1.4) and \mathbf{I} is the identity matrix. It might be argued that the norm of the gradient of SNRo is a measure of the local variations of the SNRo function in weight-space. The Laplacian is the norm-squared of the gradient:

$$\|\nabla_{\mathbf{w}} SNRo\|^2 = \frac{4SNRo}{\|\mathbf{w}\|^2} [NSNRi - SNRo] \quad (\text{A.4})$$

Some things to note here are that the norm of the gradient is zero when the output SNR is maximum (= NSNRi) and that the gradient norm decreases as the weight vector norm increases. It is possible to express output SNR in weight-space angles:

$$SNRo = SNRi \frac{|\mathbf{w}^T \mathbf{u}|^2}{\|\mathbf{w}\|^2} = N \cdot SNRi \cos^2 \alpha \quad (\text{A.5})$$

where α is the angle between \mathbf{w} and \mathbf{u} in weight space. If equation (A.5) is substituted into equation (A.4) the norm-squared of the gradient becomes:

$$\|\nabla_{\mathbf{w}} SNRo\|^2 = \left[\frac{1}{\|\mathbf{w}\|} \frac{dSNRo}{d\alpha} \right]^2 \quad (\text{A.6})$$

This relationship is apparent in Figure (A.1) above, variations in SNRo occur when the weight vector is displaced in angle α from the phase-shift vector (which is collinear with \mathbf{w}_o in the figure).

For a two-user system with a weak user (1) and a strong user (2) the optimum weight is almost collinear with the weaker user's phase-shift vector. Perturbations from the steady-state weight vector, caused by the noisy gradient estimates of the LMS algorithm, will have little effect on the weaker user since α_1 (the angle between \mathbf{u}_1 and \mathbf{w}_o) is small. Or, put another way, the difference term in the brackets of equation (A.4) is small since $SNRo_1 \approx NSNR_{i1}$, and the resulting variations are small. For a strong user, the difference in the bracketed term may be large since $SNRo_2 \approx SNRo_1$ and the weight variations may cause the large fluctuations in the strong user's output.

LIST OF REFERENCES

- ¹ R. A. Scholtz, "The Origins of Spread-Spectrum Communications," IEEE Transactions on Communications, Vol. COM-30, No. 5, pp. 822-854, May 1982
- ² A. J. Viterbi, "The Evolution of Digital Wireless Technology from Space Exploration to Personal Communication Services," IEEE Transactions on Vehicular Technology, Vol. 43, No. 3, pp. 638-644, August 1994
- ³ D. L. Schilling, "Wireless Communications Going into the 21st Century," IEEE Transactions on Vehicular Technology, Vol. 43, No. 3, pp. 645-652, August 1994
- ⁴ R. L. Pickholtz, L. B. Milstein, D. L. Schilling, "Spread Spectrum for Mobile Communications," IEEE Transactions on Vehicular Technology, Vol. 40, No. 2, pp. 313-321, May 1991
- ⁵ W. C. Y. Lee, "Overview of Cellular CDMA," IEEE Transactions on Vehicular Technology, Vol. 40, No. 2, pp. 291-302, May 1991
- ⁶ TIA/EIA IS-95, "Mobile Base-Station Compatibility Standard for Dual-Mode Wideband Spread-Spectrum Cellular Systems," Telecommunications Industry Association, July 1993
- ⁷ R. Padovani, "Reverse Link Performance of IS-95 Based Cellular Systems," IEEE Personal Communications, Vol. 1, No. 3, pp. 28-35, Third Quarter 1994
- ⁸ A. J. Viterbi, "The Orthogonal-Random Waveform Dichotomy for Digital Mobile Personal Communication," IEEE Personal Communications, Vol. 1, No. 1, pp. 18-24, First Quarter 1994
- ⁹ S. C. Swales, T. Busby, D. J. Purl, M. A. Beach, J. P. McGeehan, "A Comparison of CDMA Techniques for Third Generation Mobile Radio Systems," Proceedings of the 43rd IEEE Vehicular Technology Conference, Seacaucus, New Jersey, May 1993, pp. 424-427
- ¹⁰ M. Ewerbring, B. Gudmundson, P. Teder, P. Willars, "CDMA-IC: a Proposal for Future High Capacity Digital Cellular Systems," Proceedings of the 43rd IEEE Vehicular Technology Conference, Seacaucus, New Jersey, May 1993, pp. 440-443

- ¹¹ K. S. Gilhousen, I. M. Jacobs, R. Padovani, A. J. Viterbi, L. A. Weaver, C. E. Wheatley, "On the Capacity of a Cellular CDMA System," IEEE Transactions on Vehicular Technology, Vol. 40, No. 2, pp. 303-311, May 1991
- ¹² A. J. Viterbi, "Implications of Mobile Cellular CDMA," IEEE Communications Magazine, Vol. 30, No. 12, pp. 38-41, December 1992
- ¹³ W. Hundley, S. Rowson, "DGPS Precision Approaches: Airport-Friendly," GPS World, Vol. 4, No. 3, pp. 28-34, March 1993
- ¹⁴ D. V. Sarwate, M. B. Pursley, "Properties of Pseudorandom and Related Sequences," The Proceedings of the IEEE, Vol. 68, No. 5, pp. 593-619, May 1980
- ¹⁵ M. B. Pursley, D. V. Sarwate, W. E. Stark, "Error Probability for Direct-Sequence Spread-Spectrum Multiple-Access Communications - Part 1: Upper and Lower Bounds," IEEE Transactions on Communications, Vol. Com-30, No. 5, pp. 975-984, May 1982
- ¹⁶ E. A. Geraniotis, M. B. Pursley, "Error Probability for Direct-Sequence Spread-Spectrum Multiple-Access Communications - Part 2: Approximations," IEEE Transactions on Communications, Vol. Com-30, No. 5, pp. 985-995, May 1982
- ¹⁷ A. M. Viterbi, A. J. Viterbi, "Erlang Capacity of a Power-Controlled CDMA System," IEEE Journal on Selected Areas of Communications, Vol. 11, No. 6, pp. 892- 900, August 1993
- ¹⁸ A. J. Viterbi, A. M. Viterbi, E. Zehavi "Performance of Power-Controlled Wideband Terrestrial Digital Communication," IEEE Transactions on Communications, Vol. 41, no. 4, pp. 559-568, April 1993
- ¹⁹ A. J. Goldsmith, L. J. Greenstein, G. J. Foschini, "Error Statistics of Real-Time Power Measurements in Cellular Channels with Multipath and Shadowing," IEEE Transactions on Vehicular Technology, Vol. 43, No. 3, pp. 439-446, August 1994
- ²⁰ A. M. Monk, L. B. Milstein, "Open-Loop Power Control in a Land-Mobile Satellite System," IEEE Journal on Selected Areas of Communications, Vol. 13, No. 2, February 1995
- ²¹ B. R. Vojcic, R. L. Pickholtz, L. B. Milstein, "Performance of DS-CDMA with Imperfect Power Control Operating Over a Low Earth Orbiting Satellite Link," , IEEE Journal on Selected Areas of Communications, Vol. 12, No. 4, May 1994

- ²² Simon Haykin, *Adaptive Filter Theory, Second Edition*, Englewood Cliffs, NJ, Prentice Hall, 1991
- ²³ J. H. Winters, "Optimum Combining in Digital Mobile Radio with Cochannel Interference," *IEEE Transactions on Vehicular Technology*, Vol. VT-33, No. 3, pp. 144-155, August 1984
- ²⁴ H. Cox, "Resolving Power and Sensitivity Mismatch of Optimum Array Processors," *Journal of the Acoustical Society of America*, Vol. 54, No. 3, pp. 771-785, March 1973
- ²⁵ B. D. Van Veen, K. M. Buckley, "Beamforming, a Versatile Approach to Spatial Filtering," *IEEE ASSP Magazine*, pp. 4-24, April 1988
- ²⁶ D. G. Brennan, "Linear Diversity Combining Techniques," *Proceedings of the IRE*, Vol. 47, No. 6, pp. 1075-1102, June 1959
- ²⁷ R. T. Compton, Jr., *Adaptive Antennas, Concepts and Performance*, Englewood Cliffs, NJ, Prentice-Hall, 1988
- ²⁸ W. C. Jakes, ed., *Microwave Mobile Communications*, New York, Wiley, 1974
- ²⁹ S. P. Applebaum, "Adaptive Arrays," Syracuse University Research Corporation Report SPL TR 66, August 1966.
- ³⁰ S. P. Applebaum, "Adaptive Arrays," *IEEE Transactions on Antennas and Propagation*, Vol. AP-24, No. 5, pp. 585-598, September 1976
- ³¹ B. Widrow, P. E. Mantey, L. J. Griffiths, B. B. Goode, "Adaptive Antenna Systems," *Proceedings of the IEEE*, Vol. 55, No. 12, pp. 2143-2159, December 1967
- ³² "Special Issue on Active and Adaptive Antennas," *IEEE Transactions on Antennas and Propagation*, Vol. AP-12, March 1964
- ³³ "Special Issue on Active and Adaptive Antennas," *IEEE Transactions on Antennas and Propagation*, Vol. AP-24, September 1976
- ³⁴ "Special Issue on Active and Adaptive Antennas," *IEEE Transactions on Antennas and Propagation*, March 1986
- ³⁵ O. L. Frost, "An Algorithm for Linearly Constrained Adaptive Array Processing," *Proceedings of the IEEE*, Vol. 60, No. 8, pp. 926-935, August 1972

- ³⁶ L. J. Griffiths, "A Simple Adaptive Algorithm for Real-Time Processing in Antenna Arrays," *Proceedings of the IEEE*, Vol. 57, No. 10, pp. 1696-1704, October 1969
- ³⁷ S. W. W. Shor, "Adaptive Technique to Discriminate against Coherent Noise in a Narrowband System," *Journal of the Acoustical Society of America*, Vol. 39, No. 1, pp. 74-78, January 1966
- ³⁸ C. M. Hackett, "Adaptive Arrays Can Be Used to Separate Communication Signals," *IEEE Transactions on Aerospace and Electronic Systems*, Vol. AES-17, No. 2, pp. 234-247, March 1981
- ³⁹ R. T. Compton, Jr., R. J. Huff, W. G. Swarner, A. G. Ksienski, "Adaptive Arrays for Communication Systems: An Overview of Research at The Ohio State University," *IEEE Transactions on Antennas and Propagation*, Vol. AP-24, pp. 599-606, September 1976
- ⁴⁰ R. T. Compton, Jr., "An Adaptive Array in a Spread Spectrum Communication System," *Proceedings of the IEEE*, Vol. 66, No. 3, pp. 289-298, March 1978
- ⁴¹ J. H. Winters, "Spread Spectrum in a Four-Phase Communication System Employing Adaptive Antennas," *IEEE Transactions on Communications*, Vol. Com-30, No. 5, pp. 929-936, May 1982
- ⁴² M. W. Ganz, "Protection of PSK Communication Systems with Adaptive Arrays," *IEEE Transactions on Aerospace and Electronic Systems*, Vol. AES-23, No. 4, pp. 528-536, July 1987
- ⁴³ V. M. Bogachev, I. G. Kiselev, "Optimum Combining of Signals in Space-Diversity Reception," *Telecommunications Radio Engineering*, Vol. 34/35, pp. 83, October 1980
- ⁴⁴ J. H. Winters, "Optimum Combining for Indoor Radio Systems with Multiple Users," *IEEE Transactions on Communications*, Vol. Com-35, No. 11, pp. 1222-1230, November 1987
- ⁴⁵ J. H. Winters, "Signal Acquisition and Tracking Performance with Adaptive Arrays in the Digital Mobile Radio System IS-54 with Flat Fading," *IEEE Transactions on Vehicular Technology*, Vol. 42, No. 4, pp. 377-384, November 1993
- ⁴⁶ Y. S. Yeh, D. G. Ruedink, "Efficient Spectrum Utilization for Mobile Radio Systems Using Space Diversity," *IEEE Transactions on Communications*, Vol. Com-30, No. 3, pp. 447-455, March 1982

- 47 B. Glance, L. J. Greenstein, "Frequency-Selective Fading Effects in Digital Mobile Radio with Diversity Combining," IEEE Transactions on Communications, Vol. Com-31, No. 9, pp. 1085-1094, September 1983
- 48 R. G. Vaughan, "On Optimum Combining at the Mobile," IEEE Transactions on Vehicular Technology, Vol. 37, No. 4, pp. 181-188, November 1988
- 49 S. C. Swales, M. A. Beach, D. J. Edwards, J. P. McGeehan, "The Performance Enhancement of Multibeam Base Station Antennas for Cellular Land Mobile Radio Systems," IEEE Transactions on Vehicular Technology, Vol. 39, No. 1, pp. 56-67, February 1990
- 50 B. Suard, G. Xu, H. Li, T. Kailath, "Channel Capacity of Spatial Division Multiple-Access Schemes," Conference Record of the 28th Asilomar Conference on Circuits, Systems and Computers, Pacific Grove, California, November 1994, pp. 1159-1163
- 51 G. Xu, H. Liu, W. J. Vogel, H. P. Lin, S. S. Jeng, G. W. Torrence, "Experimental Studies of Space-Division-Multiple-Access Schemes for Spectral Efficient Wireless Communications," Proceedings of the 1994 IEEE International Conference on Communications, New Orleans, Louisiana, May 1994, pp. 800-804
- 52 H. P. Lin, S. S. Jeng, I. Parra, G. Xu, W. J. Vogel, G. W. Torrence, "Experimental Studies of SDMA Schemes for Wireless Communications," The 1995 International Conference on Acoustics, Speech and Signal Processing, Conference Proceedings, Detroit, Michigan, May 1995, pp.1760-1763
- 53 R. O. Schmidt, "Multiple Emitter Location and Signal Parameter Estimation," IEEE Transactions on Antennas and Propagation, Vol. AP-34, No. 3, pp. 276-280, March 1986
- 54 R. Roy, T. Kailath, "ESPRIT-Estimation of Signal Parameters via Rotational Invariance Techniques," IEEE Transactions on Acoustics, Speech, and Signal Processing, Vol. 37, No. 7, pp. 984-995, July 1989
- 55 G. Xu, S. Li, "Throughput Multiplication of Wireless LANs for Multimedia Services: SDMA Protocol Design," Proceedings of the 1994 IEEE Global Telecommunications Conference - Globecom '94, San Francisco, California, November 1994, pp. 1326-1332
- 56 J. Ward, R. T. Compton, Jr., "High Throughput Radio Networks with Adaptive Antenna Arrays," IEEE Transactions on Communications, Vol. 14, No. 3, pp. 460-470, March 1993

- 57 J. Ward, R. T. Compton, Jr., "Improving the Performance of the Slotted Aloha Packet Radio Network with an Adaptive Array," IEEE Transactions on Communications, Vol. 13, No. 2, pp. 292-300, February 1992
- 58 R. Kohno, H. Imai, M. Hatori, S. Pasupathy, "Combination of an Adaptive Array Antenna and a canceller of interference for Direct-Sequence Spread-Spectrum Multiple-Access Systems," IEEE Journal on Selected Areas of Communications, Vol. 8, No. 5, pp. 675-681, May 1990
- 59 C. C. Ko, Francois Chin, S. S. Foo, "An Adaptive Algorithm for Separating and Tracking Multiple Directional Sources in Linear Arrays," IEEE Transactions on Antennas and Propagation, Vol. 40, No. 3, pp. 261-267, March 1992
- 60 P. Balaban, J. Salz, "Optimum Diversity Combining and Equalization in Digital Data Transmission with Applications to Cellular Mobile Radio - Part 1: Theoretical Considerations," IEEE Transactions on Communications, Vol. 40, No. 5, pp. 885-894, May 1992
- 61 P. Balaban, J. Salz, "Optimum Diversity Combining and Equalization in Digital Data Transmission with Applications to Cellular Mobile Radio - Part 2: Numerical Results," IEEE Transactions on Communications, Vol. 40, No. 5, pp. 895-907, May 1992
- 62 R. Price, P. E. Green, Jr., "A Communication Technique for Multipath Channels," Proceedings of the IRE, Vol. 46, pp. 555-570, March 1958
- 63 G. L. Turin, "Introduction to Spread-Spectrum Antimultipath Techniques and Their Application to Urban Digital Radio," Proceedings of the IEEE, Vol. 68, No. 3, pp. 328-353, March 1980
- 64 J. L. Lehnert, M. B. Pursley, "Multipath Diversity Reception of Spread-Spectrum Multiple-Access Communications," IEEE Transactions on Communications, Vol. Com-35, No. 11, pp. 1189-1198, November 1987
- 65 J. Wang, M. Moeneclay, L. B. Milstein, "DS-CDMA with Predetection Diversity for Indoor Radio Communications," IEEE Transactions on Communications, Vol. 42, No. 2/3/4, pp. 1929-1938, February/March/April 1994
- 66 G. V. Tsoulos, M. A. Beach, S. C. Swales, "Application of Adaptive Antenna Technology to Third Generation Mixed Cell Radio Architecture," Proceedings of the 1994 IEEE 44th Vehicular Technology Conference, Stockholm, Sweden, June 1994, pp. 615-619

- 67 G. V. Tsoulos, M. A. Beach, S. C. Swales, "DS-CDMA Capacity Enhancement with Adaptive Antennas," *Electronics Letters*, Vol. 31, No. 16, pp. 1319-1320, August 3, 1995
- 68 J. H. Winters, J. Salz, R. D. Gitlin, "The Impact of Antenna Diversity on the Capacity of Wireless Communication Systems," *IEEE Transactions on Communications*, Vol. 42, No. 2/3/4, pp. 1740-1751, February/March/April 1994
- 69 B. H. Khalaj, A. Paulraj, T. Kailath, "Antenna Arrays for CDMA Systems with Multipath," *Proceedings of the 1993 Military Communications Conference*, pp. 624-628
- 70 D. Pal, B. H. Khalaj, "RAKE-Type Receiver Structure for Narrowband Wireless Systems can be Designed Using Multiple Antennas at the Receiver," *Proceedings of the 1994 IEEE International Conference on Communications*, New Orleans, Louisiana, May 1994, pp. 1701-1705
- 71 B. H. Khalaj, A. Paulraj, T. Kailath, "Spatio-Temporal Channel Estimation Technique for Multiple Access Spread-Spectrum with Antenna Arrays," *Proceedings of the 1995 IEEE International Conference on Communications*, Seattle, Washington, June 1995, pp. 1520-1524
- 72 H. Yoshino, K. Fukawa, H. Suzuki, "Interference Canceling Equalizer (ICE) for Mobile Radio Communications," *Proceedings of the 1994 IEEE International Conference on Communications*, New Orleans, Louisiana, May 1994, pp. 1427-1432
- 73 Y. Wang, J. R. Cruz, "Adaptive Antenna Arrays for Cellular CDMA Communication Systems," *The 1995 International Conference on Acoustics, Speech and Signal Processing*, Conference Proceedings, Detroit, Michigan, May 1995, pp. 1725-1728
- 74 T. Liu, "The Modular Covariance Adjustment Adaptive Array for CDMA Wireless Communications," *Proceedings of the 1993 International Conference on Acoustics, Speech and Signal Processing*, Vol. 4, pp. IV-180 - IV-183, 1993
- 75 S. A. Hanna, M. El-Tanany, S. A. Mahmoud, "An Adaptive Combiner for Co-Channel Interference Reduction in Multiuser Indoor Radio Systems," *Proceedings of the 41st IEEE Vehicular Technology Conference*, St. Louis, Missouri, May 1991, pp. 222-227
- 76 B. Suard, A. F. Naguib, G. Xu, A. Paulraj, "Performance of CDMA Mobile Communication Systems Using Antenna Arrays," *Proceedings of the 1993 IEEE International Conference on Acoustics, Speech, and Signal Processing*, Minneapolis, Minnesota, April 1993, pp. 153-156

- 77 A. F. Naguib, A. Paulraj, T. Kailath, "Capacity Improvement with Base-Station Antenna Arrays in Cellular CDMA," IEEE Transactions on Vehicular Technology, Vol. 43, No. 3, pp. 691-698, August 1994
- 78 A. F. Naguib, A. Paulraj, T. Kailath, "Performance of CDMA Cellular Networks with Base Station Antenna Arrays," Proceedings of the 1994 International Zurich Seminar on Digital Communications, Zurich, Switzerland, March 1994, pp. 87-100
- 79 A. F. Naguib, A. Paulraj, "Effects of Multipath and Base Station Antenna Arrays on Uplink Capacity of Cellular CDMA," Proceedings of the 1994 IEEE Global Telecommunications Conference - Globecom '94, San Francisco, California, November 1994, pp. 395-399
- 80 A. F. Naguib, A. Paulraj, "Performance of DS/CDMA with M-ary Modulation Cell Site Antenna Arrays," Proceedings of the 1995 IEEE International Conference on Communications, Seattle, Washington, June 1995, pp. 697-702
- 81 A. F. Naguib, A. Paulraj, "Recursive Adaptive Beamforming for Wireless CDMA," Proceedings of the 1995 IEEE International Conference on Communications, Seattle, Washington, June 1995, pp. 1515-1519
- 82 A. F. Naguib, A. Paulraj, "Performance Enhancement and Trade-offs of Smart Antennas in CDMA Cellular Networks," Proceedings of the 44th Vehicular Technology Conference, Chicago, Illinois, July 1995, pp. 40-44,
- 83 A. F. Naguib, A. Paulraj, "Power Control in Wireless CDMA: Performance with Cell Site Antenna Arrays," The Proceedings of the 1995 IEEE Global Telecommunications Conference, Singapore, November 1995, pp. 225-229
- 84 A. F. Naguib, A. Paulraj, "Performance of Cellular CDMA with M-ary Orthogonal Modulation and Cell Site Antenna Arrays," IEEE Journal on Selected Areas of Communications, Vol. 14, No. 6, pp. 100-110, July 1996
- 85 M. A. Beach, A. J. Copping, D. J. Edwards, K. W. Yates, "An Adaptive Antenna for Multiple Signal Sources," Proceedings of the IEE Fifth International Conference on Antennas and Propagation, pp. 347-350, University of York, April 1987
- 86 F. Simpson, J. M. Holtzman, "Direct Sequence CDMA Power Control, Interleaving, and Coding," IEEE Journal on Selected Areas of Communications, Vol. 11, No. 7, pp. 1085-1095, September 1993
- 87 G. L. Stuber, C. Kchao, "Analysis of a Multiple-Cell Direct-Sequence CDMA Cellular Mobile Radio System," IEEE Journal on Selected Areas of Communications, Vol. 10,

No. 4, pp. 669-678, May 1992

- ⁸⁸ A. Jalali, P. Mermelstein, "Effects of Diversity, Power Control, and Bandwidth on the Capacity of Microcellular CDMA Systems," IEEE Journal on Selected Areas of Communications, Vol. 12, No. 5, pp. 952-961, June 1994
- ⁸⁹ L. B. Milstein, T. S. Rappaport, R. Barghouti, "Performance Evaluation for Cellular CDMA," IEEE Journal on Selected Areas of Communications, Vol. 10, No. 4, pp. 680-687, May 1992
- ⁹⁰ P. Newson, M. R. Heath, "The Capacity of a Spread Spectrum CDMA System for Cellular Mobile Radio with Consideration of System Imperfections," IEEE Journal on Selected Areas of Communications, Vol. 12, No. 5, pp. 673-683, May 1994
- ⁹¹ I. J. Gupta, "Adaptive Arrays for Multiple Simultaneous Desired Signals," IEEE Transactions on Aerospace and Electronic Systems, Vol. AES-19, No. 5, pp. 761-767, September 1983
- ⁹² C. A. Baird, Jr., C. L. Zahm, "Performance Criteria for Narrowband Array Processing," Proceedings of the IEEE Conference on Decision and Control, Miami Beach, Florida., December 1971, pp. 564-565
- ⁹³ B. W. Widrow, S. D. Stearns, *Adaptive Signal Processing*, Englewood Cliffs, NJ, Prentice-Hall, 1985
- ⁹⁴ B. Widrow, J. McCool, M. Ball, "The Complex LMS Algorithm," Proceedings of the IEEE, Vol. 63, pp. 719-720, April 1975
- ⁹⁵ K. D. Senne, "Adaptive Linear Discrete-Time Estimation," Ph. D. Dissertation, Stanford University, June 1968
- ⁹⁶ L. L. Horowitz, K. D. Senne, "Performance Advantage of Complex LMS for Controlling Narrow-band Adaptive Arrays," IEEE Transactions on Acoustics, Speech and Signal Processing, Vol. ASSP-29, No. 3, pp. 722-736, June 1981
- ⁹⁷ B. Fisher, N. J. Bershad, "The Complex LMS Algorithm - Transient Weight Mean and Covariance with Applications to the ALE," IEEE Transactions on Acoustics, Speech and Signal Processing, Vol. ASSP-31, No. 1, pp. 722-736, June 1981
- ⁹⁸ L. P. Winkler, "Constrained Array Optimization by Penalty Function Techniques," Journal of the Acoustical Society of America, Vol. 55, No. 5, pp. 1042-1048, May 1974

- 99 L. P. Winkler, M. Schwartz, "Adaptive Nonlinear Optimization of the Signal-to-Noise Ratio of an Array Subject to a Constraint," *Journal of the Acoustical Society of America*, Vol. 52, No. 1, Part 1, pp. 39-51, 1972
- 100 R. T. Compton, Jr., "On Eigenvalues, SINR, and Element Patterns in Adaptive Arrays," *IEEE Transactions on Antennas and Propagation*, Vol. AP-32, No. 6, pp. 643-647, June 1984
- 101 K. S. Miller, *Complex Stochastic Processes, an Introduction to Theory and Applications*, Reading, Massachusetts: Addison-Wesley, 1974
- 102 M. B. Pursley, "Performance Evaluation for Phase-Coded Spread-Spectrum Multiple-access Communication - Part 1: System Analysis," *IEEE Transactions on Communications*, pp. 795-799, Vol. COM-25, No. 8, August 1977
- 103 D. J. Torrieri, "Performance of Direct-Sequence Systems with Long Pseudonoise Sequences," *IEEE Journal on Selected Areas of Communications*, Vol. 10, No. 4, pp. 770-781, May 1992
- 104 J. M. Holtzman, "A Simple, Accurate Method to Calculate Spread-Spectrum Multiple-Access Error Probabilities," *IEEE Transactions on Communications*, Vol. 40, No. 3, pp. 461-464, March 1992
- 105 R. K. Morrow, J. S. Lehnert, "Bit-to-Bit Error Dependence in Slotted DS/SSMA Packet Systems with Random Signature Sequences," *IEEE Transactions on Communications*, Vol. 37, No. 10, pp. 1052-1061, October 1989
- 106 R. L. Pickholtz, D. L. Schilling, L. B. Milstein, "Theory of Spread-Spectrum Communications - A Tutorial," *IEEE Transactions on Communications*, Vol. COM-30, No. 5, pp. 855-884, May 1982
- 107 Special Issue on Mobile Radio Propagation, *IEEE Transactions on Vehicular Technology*, Vol. 37, No. 1, February 1988
- 108 R. G. Vaughan, J. B. Anderson, "Antenna Diversity in Mobile Communications," *IEEE Transactions on Vehicular Technology*, Vol. VT-36, No. 4, pp. 149-172, November 1987
- 109 J. Salz, J. H. Winters, "Effect of Fading Correlation on Adaptive Arrays in Digital Mobile Radio," *IEEE Transactions on Vehicular Technology*, Vol. 43, No. 4, pp. 1049 - 1057, November 1994
- 110 G. Raleigh, S. N. Diggavi, A. F. Naguib, A. Paulraj, "Characterization of Fast Fading Vector Channels for Multi-Antenna Communication Systems," *Proceedings of the 28th*


- Asilomar Conference on Circuits, Systems and Computers, Pacific Grove, California, October 1994, pp. 800-804
- ¹¹¹ A. J. Viterbi, A. M. Viterbi, E. Zehavi, "Other-Cell Interference in Cellular Power-Controlled CDMA," IEEE Transactions on Communications, Vol. 42, No. 4, pp. 1501-1504, February/March/April 1994
 - ¹¹² D. D. Lee, D. H. Lee, Y. J. Chung, H. G. Kim, K. C. Whang, "Other-cell Interference with Power Control in Macro/Microcell CDMA Networks," Proceedings of the 1996 IEEE 46th Vehicular Technology Conference, Atlanta, Georgia, Vol. 2, pp. 1120-1124, April 1996
 - ¹¹³ M. Gudmundson, "Correlation Model for Shadow Fading in Mobile Radio Systems," Electronics Letters, Vol. 27, pp. 2145-2146, November 7, 1991
 - ¹¹⁴ R. Vijayan, J. M. Holtzman, "Foundations for Level-Crossing Analysis of handoff Algorithms," Proceedings of the 1993 IEEE International Communications Conference, Geneva, Switzerland, May 1993, pp. 935-939
 - ¹¹⁵ S. C. Schwartz, Y. S. Yeh, "On the Distribution Function and Moments of Power Sums with Log-Normal Components," The Bell System Technical Journal, Vol. 61, No. 7, pp. 1441-1462, September 1982
 - ¹¹⁶ Y. S. Yeh, S. C. Schwartz, "Outage Probability in Mobile Telephony Due to Multiple Log-Normal Interferers," IEEE Transactions on Communications, Vol. Com-32, No. 4, pp. 380-388, April 1984
 - ¹¹⁷ M. Guillen, "Simulation of a DS-CDMA System for Performance Analysis over Different Channel Conditions," M. Sc. Thesis, University of Florida, December 1994
 - ¹¹⁸ E. Eleftheriou, D. D. Falconer, "Tracking Properties and Steady-State Performance of RLS Adaptive Filter Algorithms," IEEE Transactions on Acoustics, Speech, and Signal Processing," Vol. ASSP-34, No. 5, pp. 1097-1109, October 1986
 - ¹¹⁹ N. R. Goodman, "Statistical Analysis Based on a Certain Multivariate Complex Gaussian Distribution (An Introduction)," Ann. Stat. Math., Vol. 34, pp. 152-177, March 1963
 - ¹²⁰ D. M. Dlugos, R. A. Scholtz, "Acquisition of Spread Spectrum Signals by an Adaptive Array," IEEE Transactions on Acoustics, Speech and Signal Processing, Vol. 37, No. 8, pp. 1253-1269, August 1989

- ¹²¹ I. S. Reed, J. D. Mallet, L. E. Brennan, "Rapid Convergence Rate in Adaptive Arrays," *IEEE Transactions on Aerospace and Electronic Systems*, Vol. AES-10, No. 6, pp. 853-863, November 1974
- ¹²² I. P. Kirksteins, D. W. Tufts, "On the Probability Density of Signal-to-Noise Ratio in an Improved Adaptive Detector," *Proceedings of ICASSP*, Vol. 2, pp. 572-575, 1985
- ¹²³ K. Gerlach, "Convergence Rate of an SMI Canceller in Nonstationary Noise," *IEEE Transactions on Aerospace and Electronic Systems*, Vol. 30, No. 2, pp. 599-604, April 1994
- ¹²⁴ J. Cui, D. D. Falconer, A. U. H. Sheikh, "SINR of an Antenna Array with a Large Number of Interfering Users," *Proceedings of the IEEE VTS 46th Vehicular Technology Conference*, Atlanta, Georgia, April 1996, Vol. 1, pp. 1486-1490
- ¹²⁵ J. C. Liberti, T. S. Rappaport, "Analysis of CDMA Cellular Radio Systems Employing Adaptive Antennas in Multipath Environments," *Proceedings of the IEEE VTS 46th Vehicular Technology Conference*, Atlanta, Georgia, April 1996, Vol. 2, pp. 1076-1080
- ¹²⁶ H. R. Anderson, "A Second Generation 3-D Ray-Tracing Model Using Rough Surface Scattering," *Proceedings of the IEEE VTS 46th Vehicular Technology Conference*, Atlanta, Georgia, April 1996, Vol. 1, pp. 46-50
- ¹²⁷ G. E. Athanasiadou, A. R. Nix, J. P. McGeehan, "Indoor 3-D Ray Tracing Predictions and Their Comparison with High Resolution Bandwidth Measurements," *Proceedings of the IEEE VTS 46th Vehicular Technology Conference*, Atlanta, Georgia, April 1996, Vol. 1, pp. 36-40
- ¹²⁸ L. P. Winkler, "Optimum and Adaptive Detector Arrays," Ph. D. Thesis, Polytechnic Institute of Brooklyn, 1971

BIOGRAPHICAL SKETCH

John Miller received his Bachelor of Science degree from the University of Florida in December, 1981. From February 1982 to April 1989 he worked at the Portable Products Division of Motorola Inc. in Plantation, Florida. He returned to the University of Florida in August 1989 and was awarded a Masters of Science degree in electrical engineering in May 1991. Since this time he has been working towards a Ph.D.

I certify that I have read this study and that in my opinion it conforms to acceptable standards of scholarly presentation and is fully adequate, in scope and quality, as a dissertation for the degree of Doctor of Philosophy.



Scott L. Miller, Chairman
Associate Professor of Electrical
and Computer Engineering

I certify that I have read this study and that in my opinion it conforms to acceptable standards of scholarly presentation and is fully adequate, in scope and quality, as a dissertation for the degree of Doctor of Philosophy.



Leon W. Couch, II
Professor of Electrical and Computer
Engineering

I certify that I have read this study and that in my opinion it conforms to acceptable standards of scholarly presentation and is fully adequate, in scope and quality, as a dissertation for the degree of Doctor of Philosophy.



John M. M. Anderson
Assistant Professor of Electrical
and Computer Engineering

I certify that I have read this study and that in my opinion it conforms to acceptable standards of scholarly presentation and is fully adequate, in scope and quality, as a dissertation for the degree of Doctor of Philosophy.



Jose C. Principe
Professor of Electrical and Computer
Engineering

I certify that I have read this study and that in my opinion it conforms to acceptable standards of scholarly presentation and is fully adequate, in scope and quality, as a dissertation for the degree of Doctor of Philosophy.



Ramesh Shrestha
Associate Professor of Civil
Engineering

This dissertation was submitted to the Graduate Faculty of the College of Engineering and to the Graduate School and was accepted as partial fulfillment of the requirements for the degree of Doctor of Philosophy.

August, 1996



Winfred M. Phillips
Dean, College of Engineering

Karen A. Holbrook
Dean, Graduate School

LD
1780
1996
. M648

SCIENCE
LIBRARY

UNIVERSITY OF FLORIDA



3 1262 08555 0654